POLITECNICO DI MILANO

School of Industrial and Information Engineering

Mastero of Science in Mathematical Engineering

Ion Electrodiffusion across the Ciliary Epithelium in the Human Eye

Advisor: Prof. Riccardo Sacco

Co-advisor: Ing. Greta Chiaravalli

Riccardo Griffo

ID: 928292

Academic Year 2020-2021

Ai miei nonni,
ai miei genitori,
ai miei fratelli.

Contents

List of Figures

xiii

List of Tables

Abstract

Ion electrodynamics across the Ciliary Epithelium (CE) results to be a fundamental mechanism in the secretion of aqueous humor (AH), which is the biological solution that permits the transport of nutrients in the internal structures of the eye. A malfunction of the AH secretion process, as well as a defect in the outflow of AH can lead to an increase of intraocular pressure and to the onset of diseases of the visual apparatus. A study of the mechanisms involved in the transepithelial flow of ions across the ciliary body is an important physiological question and represents an obligatory step for an accurate analysis of AH secretion and, eventually, the design of therapeutical treatment of ocular pathologies such as glaucoma.

This Master thesis deals with the study of a mathematical model for the stationary description of ion electrodynamics in the human ciliary epithelium. The model represents an adaptation to the specific case of the well known velocity-extended Poisson-Nernst-Planck model (VE-PNP), which has been used for the continuous description of intracellular and extracellular spaces. In Chapter 1 we give a review of eye physiology, focusing our attention to the biological structures that are most relevant in our description. Moreover, we illustrate the processes involved in the AH formation and introduce the concept of compartmental model, which we will use for the description of the interested area. Chapter 2 deals with the transmembrane transport:we report theoretical concept and description of transmembrane transporters. In Chapter 3 we derive the general VE-PNP model, that we will adapt for our purpose in Chapter 4. Chapter 4 also contain an accurate description of the domain upon which we applied the derived model. In Chapter 5 we discuss the numerical discretization of the problem, introducing a solution map for its iterative solution which is the extension to the present model

of the Gummel Decoupled Algorithm conventionally employed in semiconductor device simulation. In Chapter 6 we illustrate and discuss the model predictions obtained by running a computer code written using the MatLab scientific environment in the simulation of numerical tests in working conditions of increasing complexity.

Summarizing conclusions and future model developments are discussed in Chapter 7.

Sommario

L'elettrodinamica ionica attraverso l'epitelio ciliare (CE) è un meccanismo fisico fondamentale nel processo di secrezione dell'umor acqueo (AH), il quale è una soluzione biologica che permette il trasporto dei nutrienti nelle strutture interne dell'occhio. Un malfunzionamento di tale processo, o un difetto nel deflusso di umore acqueo attraverso i canali preposti, possono portare ad un aumento della pressione intraoculare e all'insorgenza di patologie dell'apparato visivo. Lo studio dei meccanismi coinvolti nel flusso transepiteliale degli ioni all'interno del corpo ciliare rappresenta un passaggio obbligato per un'analisi accurata della secrezione di umor acqueo, pertanto esso è senza dubbio un argomento di grande interesse medico.

In questa tesi viene trattato lo studio di un modello matematico per la descrizione dello stato stazionario dell'elettrodinamica ionica nell'epitelio ciliare umano. In particolare, il noto modello Poisson-Nernst-Planck generalizzato (VE-PNP) viene adattato al caso specifico ed utilizzato per la descrizione delle concentrazioni ioniche in spazi intracellulari ed extracellulari.

Nel Capitolo 1 sono presenti dei richiami alla fisiologia dell'occhio, in particolare alle strutture biologiche più rilevanti per la nostra descrizione. Inoltre, vengono illustrati i processi coinvolti nella formazione di umore acqueo ed introdotto il concetto di modello compartimentale, utilizzato per la descrizione dell'area interessata. Il Capitolo 2 tratta del trasporto ionico attraverso la membrana epiteliale: vengono descritti i concetti teorici del trasporto transmembranale ed i diversi tipi di trasportatori esistenti, dandone una caratterizzazione matematica. Nel Capitolo 3 viene derivato il modello VE-PNP, adattato per il nostro scopo nel Capitolo 4, che contiene una descrizione accurata del dominio su cui abbiamo applicato il modello derivato. Nel Capitolo 5 si discute la discretizzazione numerica del problema, introducendo un algo-

ritmo iterativo chiamato Mappa di Gummel. Nel Capitolo 6 sono riportati alcuni risultati numerici. Infine, il lavoro viene concluso illustrando alcune future direzioni di ricerca.

Per le simulazioni numeriche è stato utilizzando un codice sviluppato in $MATLAB$.

Chapter 1

Introduction

The particular functions that the visual system performs make the eye an extremely complicated biological structure. In fact, being the eye a receptor of light signals, the tissues that compose it must necessarily be transparent, so that the transmission of light cannot be disturbed by the blood supply. Furthermore, since the eye is responsible for sending signals to the brain for image creation, it is of fundamental importance to maintain optimal optical alignment between cornea, retina and lens. To comply with these restrictions, the eye is incessantly employed in the production, circulation and drainage of aqueous humor (AH), a transparent liquid that contributes to the nourishment of the tissues not reached by the blood vessels and keeps constant the pressure inside the eye (intraocular pressure, IOP) ($\approx 15 mmHg$) [15]. Aqueous humor therefore plays a very important role within the dynamics of the bulb and an imbalance in its functioning may lead to the development of pathological conditions. For example, excessive production of AH or insufficient drainage are responsible for an excess of fluid that causes high intraocular pressure. This pathological condition is referred to as glaucoma and can cause partial or total loss of vision. It is clear then that understanding the

1

mechanisms of AH production is relevant to understand eye pathophysiology.

1.1 Eye Physiology

With the aim of analyzing the physical mechanisms behind the production of aqueous humor, in this section is given a brief review of the anatomy of the eye. In particular, the focus will be given to the Ciliary Body, a ring of tissue positioned just behind the posterior surface of the iris, which is responsible for the production of AH.

1.1.1 Eye structure

The eye has a spherical shape, with an averaged diameter of 24 mm, and it is inserted within a bone cavity, called *ocular cavity* or *orbit*, which contains and protects it. The bulb wall of the eye is composed of three concentric tunics (see figure 1.1):

- **Fibrous tunic**, containing *sclera* and *cornea*. It acts as an external attachment for the muscles that allow the movement, providing the mechanical support for the eye. The sclera is composed of connective tissue and it covers most of the eye, while the cornea is located in the front and, unlike the sclera, it contains no blood vessels.

- **Vascular tunic**, formed by the *choroid*, the *ciliary body* (CB) and the *lens*. Its primary functions are to provide a pathway for blood and lymphatic vessels, to supervise the amount of light entering the eye, to modify the shape of the lens and to manage the production and absorption of aqueous humor.

- **Neural tunic**, containing the *retina*. The inner part of the tunic is called *neural part* and contains the photoreceptors of the eye. The outer part is called *pigmented part* and its primary function is to avoid reflection of light that has passed through the neural part, in order to prevent the return of the light into the eye structure.
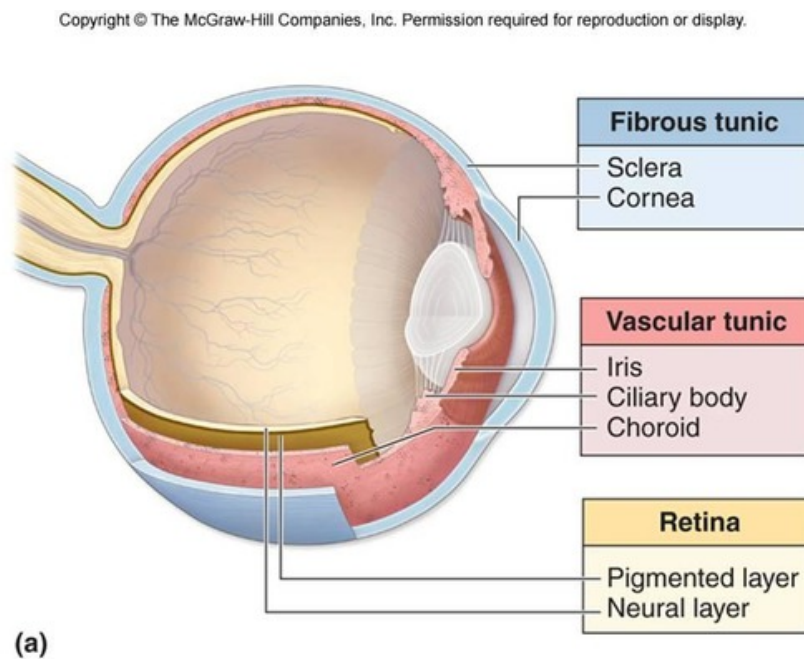
Figure 1.1: The eye's bulb wall subdivision in tunics. Source: Mescher AL. Junqueira's Basic Histology: Text and Atlas, 12th Edition: http://www.accessmedicine.com

The interior portion of the eye in composed of two chambers: the *anterior cavity* and the *posterior cavity*, which are separated by the lens and the CB. The anterior cavity is in turn subdivided into two chambers connected by the pupil aperture: the *anterior chamber* (AC), delimited by the cornea and the iris, and the *posterior Chamber* (PC), which is between the iris and the lens. These two chambers are filled with aqueous humor, a mixture composed

by water, electrolytes, organic solutes, and other proteins, produced by the ciliary body in the PC at a rate of approximately $2.4\pm0.6\mu l/min$ [8]. AH then flows into the AC and is drained outside the eye by following two different pathways, which will be described later.

The posterior cavity, also named *vitreous chamber*, occupies approximately the 90% of the hollow portion of the eye and it is filled with the *vitreous body*, a jelly-like substance composed by water and proteins. This very viscous fluid is only produced during fetal development.

1.1.2 Anatomy of the Ciliary Body

The Ciliary Body (CB) is a ring of tissue positioned behind the iris. It has two roles that make it fundamental for the natural functioning of the system: it is responsible for the production of aqueous humor and contains the *ciliary muscles*, which regulate, through their contraction, the shape of the lens to which they are linked by means of ligaments called *zonules*.

Since the aqueous humor is an extremely important component, the shape of the ciliary body is modeled to allow for as much AH production as possible. Indeed, in order to increase the surface available for fluid secretion, it is organized into a series of ridges, called *ciliary processes*, arranged radially and oriented towards the pupil.

Each ciliary process is composed by: blood vessels, *stroma* and *ciliary epithelium* (CE), see fig 1.2.

The internal part of the ciliary processes is supplied by a complex network of blood vessels, which play an active role in the production of aqueous humor. In fact, they not only offer nutrients to the cells of the ciliary epithelium, but the constituents of the blood plasma are also used directly in the production
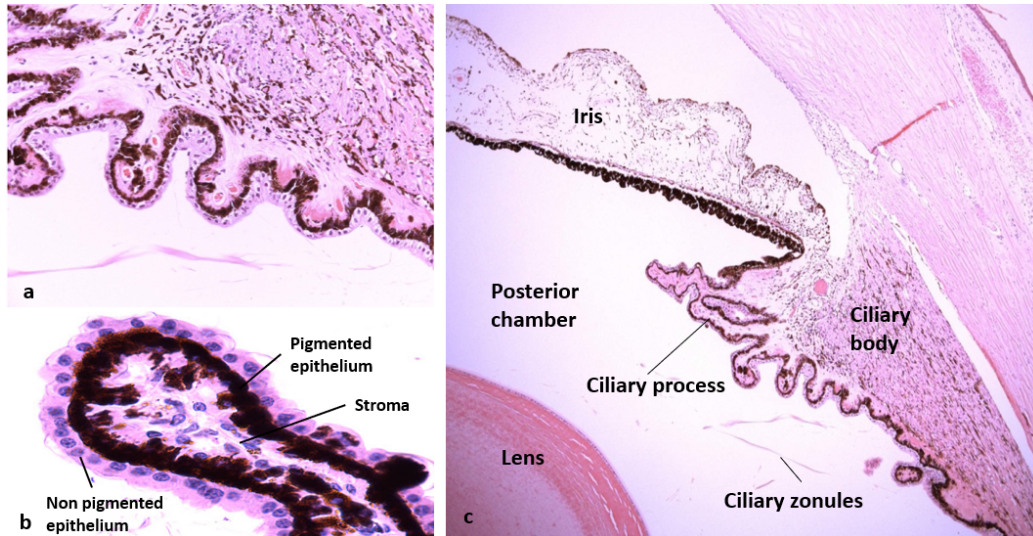
Figure 1.2: Anatomy of the Ciliary Body. (a) Detail of a portion of Ciliary Body: a series of Ciliary Processes, (b) Detail of a single Ciliary Process, (c) Sectional picture of a portion of the eye. Source Histology of human ciliary body (Prof. Ruth Santo).

of aqueous humor. This dual role indicates that the body probably regulates the secretion of aqueous humor by regulating the blood supply in the ciliary processes [15].

The surface of the ciliary processes is covered by a double epithelial layer, the ciliary epithelium, generated by the cooperation of two layers that have different origins: the outermost layer, placed in contact with the posterior chamber, is called non-pigmented ciliary epithelium (NPE), while the innermost layer, placed in contact with the stroma, is called pigmented ciliary epithelium (PE). The two epithelial layers are connected to each other by junctions placed on the apical membranes of the cells. The cells of the NPE layer are much wider than the cells of the PE layer and exhibit a higher rate of metabolic activity. Furthermore, the basolateral membrane of the non-pigmented cells, placed in contact with the posterior chamber, presents

invaginations which allow to increase even more the available secretion area (the surface area available for the secretion is approximately $6cm^2$) .

This particular double layer structure composed by different cell types is a unique example in the whole human body and the advantages over a single layer conformation are not yet clear.

Certainly, the ciliary epithelium plays an extremely important role, as it acts as a barrier between a compartment heavily supplied with blood vessels and a compartment that is not supplied at all. In fact, one should take in mind that the main activity of the ciliary body is the production of a watery like substance starting from the blood carried by the blood vessels. To accomplish this task, the CB is organized into a series of filters that act as a sieve. The combination of these filters is generally referred to as *the Blood-Aqueous barrier.*

1.1.3   The Blood-Aqueous barrier

Fortunately, the internal structures of the eye, such as the cornea, the anterior chamber or the lens, are not reached by the vascular network. The blood in fact does not allow the passage of light at all. Even if deprived of blood cells, blood contains a high concentration of protein molecules that scatter light.

A series of laboratory experiments [17] [10] have shown that the CE is able to filter blood step by step along a path that goes from the blood vessels to the anterior chamber thanks to a series of "obstacles" that form the Blood-Aqueous barrier. From a pharmacological point of view, understanding the functioning of this barrier is essential to find components that reach the eye in an acceptable concentration.

The Blood-Aqueous barrier is formed by:

1. The vascular endothelium layer that covers the vessels. Capillaries in

the ciliary processes are fenestrated, permitting the passage of plasma proteins into the stroma, while blocking blood cells.

2. The ciliary epithelium. It blocks the diffusion of large protein molecules, that cannot move from the stroma into the PC, mainly thanks to the presence of the *tight junctions* in the epithelium.

Tight junctions are protein structures that form a bridge between adjacent cells of the non-pigmented layer. This tangled network of protein fibrils prevents the diffusion of large protein molecules from the extracellular space between the epithelial cells towards the PC. The result is that the liquid obtained from the filtration of the tight junctions is a transparent mixture containing water and mostly ionic compounds.

Moreover, tight junctions mark the separation boundary between the two different types of membrane that cover epithelial cells (apical membrane and basolateral membrane). As we will see, the distinction between these two types of membrane is fundamental in the secretion process of AH, as each of them is specialized in a specific task.

1.2 Aqueous Humor formation

The production of aqueous humor is a complex electric-fluid-dynamic mechanism. The volumetric flow secreted through the epithelium layer is mainly driven by three forces [15] (see figure 1.3):

1. **Hydrostatic pressure**. Between the stroma and the PC there is a pressure gradient due to the difference between the IOP and the blood pressure in the capillaries. This jump of pressure generates a flow of water from the stroma to the posterior chamber.

2. **Oncotic pressure**. Thanks to the presence of tight junctions, a concentration gradient of large molecules is generated between the stroma and the posterior chamber. This is the result of a mechanism known as *ultrafiltration*. Ultrafiltration establish a difference in oncotic pressure which generates a direct flow of water from the PC towards the stroma.

3. **Osmotic pressure**. Ions are actively transported through the ciliary epithelium. This generates a difference in osmotic pressure across the layer due to a difference in ion concentrations. As a result, a net water flow is generated from the stroma towards the PC, as the water is forced to follow the ion flow.

   This driving force has been highlighted by more recent studies which reveal how the concentration of some solutes in PC is different from that expected from ultrafiltered plasma.

1.2.1 Active transport of ions

Tight junctions represent a dividing line between the two types of membrane that cover the cells of the ciliary epithelium. The fundamental distinction between the apical part and the basolateral part of the surface is the different distribution of ionic transporters, which are not uniformly distributed on the cell surface. This condition is known as *polarized distribution* [15].
A polarized distribution of ionic transporters appears to be a fundamental characteristic of cells, which in this way can preferentially import some solutes on one side and export them on the other side. Laboratory experiments [3] have shown that the active Na-K-ATPase transporter is much denser on the basolateral surface of the NPE layer cells. Furthermore, the presence of different molecular variants of the same transporter denote how the non-
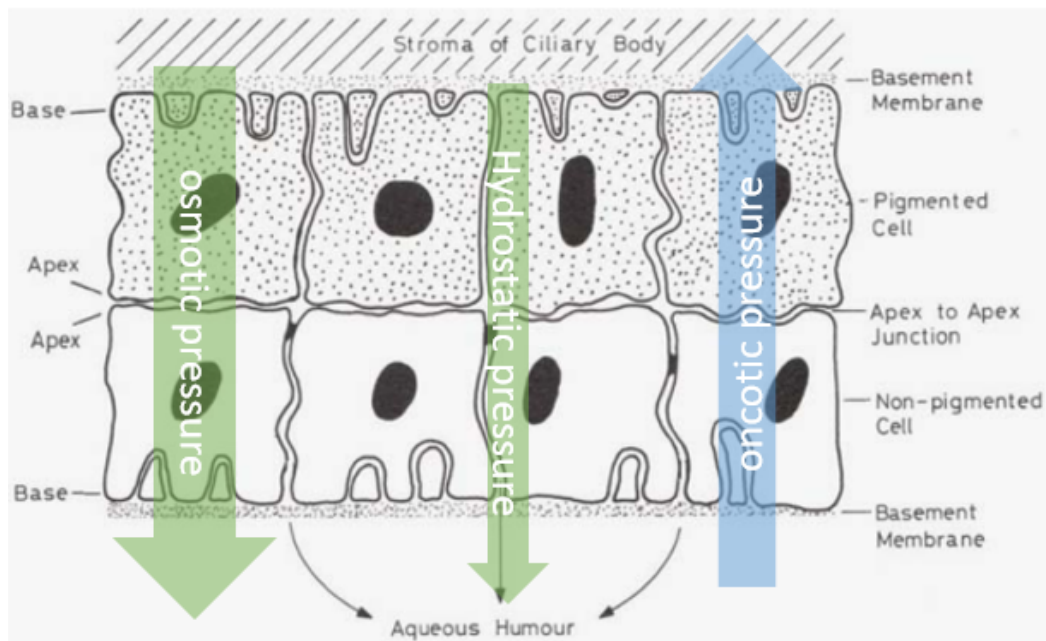
Figure 1.3: Forces involved in the process of AH secretion. Source: Shahidullah, Mohammad Al-Malki, Waleed Delamere, Nicholas. (2011). Mechanism of Aqueous Humor Secretion, Its Regulation and Relevance to Glaucoma. 10.5772/26559.

pigmented cell is specialized in the transport of sodium from the plasma present in the stroma towards the AH. On the other hand, the apical membrane of non-pigmented cells has different transporters which have the task of importing sodium into the cytoplasm. This combined action generates a rather high difference in transmembrane sodium concentration. Similarly, chlorine also passes through cells by exploiting the polarized distribution of transporters. This transepithelial movement generates a potential difference across the CE which tends to influence the movement of other ions through the extracellular space.

Active transport results to be fundamental for the secretion of aqueous humor: the efflux of ions described above causes an increase in the osmotic

pressure of the intracellular space and, in order to balance this force, water moves from the stroma into the posterior chamber, passing through the intercellular space.

1.3 Flow of aqueous humor

After the secretion within the intercellular space of the ciliary processes, AH passes throughout the anterior chamber of the eye and it flows through a trabecular meshwork, which acts as a filter, removing the debris that may come from bacterial infections. From the trabecular, AH passes into the Schlemm canal which is a thin-walled vein that connects the extraocular vein to the vascular tunic. Flow of AH through the Schlemm canal can be represented by a pressure-flow relationship [4]:

$$\frac{dQ}{dx} = \frac{IOP - p(x)}{R} \tag{1.1}$$

where Q is the flow rate of AH, IOP is the intraocular pressure, $p(x)$ is the pressure within the canal, R is the resistance to flow and x is the distance along the canal's length [12].

Although almost the whole flux of AH follows the pathway described above, a small quantity of AH enters the posterior cavity (on the order of a few nanoliters every hour), where it is diffused slowly inside the vitreous body.

1.4 Glaucoma

Glaucoma is an optic neuropathy characterized by damage to the optic nerve and visual field loss [5]. This degeneration results to be progressive and irreversible since glaucoma brings to the death of the retinal ganglion cell (RCG). Although the mechanism which leads to the ganglion cell injury is

not clear, researchers are focusing their attention to a defect in the blood supply to the optic nerve caused by high IOP.

One can distinguish between two types of glaucoma (see figure (1.4)):

1. *Primary glaucoma*: caused essentially by a defection in the circulating pathway of AH. The most important types of primary glaucoma are Primary open angle glaucoma (POAG), which is the most prevalent type of glaucoma, characterized by a an significant optic nerve damage associated with an open anterior chamber angle, and Primary closed angle glaucoma (PCAG), occurring in patients with obstruction of trabecular meshwork and glaucomatous optic neuropathy.

2. *Secondary glaucoma*: glaucomatous symptoms are caused by ocular or systemic disease such as *uveitis, ocular trauma* or *ocular neovascularization*.

Despite there may be different causes to glaucoma, the most important risk factor results to be an elevated intraocular pressure, which in chronic conditions can conduct to optic nerve damage. In fact, an increase of the IOP to about 30 mmHg is common during glaucoma and, under severe conditions, the intraocular pressure can even rise to 60 mmHg, leading to blindness within weeks. For this reason medical treatments of glaucoma include the use of drugs to reduce IOP by reducing the secretion of AH [19]. These types of medical care are not curative, but they can prevent the progression of the disease.

It is therefore evident how a deep knowledge of production and drainage of aqueous humor can bring significant benefits and influence future treatments of the disease.
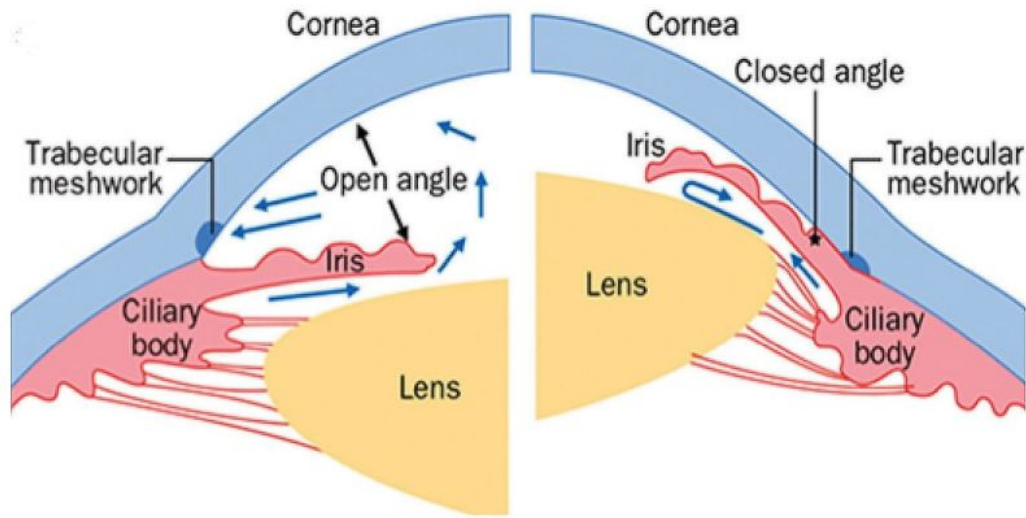
Figure 1.4: Two types of primary glaucoma: Open angle glaucoma (left), Closed angle glaucoma (right). Source: Wiggs JL, Pasquale LR. Genetics of glaucoma. Hum Mol Genet. 2017 Aug 1;26(R1):R21-R27. doi: 10.1093/hmg/ddx184. PMID: 28505344; PMCID: PMC6074793.

1.5 Compartmental model

The aim of this section is to provide a mathematical approach to the analysis of the production of aqueous humor. This is in line with the trend of recent years, during which the use of mathematical models to describe complex biophysical phenomena is becoming indispensable alongside experimental research.

A mathematical model offers a simplified view of the physical phenomenon, making a trade off between model complexity and biological accuracy. A well-constructed model can be a useful tool for clinical researchers, who are provided with a kind of virtual laboratory. Furthermore, the mathematical formalism can help to better understand complex biological phenomena, making a synthesis of all the physical processes that occur simultaneously.

1.5.1 A multiscale problem

The production of aqueous humor involves several physical processes at different spatial scales. At the highest scale, AH production occurs through the synergistic action of all the structures of the ciliary body. Having the possibility to shrink ourselves until we can walk among the zonules, we would see how the plasma present in the stroma is filtered passing through the ciliary epithelium. However, if we want to know how this filter works we should equip ourselves with a magnifying glass, approach the ciliary epithelium and observe its structures. At this point, we would observe how the different particles enter and leave the epithelial cells following a path that depends on the type of particle itself. At this level, which corresponds to the cellular level, we would observe a flow of particles, but we would not be able to observe the different mechanisms that take place on the membranes that cover the cells. Having decided that we want to know more, let's reduce ourselves further, until we reach the size of a molecule. Now we would observe special entrance doors on the cellular membrane, which only certain types of ions are allowed to pass through and thanks to which the cell communicates with the extracellular environment.

Therefore, to correctly describe all the mechanisms of our problem, we should be aware that it is necessary to describe physical phenomena that occur at different spatial scales. In the model presented in this thesis, this objective is pursued considering the cellular level and trying to take into account the membrane transporters through lumped models.

1.5.2 Derivation of a compartmental geometry

The focus of this thesis is on a portion of the ciliary body which includes stroma, ciliary epithelium and posterior chamber. Due to the extremely complicated morphology of the interested area, we introduced a simplified version of the geometry as a reference domain on which to apply the model equations.

To this purpose, the interested portion of the Ciliary Body is described by means of a compartmental model. It results that this idea fits very well in this context, because CB is naturally divided in compartments, separated by biological barriers.

In figure 1.5 a portion of the ciliary epithelium layer is shown, together with its compartmental counterpart. The domain is divides into 5 compartments: Stroma (S), pigmented epithelial cell (PE), non pigmented epithelial cell (NPE), paracellullar side (P), posterior chamber (PC). These compartments communicate through biological mechanisms illustrated in the following section.
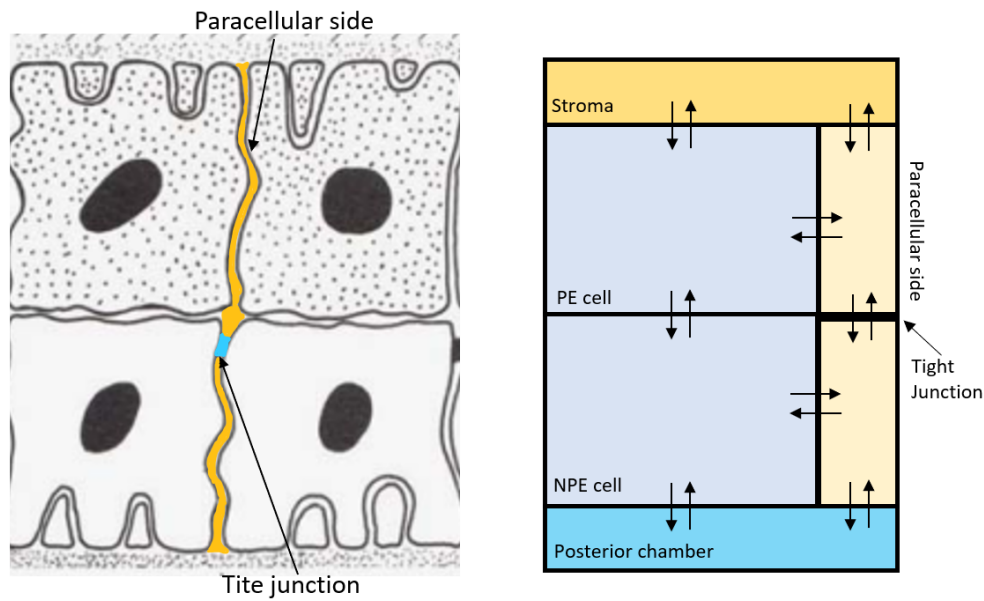
Figure 1.5: (left) Portion of the cilary epithelium layer. (right) Schematic compartmental description of the interested area

1.5.3 Communication between different compartments

PE - NPE commumication Intracellular fluids of pigmented and non-pigmented ciliary epithelial cells result to be strictly linked thanks to special conduits: the *gap junctions*. Gap junctions are specialized cell-cell junctions which form a mirror image of protein units (connexons) between apical membranes of cells. They directly connect the cytoplasms, allowing various molecules, ions and electrical impulses to directly pass through a regulated gate. For this reason,we assume that the two epithelial layers actually constitute a connected region, so that the electrical potential and intracellular ion concentrations are continuous across the separation surface [16].

Communication via channels and transporters   As mentioned above, the cytoplasm of the cells is in communication with the extracellular region thanks to special transmembrane proteins distributed along the cell membrane. These proteins act as gateways to permit the transport of specific substances across the membrane. In cellular biology, the characterization of the mechanisms that regulate the passage of substances through the cellular membrane is extremely important, since the physiology of distinct cells is related to their capacity to attract elements from the extracellular side.

Transport across the membrane can be classified as *passive transport* or *active transport*. Passive transport, or passive diffusion, occurs thanks to the so-called *transmembrane channels*, and is a spontaneous phenomenon (linked to a decrease in free energy) that depends on the concentration gradients across the membrane. In the context of the ciliary epithelium, two types of channels are particularly important: *ion channels*, which are responsible for the passive transport of charged ions (sodium, potassium, calcium, hydrogen, hydrogen carbonate), and the so-called *Aquaporins*, which are channels specialized to handle the movement of water through the hydrophobic interior of the cell membrane. Active transport occurs when a solute is moved against a concentration gradient. Since this process requires energy, the proteins involved in active transport consume metabolic energy, such as ATP.

Both active and passive transporters will be used to describe the flux of solutes between the intracellular compartments and the extracellular sides. A more detailed analysis of these concepts will be the subject of the next chapter.

Tight junctions   Tight junctions constitute the barrier to the passage of plasma proteins from the stroma of the ciliary process into the posterior

chamber. However, they allow the passage of small molecules and ions, so that we can define a membrane permeability P_α for each ion α, physically determined by claudins and occludins, which are the main components of the tight junctions.

The conductance of a tight junction depends lineraly on the ion permeabilities: given P_α and the concentrations c_α^M and c_α^N in the two compartments M and N separated by the barrier, the conductance to a charged solute α is [12]:

$$G_\alpha = \frac{P_\alpha z_\alpha^2 F^2 \bar{c}_\alpha}{RT} \tag{1.2}$$

where z_α is the chemical valence of the charged solute, R and T are the gas constant and temperature, respectively, whereas $\bar{c}_\alpha$ is a mean transmembrane concentration defined as:

$$\bar{c}_\alpha = \frac{c_\alpha^M - c_\alpha^N}{\ln c_\alpha^M - \ln c_\alpha^N} \tag{1.3}$$

The overall transepithelial conductance can be then calculated as:

$$G_{TJ} = \sum_\alpha G_\alpha = \frac{F^2}{RT} \sum_\alpha z_\alpha^2 P_\alpha \bar{c}_\alpha \tag{1.4}$$

Chapter 2

Transmembrane transport

Solutes and water can be transported across the ciliary epithelium following a transcellular pathway or through the paracellular side between the epithelial cells (figure 1.5). Laboratory experiments have demonstrated that, despite the significant paracellular contribution, the secretory pathway is largely transcellular, thus it is basically driven by transfer of net solute from stroma to AH passing through the ciliary epithelium. Secretion of $NaCl$ assumes a central role in this mechanism and, as a first approximation, the formation of the AH can be viewed as an energy dependent transfer of $NaCl$ which induces a transfer of water across the ciliary epithelium. Minor constituents present in the extracellular fluids (HCO_3^-, K^+, Ca^{2+}, H^+) are known to modulate secretion and act indirectly on Na^+ and Cl^- transfer.

The transcellular epithelial transfer is due to an ensamble of ion and water channels and other types of transmembrane proteins, such as co-transporters (symports) and counter-transporters (antiports).

In the following, the basic concepts of transmembrane transport will be discussed, then we will introduce the mathematical characterization of all the processes included for the description of the mechanisms occurring among

the compartments of figure 1.5.

2.1 Theoretical concepts

One of the most important characteristics of the lipid bilayer that composes the cell membrane is its *selective permeability*. In fact it constitutes a barrier for the transit of polar molecules, which pass through the membrane only thanks to special constituents, named membrane transporters. The main subdivision of transmembrane transport is:

- **Passive transport**. It occurs without expenditure of energy by the cell. One can distinguishes between *simple diffusion* (e.g. osmosis), and the passive transport dependent by transmembrane proteins. In particular, the two types of protein transporters are: *channel proteins*, which contain aqueous spaces for the transit of H_2O (aquaporins) or ions (ion channels), and *carrier proteins* which, combining with the ions to be transported, carry them through conformational modifications of the protein structure.

- **Active transport**. It is characterized by cellular energy expenditure and it occurs through transmembrane proteins. In particular, it is possible to further subdivide this type of transport by distinguishing between *primary* and *secondary* transport.

Figure 2.1 reports a schematic subdivision of the transport mechanisms.
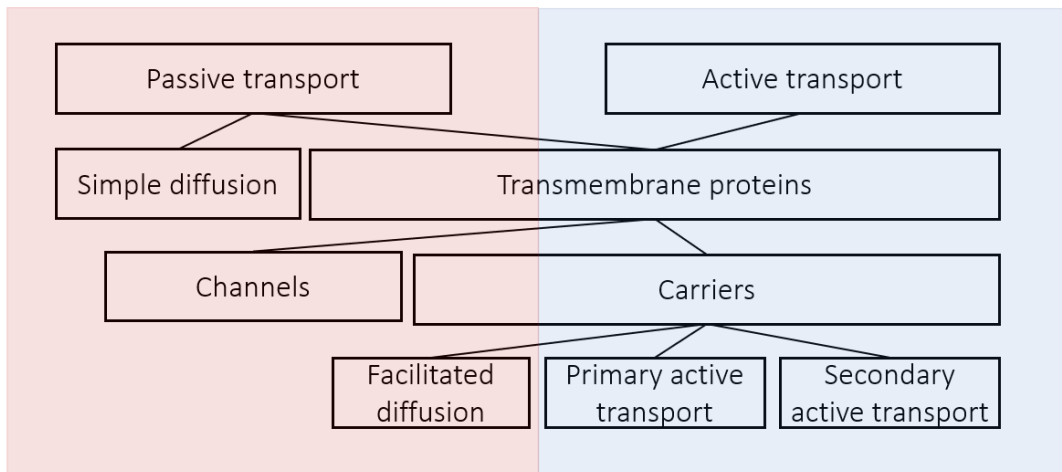
Figure 2.1: A block scheme of the transmembrane transport process

Diffusion through channels. The diffusion of H_2O and small ions occurs thanks to protein channels (aquaporins and ion channels). Some channels, named *passive channels*, are constantly open, allowing a continuous transit of H_2O or ions, while in others, named *gates*, the opening is regulated by a series of extracellular or intracellular signals. The forms of energy capable of regulating the opening of the gates can be of a chemical, electrical or mechanical nature. The *permeability* (P_α) of the membrane to a given ion α depends on the number of open channels allowing the transit of the ion α.

Facilitated diffusion: Uniports. Uniports are membrane proteins capable of carrying a single molecule. In this case the transport is bidirectional and occurs passively, according to the concentration gradient. Uniports, like other types of proteins, are characterized by *saturating transport*, meaning that the flow rate does not increase linearly to the gradient, but tends asymptotically to a maximum level.

Primary and secondary active transport. Active transport always takes place thanks to the presence of a transporter protein and involves the direct or indirect consumption of ATP by the cell. In this case ions move (all or at least in part) against an electrochemical concentration gradient.

1. *Primary active transport.* In this case the hydrolysis of the energy supplier is directly related to the transport of the solute. An example of primary transporter is the *ATP-asic pumps.* A pump is a protein that draws the necessary energy from the hydrolysis of ATP. The basolateral membrane of the non-pigmented cell has a large concentration of Sodium-Potassium ATPase pump which helps to create a negative resting membrane potential in the intracellular side and to limit the entry of Na^+ ions. The sodium concentration gradient generates a potential energy source that can be used with different purposes and it is often exploited by secondary active transporters.

2. *Secondary active transport.* In this case the hydrolysis is indirectly linked to the transport of solutes. An example of secondary transporters are the so-called *co-transporters.* These proteins transport two molecules at the same time: one against a gradient and the other in favor of the gradient. Two types of co-transporters are the *exchangers,* or antiporters, in which the molecules that move against the gradient and those that move along their gradient have opposite directions, and the *symporters,* in which the molecules have the same direction.

The ciliary epithelium expresses a wide range of ion channels and transporters responsible for facilitated diffusion and active transport. These mechanisms are distributed along the basolateral membrane of PE and NPE cells, inducing secretion of AH from the stroma to the posterior chamber (figure

2.2), but also reabsorption across the CE from the posterior chamber to the stroma.

2.1.1 Transmembrane secretion of AH

The transepithelial secretion pathway can be described into three main steps, through which the ciliary epithelium layer maintains a net flux of sodium:

1. **Uptake of Stromal NaCl**. Among all the transporters, at least three electroneutral mechanisms support uptake of NaCl from the stroma: the $Na^+ - K^+ - 2Cl^-$ *cotransporter*, the $Na^+ - H^+$ *antiport* and the $Cl^- - HCO_3^-$ *antiport*. The symport $Na^+ - K^+ - 2Cl^-$, which is considered the major mechanism for uptake of NaCl by both secretory and absorptive epithelia, is responsible for a thermodynamic driving force which favors net uptake of Na^+, K^+, and Cl^- from the stromal side into the PE. The two antiports are stimulated directly and indirectly by the action of the *Carbonic anhydrase II*, an enzyme which increases the turnover rates of the antiports by catalyzing the production of H^+ and HCO_3^- from CO_2 and H_2O.

2. **Transit of NaCl from PE to NPE**. The PE-NPE cell couplets can be viewed as the functional unit of the ciliary epithelium. In fact, as already mentioned, a massive presence of the PE-NPE gap junctions have been demonstrated through numerous experimental techniques [16]. These observations justify the fact that the transit of ions takes place undisturbed, thus we can consider the difference in concentration of ionic species across the two layers to be null.

3. **Extrusion of NaCl from NPE Cells to PC**. Finally, Na^+ ions are transported to the posterior chamber through the $Na^+ - K^+ - ATPase$

pump, which exploits the hydrolysis of ATP to ADP for the extrusion of three intracellular Na^+ ions in exchange for two extracellular K^+ ions. Moreover, the hydrolysis of ATP not only provides the secretion of Na^+ but also maintains the membrane potential necessary for the secretion of other ions. This mechanism is accompanied by the action of the Cl^- channels and the K^+ channels.

K^+ channels are fundamental at least for three functions: they provide a pathway for release of K^+ to the aqueous humor, maintain the intracellular potential more negative than the Cl^- equilibrium potential and provide a conduit for K^+ to act as a catalyst.
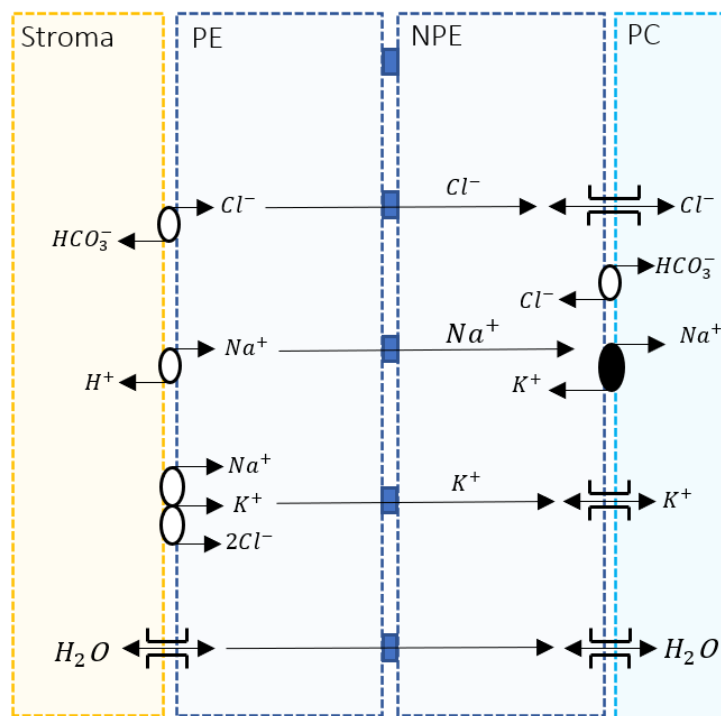
Figure 2.2: Secretion pathway

2.1.2 Transmembrane reabsorption of AH

In parallel to a flow of ions and water to the posterior chamber, one can identify a path that allows the translocation of fluid to the stromal compartment. On the basolateral surface of NPE cells, NaCl is reabsorbed by the action of two antiports, $Na^+ - H^+$ and $Cl^- - HCO_3^-$, and two symports, $Na^+ - K^+ - 2Cl^-$ and $Na^+ - Cl^-$ [6]. Once the reabsorbed fluid reaches the basolateral membrane of the PE cells it is extruded by the action of the $Na^+ - K^+$ pump, which are also present on the basolateral membrane of the pigmented epithelium, albeit in smaller quantities.
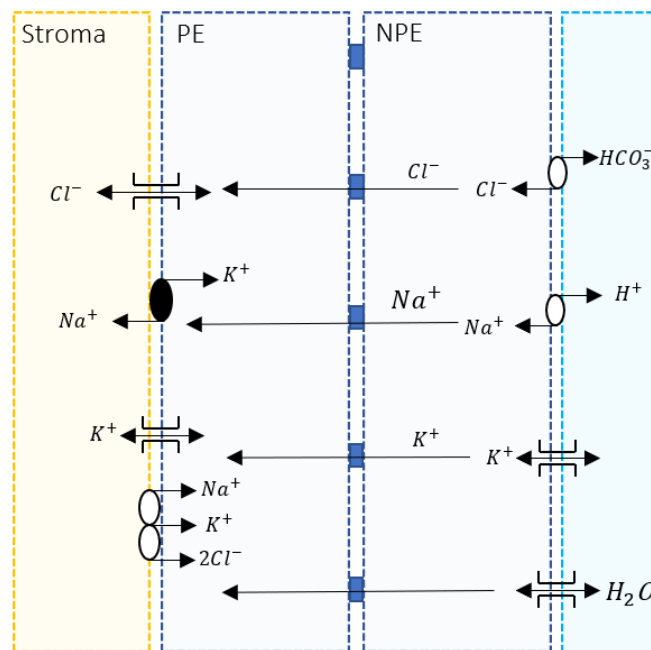
Figure 2.3: Reabsorption pathway

2.1.3 Aquaporins

Aquaporins are small water permeable channels whose contribution is crucial in the maintenance of body fluid homeostasis. Denoting M and N two

compartments which are in communication via aquaporins, the transport of water across aquaporins from M to N is driven by three forces: the osmotic pressure, which results to be predominant, the hydraulic pressure difference ($\Delta P := P^M - P^N$, where P^M and P^N are the values of hydraulic pressure in M and N respectively) and the oncotic pressure difference ($\Delta \Pi := \Pi^M - \Pi^N$, where Π^M and Π^N are the values of oncotic pressure in M and N respectively). The water flux is expressed by the following formula [12]:

$$J_{H_2O}^{AQP} = L_p^{AQP}(\Delta P - \Delta \Pi - RT \sum_\alpha \gamma_\alpha \Delta c_\alpha) \tag{2.1}$$

where L_p^{AQP} is the aquaporin permeability to water, γ is a solute activity coefficient, Δc_α is the difference of ion concentration across the surface between M and N, and the sum is over the ions present in the solution.

2.1.4 Acid-base balance

The ionization of a large number of components in the cytoplasm of the cells is determined by the intracellular pH value. For this reason, maintaining a stable pH is a vital task for the cell and is pursued by means of different mechanisms [12]. In particular, cells can control pH stabilization with the help of buffers, composed by a weak acid and its conjugate weak pair, such as the carbonic acid/bicarbonate pair (H_2CO_3/HCO_3^-) in the ciliary epithelium layer.

Since spontaneous diffusion across the membrane could lead to an imbalance in the concentration of acid molecules, the cell is equipped with so called *acid loaders* and *acid extruders*. An example of acid extruder present on the basolateral membranes of the CE layer is the Na^+/HCO_3^- cotransporter, while the HCO_3^-/Cl^- exchanger represents an example of acid loader.

2.2 Mathematical description of transmembrane transport

In this section we will introduce the mathematical description of the several transmembrane transporters that are included in the model of the basolateral membranes of the double epithelium layer.

Notice that we will consider from now on the AH as a homogeneous mixture [1] composed mainly by 5 ionic species, namely the Sodium cation Na^+, the Potassium cation K^+, the Hydrogen cation H^+, the Chlorine anion Cl^- and the Hydrogen carbonate anion HCO_3^-, while we will consider water as fluid solvent. For the computation of the ionic flux between extracellular and intracellular side we will consider as transmembrane mechanisms the following transporters:

1. the $Na^+/K^+ATPase$ pump, which is a primary active transporter;

2. the HCO_3^-/Cl^- anion exchanger which is a secondary active mechanism;

3. the Na^+/H^+ cation exchanger which is a secondary active mechanism;

4. the $Na^+/K^+/2Cl^-$ cotransporter which is a secondary active transporter;

5. the Na^+/HCO_3^- symport which is a secondary active transporter as well;

6. ionic channels for all the species, which are passive transporters.

The aim is the description of the net molar flux density J_α ($[mol\ m^{-2}s^{-1}]$) passing through a given membrane that separates two compartments. Since

27

we will adopt a one dimensional spatial description for each compartment of the model, the membrane can be viewed as a node that separates two regions. We will denote as M and N the regions adjacent to the considered node (see figure 2.4). Moreover, we will use the superscript M and N to denote the quantities on the M-side and on the N-side of the junction. In particular, c_α^i, $i = M, N$ denotes the molar concentration ([mM]) for the ion species α on the left and right side of the node, while ϕ^i, $i = M, N$ is the electric potential ([V]). Note that we are considering a lumped version model for a biological membrane, so that a jump in the electric potential $\phi^{MN} = \phi^M - \phi^N$ is perfectly admissible and it represents the so called *transmembrane potential*.
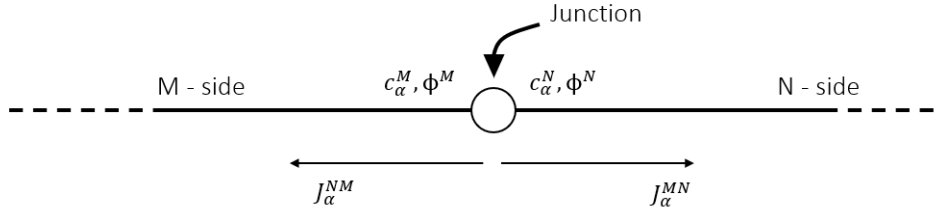
Figure 2.4: Junction separating two compartments M and N

In figure 2.4 J_α^{MN} ([$mol\ m^2 s^- 1$]) represents the net molar flux density that flows across the junction from M to N, namely, denoting by ζ the junction point, we have:

$$J_\alpha^{MN} = J_\alpha^M(\zeta)\mathrm{n}^M(\zeta) \tag{2.2}$$

where $\mathrm{n}^M(\zeta)$ is the normal unit vector at M-side at node ζ. Similarly, we have:

$$J_\alpha^{NM} = J_\alpha^N(\zeta)\mathrm{n}^N(\zeta) \tag{2.3}$$

2.2.1 $Na^+/K^+ATPase$ **pump**
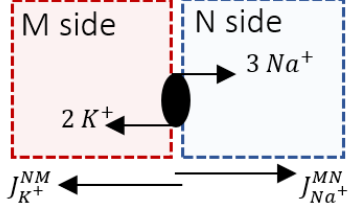
Figure 2.5: Na^+/K^+ pump

This active transporter exploits the energy retrieved from ATP hydrolysis. For each ATP molecule, three Na^+ ions are exported towards the extracellular region and two K^+ ions are imported in the cytoplasm.

The ionic flux across the $Na^+/K^+ATPase$ pump can be evaluated considering the binding of each ion to the enzyme E as an independent process [12]. Let us consider the first order, reversible reaction between one intracellular Na^+ ion and the enzime E:

$$Na^+ + E \longleftrightarrow NaE \tag{2.4}$$

Denoting as k^{on}_{NaE} and k^{off}_{NaE} the association and dissociation kinetic constants for the reaction (2.4), the rate of NaE formation is given by:

$$\frac{dc_{NaE}}{dt} = k^{on}_{NaE}c^M_{Na^+}c_E - k^{off}_{NaE}c_{NaE} = 0 \tag{2.5}$$

At steady state, one can neglect the temporal derivative, thus obtaining

$$\kappa^{on}_{NaE}c^M_{Na^+}\left(c^{tot}_E - c_{NaE}\right) = \kappa^{off}_{NaE}c_{NaE} \tag{2.6}$$

where we used the relation $c^{tot}_E = c_E + c_{NaE}$, c^{tot}_E being the total concentration of the enzyme E. Introducing the so called apparent dissociation constant $K^M_{Na^+} = k^{off}_{NaE}/k^{on}_{NaE}$, one can reformulate eq. (2.6) as:

$$c_{NaE} = \frac{c^M_{Na^+}}{c^M_{Na^+} + K^M_{Na^+}}c^{tot}_E \tag{2.7}$$

From (2.7) we can deduce that the probability p_{Na} of having one pump unit bound to one Na^+ ion is proportional $c_{Na^+}^M/(c_{Na^+}^M + K_{Na^+}^M)$. Similarly, the probability to p_K of having one pump unit bound to one K^+ ion is proportional to $c_{K^+}^N/(c_{K^+}^N + K_{K^+}^N)$.

Introducing the following relations:

$$K_{Na^+}^M = K_{M,Na^+}^{pump}(1 + \frac{c_{K^+}^M}{K_{M,K^+}^{pump}}) \tag{2.8}$$

$$K_{K^+}^N = K_{N,K^+}^{pump}(1 + \frac{c_{Na^+}^N}{K_{N,Na^+}^{pump}}) \tag{2.9}$$

the flux density across the pump J_{pump}^{MN} can be expressed as:

$$J_{pump}^{MN} = \gamma^{MN}[ATP]\left(\frac{c_{Na}^M}{\phi_{Na^+}}\right)^3 \left(\frac{c_K^N}{\phi_K^+}\right)^2 \tag{2.10}$$

where γ ($[ms^{-1}]$) is a membrane permeability and $[ATP]$ ($[mM]$) is the ATP molar concentration.

The functions $\phi_{Na^+}^M$ and $\phi_{K^+}^N$ take the form

$$\phi_{Na^+}(c_{Na^+}^M, c_{K^+}^M) = c_{Na^+}^M + K_{M,Na^+}^{pump}\left(1 + \frac{c_{K^+}^M}{K_{M,K^+}^{pump}}\right) \tag{2.11}$$

$$\phi_{K^+}(c_{Na^+}^N, c_{K^+}^N) = c_{K^+}^N + K_{N,K^+}^{pump}\left(1 + \frac{c_{Na^+}^N}{K_{N,Na^+}^{pump}}\right) \tag{2.12}$$

K_{N,Na^+}^{pump} and K_{M,K^+}^{pump} ($[mM]$) are called *inhibition constants*, while K_{M,Na^+}^{pump} and K_{N,K^+}^{pump} ($[mM]$) are called *Michaelis constants*.

For stoichiometric considerations, denoting the extracellular region as N-side, one has that the flux density across the pump is:

$$J_{Na^+}^{Na/K,MN} = J_{pump}^{MN} \tag{2.13}$$

$$J_{K^+}^{Na/K,NM} = \frac{2}{3}J_{pump}^{MN}. \tag{2.14}$$

2.2.2 HCO_3^-/Cl^- anion exchanger

This antiport works as an *acid loader* for the cell, importing Cl^- in the cytoplasm (M side) and extruding HCO_3^-.
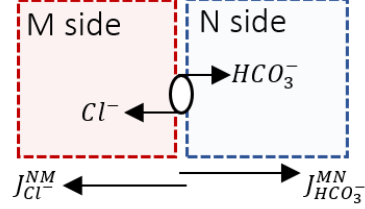
Figure 2.6: HCO_3^-/Cl^- exchanger

The mathematical description is the following

$$J_{exch,1}^{MN} = \kappa_{HCO_3^-/Cl^-} \frac{c_{Cl^-}^N \, c_{HCO_3^-}^M - c_{Cl^-}^M \, c_{HCO_3^-}^N}{\phi(c_{Cl^-}^M, c_{Cl^-}^N, c_{HCO_3^-}^M, c_{HCO_3^-}^N)} \qquad (2.15)$$

where the function ϕ takes the form $\phi = \tilde{\phi}^{MN} + \tilde{\phi}^{NM}$, with

$$\tilde{\phi}^{ij} = \left(1 + \frac{c_{Cl^-}^i}{K_{Cl^-}} + \frac{c_{HCO_3^-}^i}{K_{HCO_3^-}}\right)\left(1 + \frac{c_{Cl^-}^j}{K_{Cl^-}} + \frac{c_{HCO_3^-}^j}{K_{HCO_3^-}}\right) \qquad (2.16)$$

while $\kappa_{HCO_3^-/Cl^-}$ ($[m^4 mol^{-1} s^{-1}]$) can be described as

$$\kappa_{HCO_3^-/Cl^-} = \frac{G_{HCO_3^-/Cl^-}}{K_{Cl^-} K_{HCO_3^-}} \qquad (2.17)$$

where $G_{HCO_3^-/Cl^-}$ ($[mol \; m^{-2} s^{-1}]$), K_{Cl} and K_{HCO_3} ($[mM]$) are given constants.

Assuming the direction depicted in the figure, one obtains

$$J_{HCO_3^-}^{HCO_3/Cl,MN} = J_{exch,1}^{MN} \qquad (2.18)$$

$$J_{Cl^-}^{HCO_3/Cl,NM} = J_{exch,1}^{MN} \qquad (2.19)$$

2.2.3 Na^+/H^+ cation exchanger
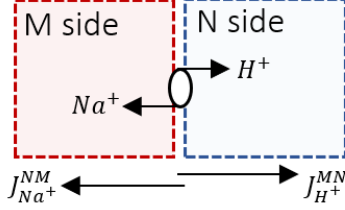
Figure 2.7: Na^+/H^+ exchanger

The aim of this antiport is to regulate the intracellular pH by expelling H^+ ions generated from metabolic processes and cellular respiration. Na^+ ions enter in the cytoplasm (M side) while H^+ ions are expelled against gradient.

Similarly to what we saw previously, its mathematical description is the following

$$J_{exch,2}^{MN} = \kappa_{Na^+/H^+} \frac{c_{H^+}^M \, c_{Na^+}^N - c_{H^+}^N \, c_{Na^+}^M}{\phi(c_{Na^+}^M, c_{Na^+}^N, c_{H^+}^M, c_{H^+}^N)} \tag{2.20}$$

where $\phi = \tilde{\phi}^{MN} + \tilde{\phi}^{NM}$ and in this case one has

$$\tilde{\phi}^{ij} = \left(1 + \frac{c_{Na^+}^i}{K_{Na^+}} + \frac{c_{H^+}^i}{K_{H^+}}\right)\left(1 + \frac{c_{Na^+}^j}{K_{Na^+}} + \frac{c_{H^+}^j}{K_{H^+}}\right) \tag{2.21}$$

moreover $\kappa_{HCO_3^-/Cl^-}$ can be described as

$$\kappa_{Na^+/H^+} = \frac{G_{Na^+/H^+}}{K_{Na^+} K_{H^+}} \tag{2.22}$$

where G_{Na^+/H^+} ($[mol \; m^{-2} s^{-1}]$), K_{Na^+} and K_{H^+} ($[mM]$) are given constants. Then, the molar flux densities are

$$J_{H+}^{MN} = J_{exch,2}^{MN} \tag{2.23}$$

$$J_{Na^+}^{NM} = J_{exch,2}^{MN} \tag{2.24}$$

2.2.4 $Na^+/K^+/2Cl^-$ **cotransporter**

It is an electroneutral transporter whose main activity is the control of cell volume. Na^+ ions enter according to gradient while K^+ ions and Cl^- ions enter against gradient.
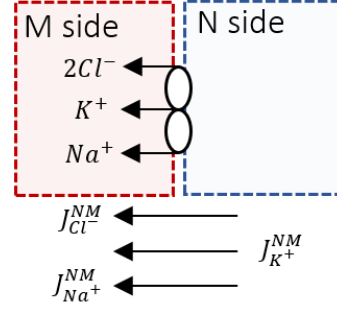
Figure 2.8: $Na^+/K^+/2Cl^-$ co-transporter

The mathematical description is the following

$$J_{co}^{NM} = J_{co,max}\left[\phi(c_{Na+}^N, c_{K+}^N, c_{Cl-}^N) - \phi(c_{Na+}^M, c_{K+}^M, c_{Cl-}^M)\right] \qquad (2.25)$$

where $J_{co,max}$ represents the maximum molar flux density that can pass through the transporter at steady state and the function ϕ takes the following form

$$\phi(x,y,z) = \left(\frac{x}{x + K_{Na+}^{co}}\right)\left(\frac{y}{y + K_{K+}^{co}}\right)\left(\frac{z}{z + K_{Cl-,1}^{co}}\right)\left(\frac{z}{z + K_{Cl-,2}^{co}}\right) \qquad (2.26)$$

where K_{Na+}^{co}, K_{K+}^{co}, $K_{Cl-,1}^{co}$ and $K_{Cl-,2}^{co}$ are suitable constants.

The resultant molar flux densities are

$$J_{Na+}^{NM} = \frac{1}{2}J_{co} \qquad (2.27)$$

$$J_{K+}^{NM} = \frac{1}{2}J_{co} \qquad (2.28)$$

$$J_{Cl-}^{NM} = J_{co} \qquad (2.29)$$

2.2.5 Na^+/HCO_3^- symport
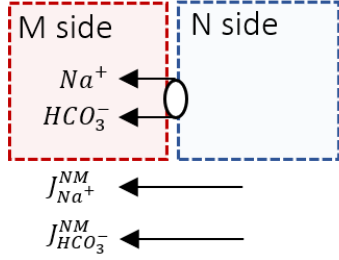
This symport shows two essential functions: import of sodium and import of bicarbonate in variable proportions. The result is an increase of the intracellular pH.

Figure 2.9: Na^+/HCO_3^- symport

The mathematical description of the symport is

$$J_{symp}^{NM} = \kappa_{Na^+/HCO_3^-} \frac{c_{HCO_3^-}^N c_{Na^+}^N - c_{HCO_3^-}^M c_{Na^+}^M}{\phi(c_{Na^+}^M, c_{Na^+}^N, c_{HCO_3^-}^M, c_{HCO_3^-}^N)} \tag{2.30}$$

where κ_{Na^+/HCO_3^-} has the following form

$$\kappa_{Na^+/HCO_3^-} = \frac{G_{Na^+/HCO_3^-}}{K_{c,Na^+} K_{c,HCO_3^-}} \tag{2.31}$$

while ϕ can be written as $\phi = \tilde{\phi}^{MN} + \tilde{\phi}^{NM}$, where

$$\tilde{\phi}^{ij} = \left(1 + R_{lk} \frac{c_{Na^+}^i c_{HCO_3^-}^i}{K_{c,Na^+} K_{c,HCO_3^-}}\right) \left(1 + \frac{c_{Na^+}^j}{K_{c,Na^+}} + \frac{c_{Na^+}^j c_{HCO_3^-}^j}{K_{c,Na^+} K_{c,HCO_3^-}}\right) \tag{2.32}$$

K_{c,Na^+}, K_{c,Na^+}, R_{lk} and G_{Na^+/HCO_3^-} being suitable parameters.
Finally, the molar flux densities are

$$J_{Na^+}^{NM} = J_{HCO_3^-}^{NM} = J_{symp}^{NM} \tag{2.33}$$

2.2.6 Ion channels

For ion channels we use the Goldman-Hodgkin-Katz model [1]:

$$J_\alpha^{MN} = P_\alpha[c_\alpha^M Be(-\eta_\alpha^{MN}) - c_\alpha^N Be(\eta_\alpha^{MN})] \tag{2.34}$$

where P_α is the permeability of the membrane to the specific ion α, $Be(x) = e^x/(x-1)$ is the inverse of the Bernoulli function and

$$\eta_\alpha^{MN} = \frac{\boldsymbol{v}_f^{MN}}{P_\alpha} + z_\alpha \frac{\psi^M - \psi^N}{V_{th}} \tag{2.35}$$

where $V_{th} = K_B T/q$ is the so called thermal potential and v_f^{MN} is the fluid velocity throughout the channel.

Note that if one wants to obtain the current densities $J_\alpha^{el,MN}$ ($[Cm^{-2}s^{-1}]$), the following relation should be applied

$$J_\alpha^{el,MN} = F z_\alpha J_\alpha^{MN} \tag{2.36}$$

where $F = 96.485,336 \ Cmol^{-1}$ is the Faraday constant.

In Table 2.1 the values of the coefficients that appeared in this section are reported.

Figure 2.10 represents the schematic distribution of the transporters along the basolateral membranes of the PE-NPE cells. As previously underlined, transporters are not evenly distributed, as each of them plays a different role in the transmembrane transport of ions.
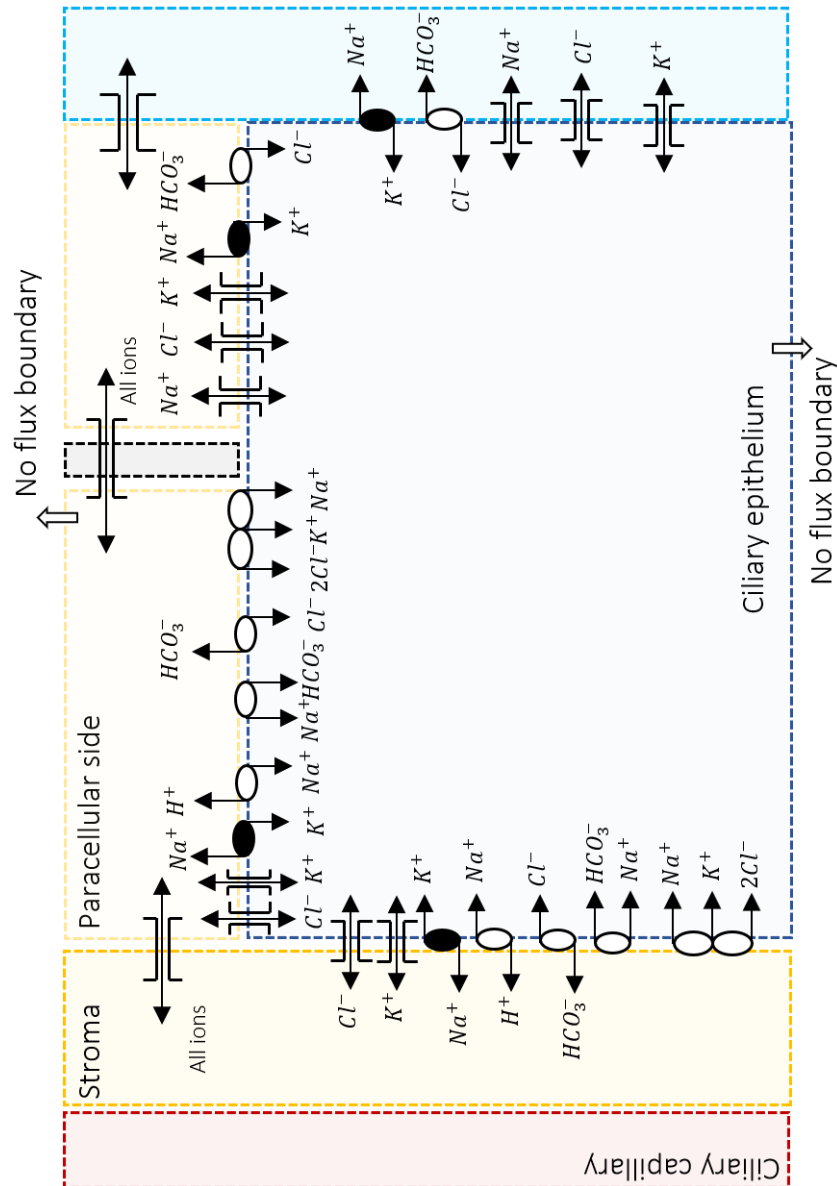
Figure 2.10: A schematic representation of transmembrane mechanisms in the ciliary epithelium.

Coefficient	Value	Unit	Transporter
K_{M,Na^+}^{pump}	1.3	mM	$Na^+/K^+ATPase$
K_{N,K^+}^{pump}	0.14	mM	$Na^+/K^+ATPase$
K_{N,Na^+}^{pump}	12	mM	$Na^+/K^+ATPase$
K_{M,K^+}^{pump}	32	mM	$Na^+/K^+ATPase$
K_{Cl^-}	10	mM	HCO_3^-/Cl^-
$K_{HCO_3^-}$	1	mM	HCO_3^-/Cl^-
$G_{HCO_3^-/Cl^-}$	$1.5 \cdot 10^{-3}$	mol cm^{2}s^{-1}	HCO_3^-/Cl^-
K_{H^+}	$5 \cdot 10^{-4}$	mM	Na^+/H^+
K_{Na^+}	100	mM	Na^+/H^+
G_{Na^+/H^+}	$3 \cdot 10^{-3}$	mol cm^{2}s^{-1}	Na^+/H^+
$K_{Na^+}^{co}$	105	mM	$Na^+/K^+/2Cl^-$
$K_{K^+}^{co}$	1.22	mM	$Na^+/K^+/2Cl^-$
$K_{Cl^-,1}^{co}$	103	mM	$Na^+/K^+/2Cl^-$
$K_{Cl^-,2}^{co}$	23.9	mM	$Na^+/K^+/2Cl^-$
K_{c,Na^+}	500	mM	Na^+/HCO_3^-
K_{c,HCO_3^-}	30	mM	Na^+/HCO_3^-
G_{Na^+/HCO_3^-}	$1.5 \cdot 10^{-3}$	mol cm^{2}s^{-1}	Na^+/HCO_3^-
R_{lk}	100	-	Na^+/HCO_3^-

Table 2.1: Values of the coefficients used in the numerical simulations.

Chapter 3

The mathematical model of ion and fluid transport

This chapter is devoted to the derivation of the *Velocity extended Poisson-Nernst-Planck* (VE-PNP) system, for the description of electrodiffusion phenomena involved in the AH secretion.

3.1 Velocity Extended PNP model

The VE-PNP model is widely used in biophysical applications for the description of ion electrodynamics coupled with fluid-dynamics mechanisms (see [1]). It results to be a continuum-based model composed by:

1. the **Poisson equation**, which takes into account the electric field generated by moving and fixed charged ions;

2. the **Nernst-Planck equation**, which describes the conservation of mass and the balance of momentum for each ion species;

3. the **Navier-Stokes equations**, which describe the conservation of

mass and the balance of momentum for the fluid.

In the following, we carry out the derivation of the equations starting from the integral form for the balance of mass charge and momentum. We consider a homogeneous mixture composed by the fluid solvent and M_{ion} ion species, which means that the mixing between ions and fluid occurs at the molecular level. Our description is based on the treatment made in [1].

3.1.1 Balance laws in local form

Let us consider a scalar quantity $u = u(\boldsymbol{x}, t)$ in the Eulerian framework. The general balance law of u in a material volume $\mathcal{V}_t \subseteq \Omega_t$ of a moving material domain Ω_t takes the form

$$\frac{d}{dt} \int_{\mathcal{V}_t} u(\boldsymbol{x}, t) d\Omega = \int_{\partial \mathcal{V}_t} (\boldsymbol{\gamma} \cdot \boldsymbol{n})(\boldsymbol{x}, t) d\sigma + \int_{\mathcal{V}_t} \beta d\Omega \qquad (3.1)$$

where $\boldsymbol{n}(\boldsymbol{x}, t)$ is the outward unit normal vector at the point $\boldsymbol{x}$ on the boundary $\partial \mathcal{V}_t$. $\boldsymbol{\gamma}$ is a vector field which describes the dynamics of $\boldsymbol{u}$ through the boundary $\partial \mathcal{V}_t$, while β, also called net production rate, acts as a source or sink in $\mathcal{V}_t$.

In a similar way one can describe the balance law for a vector-valued physical quantity. Given the vector field $\boldsymbol{u} = \boldsymbol{u}(\boldsymbol{x}, t)$, the balance law of $\boldsymbol{u}$ in Ω_t takes the form

$$\frac{d}{dt} \int_{\mathcal{V}_t} \boldsymbol{u}(\boldsymbol{x}, t) d\Omega = \int_{\partial \mathcal{V}_t} (\boldsymbol{\Sigma} \boldsymbol{n})(\boldsymbol{x}, t) d\sigma + \int_{\mathcal{V}_t} \boldsymbol{\beta}(\boldsymbol{x}, t) d\Omega \qquad (3.2)$$

where the second order stress tensor $\boldsymbol{\Sigma}$ and the vector field $\boldsymbol{\beta}$, as in the scalar case, model the dynamics of $\boldsymbol{u}$.

Starting from a balance law in integral form, one can derive the local form by means of the transport theorem (A.1), to move the time derivative inside the corresponding volume integrals, and the divergence theorem (A.2), to retrieve a volume integral from the first term on the right hand side.

In a general framework of a moving material domain, applying the transport theorem to the scalar quantity u one obtains

$$\frac{d}{dt}\int_{\mathcal{V}_t}u(\boldsymbol{x},t)d\Omega = \int_{\mathcal{V}_t}\frac{\partial u}{\partial t}(\boldsymbol{x},t)d\Omega + \int_{\partial\mathcal{V}_t}(u\boldsymbol{v}\cdot\boldsymbol{n})(\boldsymbol{x},t)d\sigma \qquad (3.3)$$

where $\boldsymbol{v}(\boldsymbol{x},t)$ is the vector field describing the velocity of the medium at each point $\boldsymbol{x}\in\partial\mathcal{V}_t$. Applying the divergence theorem to the second term on the right hand side we get

$$\frac{d}{dt}\int_{\mathcal{V}_t}u(\boldsymbol{x},t)d\Omega = \int_{\mathcal{V}_t}\left(\frac{\partial u}{\partial t}(\boldsymbol{x},t) + \nabla_{\boldsymbol{x}}\cdot(u\boldsymbol{v})(\boldsymbol{x},t)\right)d\Omega \qquad (3.4)$$

The quantity appearing as integrand in the right hand side is called *material derivative* of u

$$\frac{Du}{Dt}(\boldsymbol{u},t) := \frac{\partial u}{\partial t}(\boldsymbol{x},t) + (\boldsymbol{v}\cdot\nabla_{\boldsymbol{x}})u(\boldsymbol{x},t) \qquad (3.5)$$

Finally, applying the divergence theorem in (3.1) and considering that the integral form should be valid for any material volume $\mathcal{V}_t\subseteq\Omega_t$, the balance law in a local form for the scalar quantity u takes the form

$$\frac{Du}{Dt} = \nabla_{\boldsymbol{x}}\cdot\boldsymbol{\gamma}(\boldsymbol{x},t) + \beta(\boldsymbol{x},t), \qquad \forall x\in\Omega_t, \quad \forall t\in(0,T) \qquad (3.6)$$

Balance of mass and electric charge In order to retrieve a balance for mass and electric charge, one should apply (3.6) to the mass density field $\rho(\boldsymbol{x},t)$ and the charge density field $\zeta(\boldsymbol{x},t)$ respectively , obtaining

$$\frac{\partial\rho}{\partial t}(\boldsymbol{x},t) + \nabla_{\boldsymbol{x}}\cdot(\rho\boldsymbol{v})(\boldsymbol{x},t) = \beta(\boldsymbol{x},t), \qquad \forall\boldsymbol{x}\in\Omega_t, \quad \forall t\in(0,T) \qquad (3.7)$$

$$\frac{\partial \zeta}{\partial t}(\boldsymbol{x}, t) + \nabla_{\boldsymbol{x}} \cdot (\zeta \boldsymbol{v})(\boldsymbol{x}, t) = \pi(\boldsymbol{x}, t) \qquad \forall \boldsymbol{x} \in \Omega_t, \quad \forall t \in (0, T) \qquad (3.8)$$

where $\boldsymbol{\gamma}(\boldsymbol{x}, t)$ has been considered null since the boundary of Ω_t moves with the mass (and the charge as well) contained in it, thus implying $\boldsymbol{\gamma} = \boldsymbol{0}$ for $u(\boldsymbol{x}, t) = \rho(\boldsymbol{x}, t)$ and $u(\boldsymbol{x}, t) = \zeta(\boldsymbol{x}, t)$.

In the case when $\beta = 0$ and $\pi = 0$, the balance equations of mass and charge reduce to the following conservation laws:

$$\frac{\partial \rho}{\partial t}(\boldsymbol{x}, t) + \nabla_{\boldsymbol{x}} \cdot (\rho \boldsymbol{v})(\boldsymbol{x}, t) = 0, \qquad \forall \boldsymbol{x} \in \Omega_t, \quad \forall t \in (0, T) \qquad (3.9)$$

$$\frac{\partial \zeta}{\partial t}(\boldsymbol{x}, t) + \nabla_{\boldsymbol{x}} \cdot (\zeta \boldsymbol{v})(\boldsymbol{x}, t) = 0, \qquad \forall \boldsymbol{x} \in \Omega_t, \quad \forall t \in (0, T) \qquad (3.10)$$

Moreover, if one assumes ρ to be constant in time and space, (3.7) reduces to the incompressibility constraint on the velocity, namely

$$\nabla_{\boldsymbol{x}} \cdot \boldsymbol{v}(\boldsymbol{x}, t) = 0 \qquad \forall \boldsymbol{x} \in \Omega_t, \quad \forall t \in (0, T) \qquad (3.11)$$

It is worth to notice that one can link the mass density ρ_α of the ion species α to the number density function $n_\alpha(\boldsymbol{x}, t)$ ($[m^{-3}]$), which represents the averaged number of ions of type α per unit volume contained in the infinitesimal volume $d\Omega_t$ located at $\boldsymbol{x}$ at time t, through the following relation

$$\rho_\alpha(\boldsymbol{x}, t) := m_\alpha n_\alpha(\boldsymbol{x}, t), \qquad \boldsymbol{x} \in \Omega_t, \quad t \in (0, T) \qquad (3.12)$$

where m_α ($[Kg]$) is a positive constant representing the mass of the ion α. Equation (3.12) connects a kinetic description of the phenomena to the continuum approach and it allows us to identify the two balance laws (3.7) and (3.8), since the electric charge density for the ion α can be defined as

$$\zeta_\alpha(\boldsymbol{x}, t) := q z_\alpha n_\alpha(\boldsymbol{x}, t), \qquad \boldsymbol{x} \in \Omega_t, \quad t \in (0, T) \qquad (3.13)$$

and thus (3.8) is obtained multiplying (3.7) by the factor $q z_\alpha / m_\alpha$.

Balance of momentum Applying the Reynold's theorem (A.3) to each component of (3.2) with $\rho\eta = \rho v_k$, $k = 1, 2, 3$, one obtains the following local balance law in vectorial form for the linear momentum

$$\rho\frac{\partial \boldsymbol{v}}{\partial t} + \rho(\boldsymbol{v} \cdot \nabla_{\boldsymbol{x}})\boldsymbol{v} + \beta\boldsymbol{v} = \nabla_{\boldsymbol{x}} \cdot \boldsymbol{T} + \boldsymbol{b} \qquad (3.14)$$

where the second order tensor $\boldsymbol{T}$ is the Cauchy stress tensor and the vector field $\boldsymbol{b}(\boldsymbol{x}, t)$ is the resultant of external body forces per unit volume.

3.1.2 Ion charged fluid

If we assume to work with an isothermal mixture, the Velocity extended PNP model for an homogeneous multicomponent mixture can be derived considering the balance law for mass, electric charge and momentum. For this reason, we will apply here the general concepts illustrated above, considering first the balance equations for each α ion, with $\alpha = 1, ..., M_{ion}$, and then dealing with the equations for the fluid, denoted with the subscript f.

Ion species For each ion species α, the balance laws for mass and linear momentum, valid for $\boldsymbol{x} \in \Omega_t$ and $t \in (0, T)$, can be written as

$$m_\alpha\frac{\partial n_\alpha}{\partial t} + \nabla_{\boldsymbol{x}} \cdot (\rho_\alpha\boldsymbol{v}_\alpha) = \beta_\alpha \qquad (3.15)$$

$$m_\alpha n_\alpha\frac{\partial \boldsymbol{v}_\alpha}{\partial t} + m_\alpha n_\alpha(\boldsymbol{v}_\alpha \cdot \nabla_{\boldsymbol{x}})\boldsymbol{v}_\alpha + \beta_\alpha\boldsymbol{v}_\alpha = \nabla \cdot \boldsymbol{T}_\alpha + \boldsymbol{b}_\alpha \qquad (3.16)$$

The net production rate β_α is strongly related to the specific application. In the study of biological systems, such as protein channels, one can safely neglect the effects of generation/recombination, and thus set $\beta_\alpha = 0$ for each ion $\alpha = 1, .., M_{ion}$. However, in an intracellular environment, cellular activity is linked to internal chemical reactions, which therefore may contribute with a significant generation/recombination rate to the mass balance of the ionic

species.

The stress tensor $\boldsymbol{T}_\alpha$ can be described using the following constitutive relation [1]

$$\boldsymbol{T}_\alpha = -p_\alpha \boldsymbol{I} + \lambda_\alpha (\nabla_{\boldsymbol{x}} \cdot \boldsymbol{v}_\alpha)\boldsymbol{I} + 2\mu_\alpha \boldsymbol{D}(v_\alpha) \tag{3.17}$$

where p_α is the hydrostatic pressure exerted by ions of the same species, λ_α is the ion bulk modulus, μ_α is the ion dynamic viscosity and $\boldsymbol{D}$ is the symmetric part of $\nabla_{\boldsymbol{x}}\boldsymbol{v}$. The force density $\boldsymbol{b}_\alpha$ can be considered as the sum of two contributions [1]

$$\boldsymbol{b}_\alpha = \boldsymbol{m}_\alpha + \boldsymbol{f}_\alpha \tag{3.18}$$

The contribution $\boldsymbol{m}_\alpha$ takes into account the effect of viscous drag forces on the ions of species α exerted by other components of the mixture. Introducing the viscous drag coefficients $c_{\alpha\gamma}$ $(c_{\alpha\gamma} = c_{\gamma\alpha})$, $\boldsymbol{m}_\alpha$ assumes the following form:

$$\boldsymbol{m}_\alpha = -\sum_{\gamma=1,\gamma\neq\alpha}^{M_{ion}} c_{\alpha\gamma}(\boldsymbol{v}_\alpha - \boldsymbol{v}_\gamma) - c_{\alpha f}(\boldsymbol{v}_\alpha - \boldsymbol{v}_f) \tag{3.19}$$

The contribution $\boldsymbol{f}_\alpha$ takes into account gravitational and Lorentz forces:

$$\boldsymbol{f}_\alpha = \rho_\alpha \boldsymbol{g} + qz_\alpha n_\alpha(\boldsymbol{E} + \boldsymbol{v}_\alpha \times \boldsymbol{B}) \tag{3.20}$$

Fluid solvent For the fluid component one has, for $\boldsymbol{x} \in \Omega_t$ and $t \in (0, T)$,

$$\frac{\partial \rho_f}{\partial t} + \nabla_{\boldsymbol{x}} \cdot (\rho_f \boldsymbol{v}_f) = \beta_f \tag{3.21}$$

$$\rho_f \frac{\partial \boldsymbol{v}_f}{\partial t} + \rho_f(\boldsymbol{v}_f \cdot \nabla_{\boldsymbol{x}})\boldsymbol{v}_f + \beta_f \boldsymbol{v}_f = \nabla_{\boldsymbol{x}} \cdot \boldsymbol{T}_f + \boldsymbol{b}_f \tag{3.22}$$

where the description of β_f, $\boldsymbol{T}_f$ and $\boldsymbol{b}_f$ is similar to that performed in the case of ion species. If the fluid is water, as in the case of AH production, one can simplify (3.21) considering the incompressibility constraint, thus writing

$$\nabla_{\boldsymbol{x}} \cdot \boldsymbol{v}_f = 0 \tag{3.23}$$

Moreover, the stress tensor $\boldsymbol{T}_f$ and the force density $\boldsymbol{b}_f$ can be written in the form

$$\boldsymbol{T}_f = -p_f \boldsymbol{I} + 2\mu_f \boldsymbol{D}(\boldsymbol{v}_f) \tag{3.24}$$

$$\boldsymbol{b}_f = \rho_f \boldsymbol{g} - \sum_{\alpha=1}^{M_{ion}} c_{f\alpha}(\boldsymbol{v}_f - \boldsymbol{v}_\alpha) \tag{3.25}$$

Electromagnetic field   To solve the electromagnetic field generated by the charged ions, it is necessary to introduce the Maxwell equations:

$$\nabla_{\boldsymbol{x}} \times \boldsymbol{E} = -\frac{\partial \boldsymbol{B}}{\partial t} \tag{3.26}$$

$$\nabla_{\boldsymbol{x}} \times \boldsymbol{H} = \boldsymbol{J} + \frac{\partial \boldsymbol{D}}{\partial t} \tag{3.27}$$

$$\nabla_{\boldsymbol{x}} \cdot \boldsymbol{D} = \rho^{el} \tag{3.28}$$

$$\nabla_{\boldsymbol{x}} \cdot \boldsymbol{B} = 0 \tag{3.29}$$

where

$$\rho^{el}(\boldsymbol{x}, t) = \sum_{\alpha=1}^{M_{ion}} \zeta_\alpha(\boldsymbol{x}, t) + \rho^{fixed}(\boldsymbol{x}, t) \tag{3.30}$$

$$\boldsymbol{J}(\boldsymbol{x}, t) = \sum_{\alpha=1}^{M_{ion}} q z_\alpha n_\alpha(\boldsymbol{x}, t) \boldsymbol{v}_\alpha(\boldsymbol{x}, t) \tag{3.31}$$

ζ_α being the electric charge density of the ion species α and ρ^{fixed} being the charge density of fixed ions and/or charged immobile proteins.

Moreover, to complete the system, one can consider the following constitutive relationships

$$\boldsymbol{D} = \varepsilon_m \boldsymbol{E}, \qquad \boldsymbol{B} = \mu_m \boldsymbol{H} \tag{3.32}$$

where ε_m is the dielectric permittivity of the mixture and μ_m is the magnetic permittivity of the mixture.

3.1.3 Derivation of the VE-PNP model

In order to derive the VE-PNP from equations (3.15), (3.16), (3.21), (3.22), coupled with the Maxwell system, we introduce the following assumptions:

1. Bulk modulus coefficients are negligible for each ion species, thus $\lambda_\alpha = 0, \quad \forall \alpha = 1, ..., M_{ion}$;

2. Dynamic viscosity coefficients are negligible for each ion species, thus $\mu_\alpha = 0, \quad \forall \alpha = 1, ..., M_{ion}$;

3. Viscous drag coefficients among ion components are negligible, thus $c_{\alpha\gamma} = 0, \quad \forall \alpha, \gamma = 1, ..., M_{ion}$;

4. Characterization of viscous drag coefficients between fluid and ion species using Stokes' drag theory

$$c_{\alpha f} = 6\pi \mu_f R_{h,\alpha} n_\alpha \tag{3.33}$$

   where

$$R_{h,\alpha} = \frac{K_B T}{6\pi_\alpha} \tag{3.34}$$

   is the hydrodynamic radius ($[m]$) of the ion species α. D_α ($[m^2 s^{-1}]$) is the molecular diffusion coefficient of the species α in the fluid and T is the temperature of the mixture;

5. Einstein's relation holds, thus

$$D_\alpha = \frac{K_B T}{q|z_\alpha|} \mu_\alpha^{el} \tag{3.35}$$

   where μ^{el} is the electrical mobility ($[m^2 V^{-1} s^{-1}]$) of the ion species α;

6. Inertial terms are negligible in (3.15) and (3.21), thus

$$\frac{D\boldsymbol{v}_f}{Dt} = \boldsymbol{0}, \quad \frac{D\boldsymbol{v}_\alpha}{Dt} = \boldsymbol{0}, \forall i = 1, ..., M_{ion} \tag{3.36}$$

46

7. The effects of the gravitational field are negligible;

8. The contribution of the magnetic field $\boldsymbol{H}$ is small in comparison with that of the electric field. Moreover, the temporal variation of $\boldsymbol{B}$ is negligible in comparison with the spatial variation of $\boldsymbol{E}$.

Under the assumptions 1.-8., we obtain the following system of equations:

$$\frac{\partial n_\alpha}{\partial t} + \nabla_{\boldsymbol{x}} \cdot \boldsymbol{J}_\alpha = \beta_\alpha \qquad (3.37)$$

$$\boldsymbol{J}_\alpha = n_\alpha \boldsymbol{v}_f + \mu_\alpha^{el} \frac{z_\alpha}{|z_\alpha|} n_\alpha \boldsymbol{E} - D_\alpha \nabla_{\boldsymbol{x}} n_\alpha \qquad (3.38)$$

$$\nabla_{\boldsymbol{x}} \cdot \boldsymbol{v}_f = 0 \qquad (3.39)$$

$$-2\mu_f \nabla_{\boldsymbol{x}} \cdot \boldsymbol{D}(\boldsymbol{v}_f) + \nabla_{\boldsymbol{x}} p_f = -\sum_{\alpha=1}^{M_{ion}} K_B T \nabla_{\boldsymbol{x}} n_\alpha + \sum_{\alpha=1}^{M_{ion}} q z_\alpha n_\alpha \boldsymbol{E} \qquad (3.40)$$

$$\varepsilon_m \nabla_{\boldsymbol{x}} \cdot \boldsymbol{E} = q \sum_{\alpha=1}^{M_{ion}} z_\alpha n_\alpha \qquad (3.41)$$

$$\boldsymbol{E} = -\nabla_{\boldsymbol{x}} \psi \qquad (3.42)$$

where in (3.42) ψ represents the electrical potential. The model is composed by the *Nernst-Planck equations*, which describe conservation of mass and balance of momentum for the ion component, the *Stokes equations*, which describe the fluid dynamics, and the *Poisson equation*, which describes the electric field $\boldsymbol{E}$ in the system.

In (3.38) the flux density $\boldsymbol{J}_\alpha$ ($[m^{-2}s^{-1}]$) results to be the sum of three contributions

$$\boldsymbol{J}_\alpha = \boldsymbol{J}_{\alpha,f} + \boldsymbol{J}_{\alpha,\boldsymbol{E}} + \boldsymbol{J}_{\alpha,diff} \qquad (3.43)$$

where

1. $\boldsymbol{J}_{\alpha,f} = n_\alpha \boldsymbol{v}_f$ is the contribution due to the convective effect of the velocity of the fluid solvent;

2. $\boldsymbol{J}_{\alpha,\boldsymbol{E}} = \mu_{\alpha}^{el} \frac{z_{\alpha}}{|z_{\alpha}|} n_{\alpha} \boldsymbol{E}$ is the contribution due to the convective effect of the electric field on ions;

3. $\boldsymbol{J}_{\alpha,diff} = -D_{\alpha} \nabla_{\boldsymbol{x}} n_{\alpha}$ is the contribution due to the diffusion process, described through Fick's law.

It is worth to remember that one can associate with the flux density $\boldsymbol{J}_{\alpha}$ an ion current density $\boldsymbol{J}_{\alpha}^{el}$ ($[Am^{-2}]$), namely

$$\boldsymbol{J}_{\alpha}^{el} = qz_{\alpha}\boldsymbol{J}_{\alpha} \tag{3.44}$$

Chapter 4

The model for AH secretion

In this chapter we apply the VE-PNP model to the description of ion elec-
trodiffusion across the ciliary epithelium. With this aim, we first introduce
a one-dimensional network based on the compartmental model described in
chapter 1. Then, we derive a PNP differential system to describe ion motion
along the network.

4.1   Description of the simplified domain

In this section we will describe the geometry upon which to apply the final
system that we will derive starting from the VE-PNP equations.
With this aim, we will consider a portion of Ciliary Body which includes
the double Ciliary epithelial layer, the Stroma, the paracellular side and the
Posterior chamber, as represented in figure 4.1.

The process of aqueous humor secretion starts with the ultrafiltration of
blood through the vascular endothelium layer that covers the vessels. The
filtrated plasma flows from the Stroma to the Posterior chamber passing
through the double epithelial layer. In particular, it can be transported ac-

tively through the cytoplasm of the cells or it can flow along the paracellular side, where it will be eventually filtrated by the tight junctions.
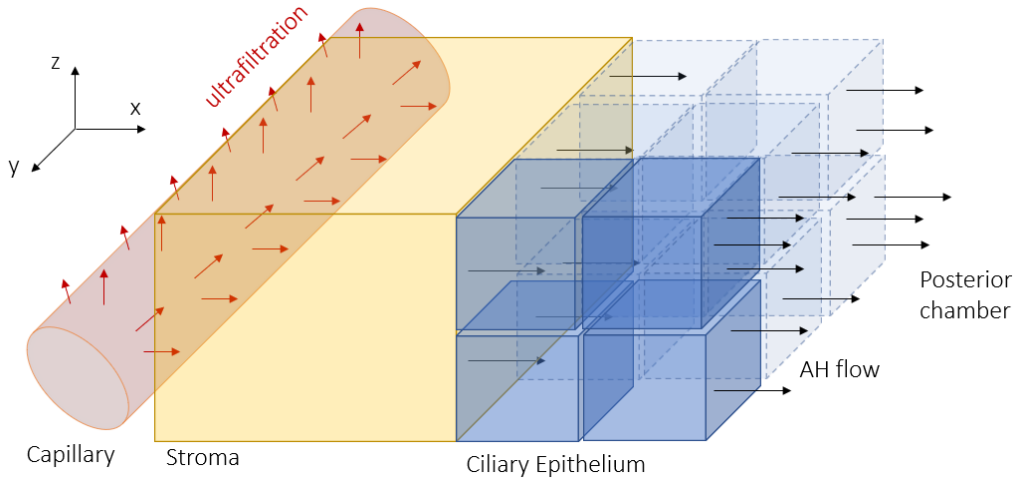
Figure 4.1: A three dimensional scheme of the ciliary epithelium illustrating the flow direction of the homogeneous mixture. The blood transported by the ciliary capillary reaches the stroma. The ultrafiltrated plasma flows across the ciliary epithelium.

As a first step, we will assume that the z component of the AH flow can be neglected, thus we are allowed to study the flow along the $x - y$ plane. Let us consider now a compartmental subdivision of the interested area, as depicted in figure 4.2. Different compartments are in communication with each other. In particular the NPE and PE compartments communicate with the extracellular compartments (Stroma (S), paracellular side (PS), posterior chamber (PC)) thanks to the transporters located along the basolateral membrane of the cells. Moreover, PE and NPE are in a strict communication with each other thanks to the gap junctions distributed along the apical surfaces. Tight junctions are positioned between two PS compartments, which

in turn communicate with S and PC.
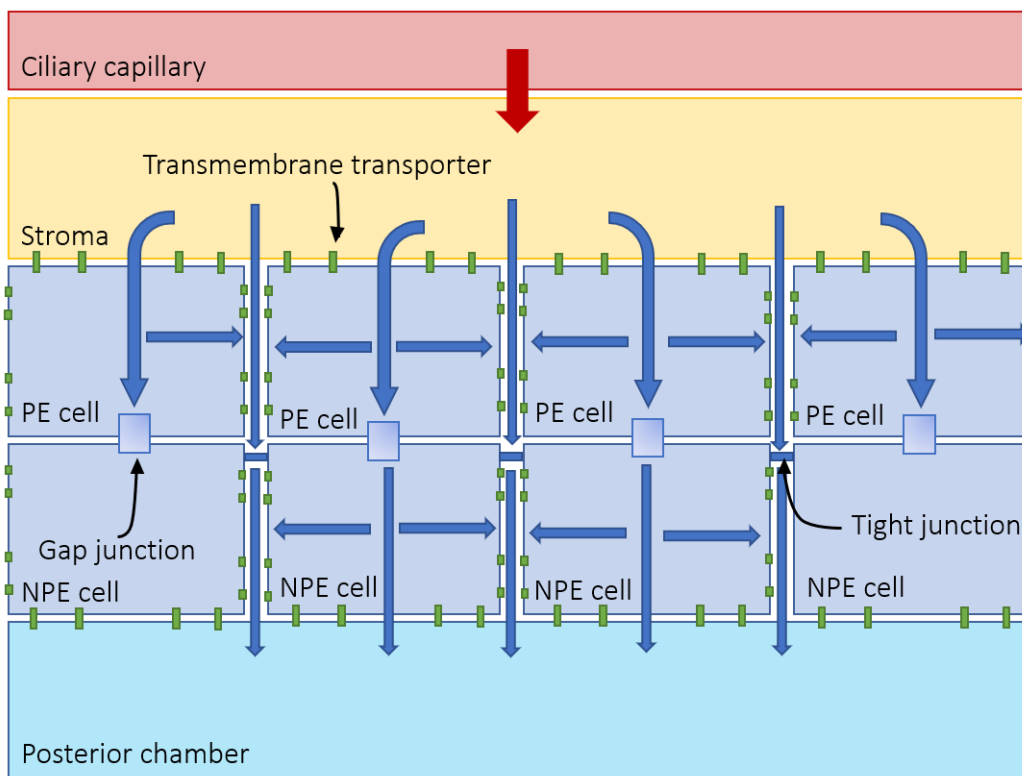
Figure 4.2: A two dimensional cross-section in the x-y plane of the scheme shown in figure 4.1.

In our model, we will investigate a portion of the scheme in figure 4.2, as illustrated in figure 4.3. In particular, we will consider half of a single cell both for PE and NPE cells, and half of the paracellular space between two adjacent cells. This choice will allow us to introduce an important assumption on the AH flux, namely, null flux on the left boundary of the PE and NPE compartment and on the right boundary of the PS compartments. This assumption is justified by symmetry motivations.
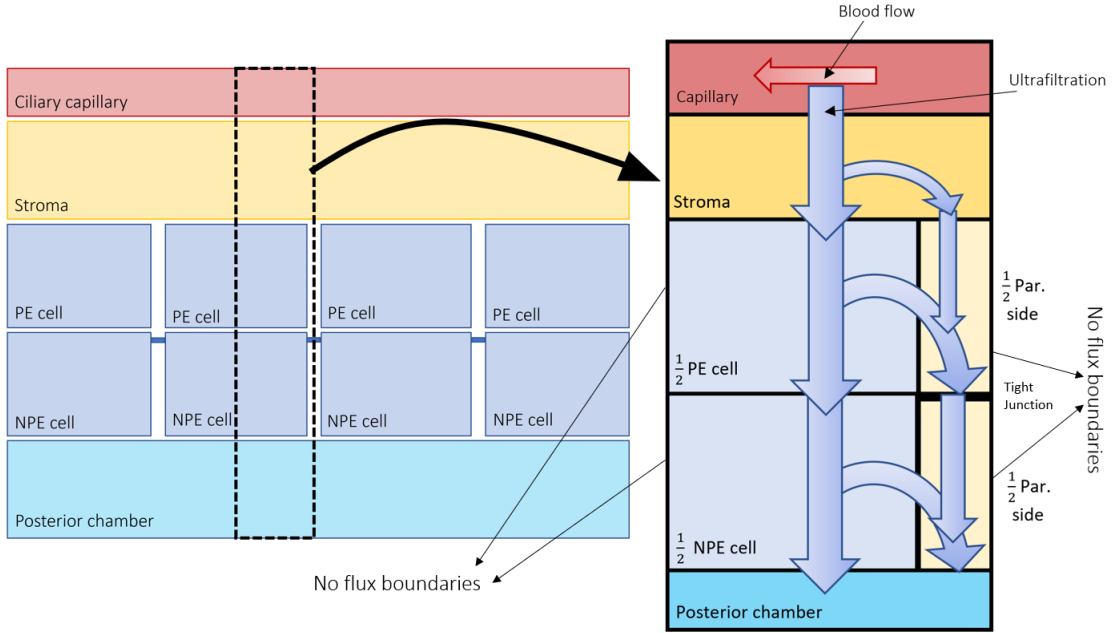
Figure 4.3: Two-dimensional geometrical model for the AH secretion

Finally, a network scheme is derived for the interested area. The use of a network for the description of the problem turns out to be a good trade-off between model simplicity and the need to describe all the electro-chemical phenomena that contribute to the secretion of AH. In fact, this network approach allows us to model the dynamics inside the compartments, which will be represented by the *edges* of the network, but it also prevents us from neglecting the phenomena that occur at the interfaces of the compartments, which are treated by including lumped models at the *nodes* of the network that separate two compartments.

The geometrical description of the network is depicted in figure 4.4 and it is composed by 11 edges distributed along the PE-NPE-PS compartments, 7 nodes (named from A to G) which represent the interface surfaces where it is necessary to establish the laws governing the flow of particles, and the L^j, $j = 1, .., 6$, nodes which do not represent a physical membrane, but

simply serve to connect adjacent sides of the network.
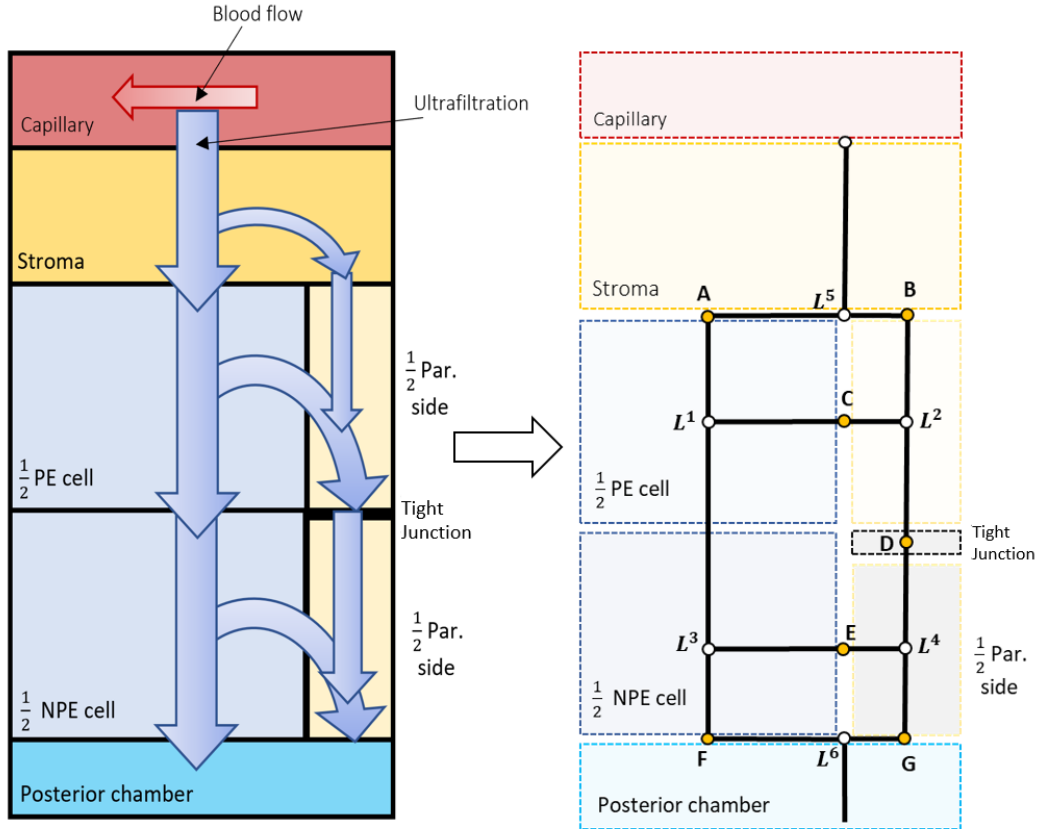
Figure 4.4: The transition between the compartmental model and the network model

It is important to notice that, passing to the network configuration, we decided not to insert any node at the interface between PE-NPE, this because we will assume that the gap junctions allow an undisturbed flow of information between the two compartments, thus we can consider the couple PE-NPE as a single compartment.

Comparing figure 2.10 to the network diagram illustrated in figure 4.5, one can observe that the transporters placed between the ciliary epithelium and the posterior chamber characterize the ionic behavior of the node F, the
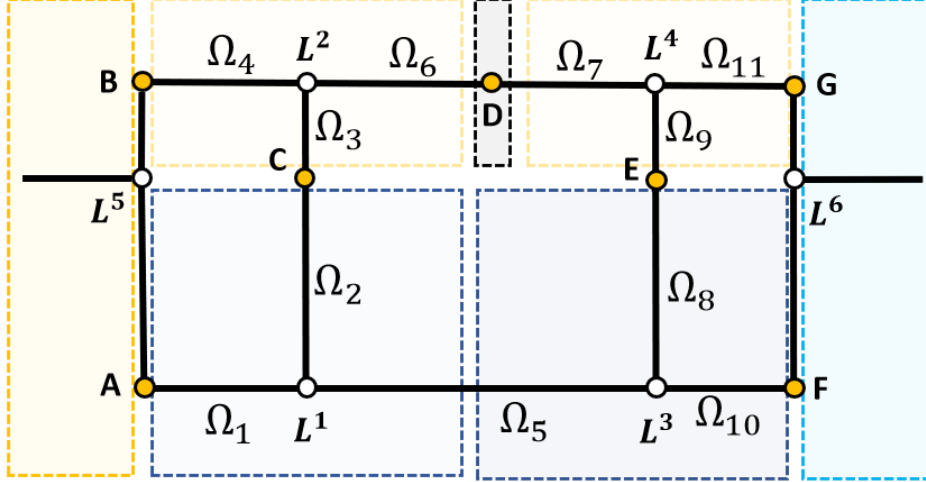
Figure 4.5: Network geometrical representation of the Ciliary epithelium.

transporters placed between the stroma and the ciliary epithelium character-
ize the node A, the mechanisms placed between the ciliary epithelium and
the paracellular side characterize the nodes C and E, while the nodes B,
D, and G have been described assuming the presence of channels for all the
ionic species.

4.2 A PNP model on the network

The aim of this section is the derivation of the final equations used for the
description of ion electrodynamics in the ciliary epithelium. Since our goal is
just to model the concentration of ions inside the compartments, we decided
to neglect the advective contribution of the fluid velocity, thus imposing
$\boldsymbol{v}_f = \boldsymbol{0}$. However, one should keep in mind that if the goal is to evaluate the
hydrostatic pressure supporting the flow of aqueous humor, then the Stokes
part of the model must be included.

We also make the assumption that phenomena occur at a smaller temporal

scale compared to our observation. This allows us to look for the stationary solution of the PNP model, thus neglecting all the temporal derivatives in (3.37)-(3.42).

The resulting one dimensional formulation of the PNP equations reads:

$$\frac{\partial J_\alpha}{\partial s} = \beta_\alpha \tag{4.1}$$

$$J_\alpha = \mu_\alpha^{el} \frac{z_\alpha}{|z_\alpha|} c_\alpha E - D_\alpha \frac{dc_\alpha}{ds} \tag{4.2}$$

$$\varepsilon \frac{\partial E}{\partial s} = F \sum_{\alpha=1}^{M_{ion}} z_\alpha c_\alpha + F(c_{fixed}^+ - c_{fixed}^-) \tag{4.3}$$

$$E = -\frac{\partial \psi}{\partial s} \tag{4.4}$$

where c_α ($[mM]$) is the molar concentration of the ion α ($n_\alpha = c_\alpha N_{AV}$), s is the curvilinear coordinate along the network, and c_{fixed}^+ ($[mM]$) and c_{fixed}^- ($[mM]$) are the positive and negative fixed molar density in the intracellular side,respectively. Equations (4.1)-(4.4) hold in Ω_i, $i = 1,..,11$. The system must be completed imposing suitable boundary conditions and compatibility conditions in correspondence of the network nodes.

4.2.1 Electric part

Collecting out $\mu_\alpha^{el} c_\alpha z_\alpha / |z_\alpha|$ in (4.2) and using (3.35), one obtain the following relation:

$$J_\alpha = -\mu_\alpha^{el} \frac{z_\alpha}{|z_\alpha|} c_\alpha \frac{\partial \varphi_\alpha^{ec}}{\partial s} \tag{4.5}$$

where φ_α^{ec} ($[V]$) is the *electrochemical potential* of ion α defined as:

$$\varphi_\alpha^{ec} = \psi + \frac{V_{th}}{z_\alpha} \ln\left(\frac{c_\alpha}{c_{ref}}\right) \tag{4.6}$$

where $V_{th} = D_\alpha |z_\alpha| / \mu_\alpha^{el}$ is the *thermal voltage* ($[V]$) and c_{ref} ($[mM]$) is a positive constant that represents the reference concentration in the ionic

solution, which we take equal to the ion bulk maximum molar density. By inverting (4.6) we obtain the generalized Maxwell-Boltzmann statistics:

$$c_\alpha = c_{ref} \exp\left(z_\alpha \frac{\varphi_\alpha^{ec} - \psi}{v_{th}} \right) \tag{4.7}$$

Replacing (4.7) in (4.3) one obtains the following nonlinear Poisson equation in mixed form, valid in $\Omega_i, \ i = 1, ..., 11$:

$$\begin{cases} \frac{\partial D(\psi)}{\partial s} = F(c_{fixed}^+ - c_{fixed}^-) + F c_{ref} \sum_{\alpha=1}^{M_{ion}} z_\alpha \exp\left(z_\alpha \frac{(\varphi_\alpha^{ec} - \psi)}{V_{th}} \right) \\ D(\psi) = -\varepsilon \frac{\partial \psi}{\partial s} \end{cases} \tag{4.8}$$

To close the system we need to enforce suitable compatibility conditions at the nodes of the networks.

With this aim, let us consider the nomenclature used in figure 4.6, where the membrane that separates the regions M and N is represented with a thickness $t_m \neq 0$. Away from ion channels and transmembrane proteins, the normal component of the electric displacement vector $D \cdot \mathrm{n}$ and the electrostatic potential ψ should be continuous functions along x. Therefore, if we make the assumption that the amount of membrane area occupied by proteins is negligible, we have:

$$\psi^M = \psi^{in}; \qquad \psi^N = \psi^{out}; \tag{4.9}$$

$$\varepsilon \frac{\partial \psi^M}{\partial \mathrm{n}^1} = \varepsilon_m \frac{\partial \psi^{in}}{\partial \mathrm{n}^1}; \qquad \varepsilon \frac{\partial \psi^N}{\partial \mathrm{n}^2} = \varepsilon_m \frac{\partial \psi^{out}}{\partial \mathrm{n}^2}; \tag{4.10}$$

where ε_m is the dielectric constant of the cell membrane. Let us now introduce two more assumptions: t_m is small compared to the typical length scale of the system and the bulk of the membrane behaves electrically as an insulator with a uniform dielectric constant [14]. Under these assumptions we have that ψ varies linearly in the membrane, thus we obtain the following conditions:

$$D^M \cdot \mathrm{n}^1 = \epsilon \frac{\partial \psi^M}{\partial \mathrm{n}^1} = \epsilon_m \frac{\partial \psi^{in}}{\partial \mathrm{n}^1} = \epsilon_m \frac{\psi^M - \psi^N}{t_m} = c_m(\psi^M - \psi^N) \tag{4.11}$$
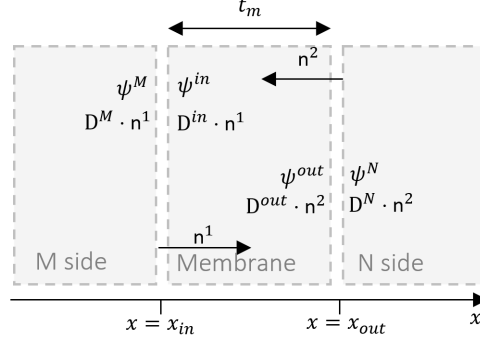
Figure 4.6: Schematic representation of the nomenclature used in this section.

$$D^N \cdot \mathrm{n}^2 = \epsilon \frac{\partial \psi^N}{\partial \mathrm{n}^2} = \epsilon_m \frac{\partial \psi^{out}}{\partial \mathrm{n}^2} = \epsilon_m \frac{\psi^N - \psi^M}{t_m} = c_m(\psi^N - \psi^M) \qquad (4.12)$$

Considering (4.11) and (4.12) we now make explicit the boundary conditions at each edge of the network.

- Node **A**

$$D^1(A) \cdot \mathrm{n}^1(A) = c_{m,A}(\psi^1(A) - \psi^S) \qquad (4.13)$$

where ψ^S is the electric potential in the Stroma compartment, $c_{m,A}$ ($[Fm^{-1}]$) is the membrane capacitance per unit area at node A and $\mathrm{n}^1(A)$ is the outward normal unit vector at A of the Ω_1 edge.

In the following we will adopt the same convention, indicating the edge number as a subscript.

- Node **B**

$$D^4(B) \cdot \mathrm{n}^4(B) = c_{m,B}(\psi^4(B) - \psi^S) \qquad (4.14)$$

where $c_{m,B}$ ($[Fm^{-2}]$) is the capacitance per unit area of the paracellular membrane.

- Node **C**

$$D^2(C) \cdot \mathrm{n}^2(C) = c_{m,C}(\psi^2(C) - \psi^3(C)) \qquad (4.15)$$

$$D^3(C) \cdot \mathrm{n}^3(C) = c_{m,C}(\psi^3(C) - \psi^2(C)) \tag{4.16}$$

Here $c_{m,C}$ ($[Fm^{-2}]$) represents the membrane capacitance per unit area of the basolateral membrane of the PE.

- Node **D**

$$D^6(D) \cdot \mathrm{n}^6(D) = c_{m,D}(\psi^6(D) - \psi^7(D)) \tag{4.17}$$

$$D^7(D) \cdot \mathrm{n}^7(D) = c_{m,D}(\psi^7(D) - \psi^6(D)) \tag{4.18}$$

where $c_{m,D}$ ($[Fm^{-2}]$) is the membrane capacitance per unit area due to the presence of the tight junction.

- Node **E**

$$D^8(E) \cdot \mathrm{n}^8(E) = c_{m,E}(\psi^8(E) - \psi^9(E)) \tag{4.19}$$

$$D^9(E) \cdot \mathrm{n}^9(E) = c_{m,E}(\psi^9(E) - \psi^8(E)) \tag{4.20}$$

where $c_{m,E}$ ($[Fm^{-2}]$) represents the membrane capacitance per unit area of the basolateral membrane of the NPE.

- Node **F**

$$D^{10}(F) \cdot \mathrm{n}^{10}(F) = c_{m,F}(\psi^{10}(F) - \psi^{PC}) \tag{4.21}$$

where ψ^{PC} is the electric potential in the posterior chamber and $c_{m,F}$ ($[Fm^{-2}]$) is the capacitance of the basolateral membrane of the NPE.

- Node **G**

$$D^{11}(G) \cdot \mathrm{n}^{11}(G) = c_{m,G}(\psi^{11}(G) - \psi^{PC}) \tag{4.22}$$

where $c_{m,G}$ ($[Fm^{-2}]$) is the capacitance per unit area of the membrane separating the paracellular side and the PC.

Together with conditions (4.13)-(4.22), one should impose a Kirchoff law for the normal component of the electric displacement D and the continuity of the electric potential ψ at nodes $L^i, i = 1, .., 4$:

- Node L^1

$$\psi^1(L^1) = \psi^2(L^1) \qquad (4.23)$$

$$\psi^1(L^1) = \psi^5(L^1) \qquad (4.24)$$

$$D^1(L^1) \cdot n^1(L^1) + D^2(L^1) \cdot n^2(L^1) + D^5(L^1) \cdot n^5(L^1) = 0 \qquad (4.25)$$

- Node L^2

$$\psi^3(L^2) = \psi^4(L^2) \qquad (4.26)$$

$$\psi^3(L^2) = \psi^6(L^2) \qquad (4.27)$$

$$D^3(L^2) \cdot n^3(L^2) + D^4(L^2) \cdot n^4(L^2) + D^6(L^2) \cdot n^6(L^2) = 0 \qquad (4.28)$$

- Node L^3

$$\psi^5(L^3) = \psi^8(L^3) \qquad (4.29)$$

$$\psi^5(L^3) = \psi^{10}(L^3) \qquad (4.30)$$

$$D^1(L^3) \cdot n^1(L^3) + D^2(L^3) \cdot n^2(L^3) + D^5(L^3) \cdot n^5(L^3) = 0 \qquad (4.31)$$

- Node L^4

$$\psi^7(L^4) = \psi^9(L^4) \qquad (4.32)$$

$$\psi^7(L^4) = \psi^{11}(L^4) \qquad (4.33)$$

$$D^7(L^4) \cdot n^7(L^4) + D^9(L^4) \cdot n^9(L^4) + D^{11}(L^4) \cdot n^{11}(L^4) = 0 \qquad (4.34)$$

4.2.2 Ionic part

Let us now describe the remaining part of the model, the balance law for ion momentum. For each ion α, in $\Omega_i, i = 1, ..., 11$, one has to solve:

$$\begin{cases} \frac{\partial J_\alpha}{\partial s} = \beta_\alpha \\ J_\alpha = \mu_\alpha^{el} \frac{z_\alpha}{|z_\alpha|} c_\alpha E - D_\alpha \frac{dc_\alpha}{ds} \end{cases} \qquad (4.35)$$

To close the system we introduce suitable boundary conditions, by imposing ion concentration in the Stromal compartment (S) and in the posterior chamber (PC):

$$c_\alpha^S(A) = \bar{c}_\alpha^A, \quad \forall \alpha = 1, .., M_{ion} \tag{4.36}$$

$$c_\alpha^S(B) = \bar{c}_\alpha^B, \quad \forall \alpha = 1, .., M_{ion} \tag{4.37}$$

$$c_\alpha^{PC}(F) = \bar{c}_\alpha^F, \quad \forall \alpha = 1, .., M_{ion} \tag{4.38}$$

$$c_\alpha^{PC}(G) = \bar{c}_\alpha^G, \quad \forall \alpha = 1, .., M_{ion} \tag{4.39}$$

where $\bar{c}_\alpha^A$, $\bar{c}_\alpha^B$, $\bar{c}_\alpha^F$ and $\bar{c}_\alpha^G$ are given data.

Moreover, we need to introduce suitable conditions for the molar flux densities J_α at the boundary points of each edge $i = 1, .., 11$. Referring to the scheme of figure 2.10 we now consider a characterization for each J_α.

Let us introduce the notation $J_\alpha^{i, M \to N}$, where α is the current ion, i is the transporter and $M \to N$ represents the direction of the flux (for example, given two adjacent edges of the network e_1 and e_2, $J_\alpha^{e_1 \to e_2}$ represents molar flux density of α from Ω_1 to Ω_2), we have:

- Node **A**

$$J_{Na}^{e_1 \to S} = J_{Na}^{Na/K, e_1 \to S} + J_{Na}^{Na/HCO_3, e_1 \to S} +$$
$$J_{Na}^{Na/H, e_1 \to S} + J_{Na}^{Na/K/2Cl, e_1 \to S} + J_{Na}^{Na, e_1 \to S}$$
$$J_K^{e_1 \to S} = J_K^{Na/K, e_1 \to S} + J_K^{Na/K/2Cl, e_1 \to S} + J_K^{K, e_1 \to S}$$
$$J_H^{e_1 \to S} = J_H^{Na/H, e_1 \to S} + J_H^{Na/HCO_3, e_1 \to S} + J_{Na}^{Na/K/2Cl, e_1 \to S} + J_{Na}^{Na, e_1 \to S}$$
$$J_{Cl}^{e_1 \to S} = J_{Cl}^{Cl/HCO_3, e_1 \to S} + J_{Cl}^{Na/K/2Cl, e_1 \to S} + J_{Cl}^{Cl, e_1 \to S}$$
$$J_{HCO_3}^{e_1 \to S} = J_{HCO_3}^{Cl/HCO_3, e_1 \to S} + J_H^{Na/HCO_3, e_1 \to S}$$

- Node **B**

$$J_\alpha^{e_4 \to S} = J_\alpha^{\alpha, e_4 \to S} \quad \forall \alpha \in [Na^+; K^+; H^+; Cl^-; HCO_3^-]$$

- Node **C**

$$J_{Na}^{e_2 \to e_3} = J_{Na}^{Na/K,e_2 \to e_3} + J_{Na}^{Na/HCO_3,e_2 \to e_3} +$$

$$J_{Na}^{Na/H,e_2 \to e_3} + J_{Na}^{Na/K/2Cl,e_2 \to e_3} + J_{Na}^{Na,e_2 \to e_3}$$

$$J_{K}^{e_1 \to S} = J_{K}^{Na/K,e_2 \to e_3} + J_{K}^{Na/K/2Cl,e_2 \to e_3} + J_{K}^{K,e_2 \to e_3}$$

$$J_{H}^{e_2 \to e_3} = J_{H}^{Na/H,e_2 \to e_3} + J_{H}^{Na/HCO_3,e_2 \to e_3} + J_{Na}^{Na/K/2Cl,e_2 \to e_3} + J_{Na}^{Na,e_2 \to e_3}$$

$$J_{Cl}^{e_2 \to e_3} = J_{Cl}^{Cl/HCO_3,e_2 \to e_3} + J_{Cl}^{Na/K/2Cl,e_2 \to e_3} + J_{Cl}^{Cl,e_2 \to e_3}$$

$$J_{HCO_3}^{e_2 \to e_3} = J_{HCO_3}^{Cl/HCO_3,e_2 \to e_3} + J_{H}^{Na/HCO_3,e_2 \to e_3}$$

- Node **D**

$$J_{\alpha}^{e_6 \to e_7} = J_{\alpha}^{\alpha,e_6 \to e_7} \quad \forall \alpha \in [Na^+; K^+; H^+; Cl^-; HCO_3^-]$$

- Node **E**

$$J_{Na}^{e_8 \to e_9} = J_{Na}^{Na/K,e_8 \to e_9} + J_{Na}^{Na,e_8 \to e_9}$$

$$J_{K}^{e_8 \to e_9} = J_{K}^{Na/K,e_8 \to e_9} + J_{K}^{K,e_8 \to e_9}$$

$$J_{Cl}^{e_8 \to e_9} = J_{Cl}^{Cl/HCO_3,e_8 \to e_9} + J_{Cl}^{Cl,e_8 \to e_9}$$

$$J_{H}^{e_8 \to e_9} = 0$$

$$J_{HCO_3}^{e_8 \to e_9} = J_{HCO_3}^{Cl/HCO_3,e_8 \to e_9}$$

- Node **F**

$$J_{Na}^{e_{10} \to e_{PC}} = J_{Na}^{Na/K,e_{10} \to e_{PC}} + J_{Na}^{Na,e_{10} \to e_{PC}}$$

$$J_{K}^{e_{10} \to e_{PC}} = J_{K}^{Na/K,e_{10} \to e_{PC}} + J_{K}^{K,e_{10} \to e_{PC}}$$

$$J_{Cl}^{e_{10} \to e_{PC}} = J_{Cl}^{Cl/HCO_3,e_{10} \to e_{PC}} + J_{Cl}^{Cl,e_{10} \to e_{PC}}$$

$$J_{H}^{e_{10} \to e_{PC}} = 0$$

$$J_{HCO_3}^{e_{10} \to e_{PC}} = J_{HCO_3}^{Cl/HCO_3,e_{10} \to e_{PC}}$$

- Node **G**

$$J_\alpha^{e_{11} \to PC} = J_\alpha^{\alpha, e_{11} \to PC} \quad \forall \alpha \in [Na^+; K^+; H^+; Cl^-; HCO_3^-]$$

Note that, denoting ζ the intersection node between sides M and N, then $J_\alpha^{M \to N} = J_{M,\alpha}(\zeta) \cdot n_M(\zeta)$. Moreover $J_\alpha^{M \to N} = -J_\alpha^{N \to M}$.

4.2.3 Scaling of the Poisson equation

Let us now non-dimensionalize (4.3). For this discussion we refer to [14], considering $c_{fixed}^+ = c_{fixed}^- = 0$.

We denote by $\bar\psi$ and $\bar c$ the positive scaling factors for the electric potential and ion molar density, respectively, $[\bar\psi] = V$ and $[\bar c] = mM$.

Then, we introduce the dimensionless dependent variables $\tilde\psi$, $\tilde c_\alpha$:

$$\tilde\psi = \frac{\psi}{\bar\psi} \tag{4.40}$$

$$\tilde c_\alpha = \frac{c_\alpha}{c_{ref}} \tag{4.41}$$

We set henceforth $\bar\psi = V_{th} = k_B T/q$ and $\bar c = c_{ref}$.

Rescaling, one obtains:

$$r_d^2 \frac{\partial^2 \tilde\psi}{\partial s^2} = -\sum_{\alpha=1}^{M_{ion}} z_\alpha \tilde c_\alpha \tag{4.42}$$

where $r_d := \sqrt{\frac{\varepsilon k_B T}{q F c_{ref}}}$ is called *Debye length*. Moreover, introducing a characteristic length l_0 such that $s = l_0 \tilde s$, we have:

$$\beta^2 \frac{\partial^2 \tilde\psi}{\partial \tilde s^2} = -\sum_{\alpha=1}^{M_{ion}} z_\alpha \tilde c_\alpha \tag{4.43}$$

where $\beta = \frac{r_d}{l_0}$. Thanks to (4.43) we are able to investigate an important property of the PNP model, namely the electroneutrality in the bulk of the

compartments (away from membranes). In fact, we can observe that, by letting $\beta \to 0$, which holds away from the cell membranes, the Poisson equation degenerates into the following limit:

$$\sum_{\alpha=1}^{M_{ion}} z_\alpha \tilde{c}_\alpha = 0 \tag{4.44}$$

which corresponds to the condition of electroneutrality away from membranes.

We can also note that the small parameter β is multiplying the highest order derivative, thus the smallness of β implies the appearance of boundary layers at the membranes whose thickness is on the order of r_d.

Regarding the boundary conditions, introducing the dimensionless parameter $\tilde{c}_m = \frac{c_m}{\varepsilon/r_d}$, one has:

$$\tilde{c}_m(\psi^M - \psi^N) = r_d \frac{\partial \psi^M}{\partial \mathrm{n}^M} \tag{4.45}$$

Chapter 5

Numerical discretization

In this chapter we illustrate the fixed-point map for the iterative solution of the PNP model introduced in chapter 4. Then, we describe a numerical discretization of the decoupled equations by using the finite Element method.

5.1   Gummel's map

To solve problem (4.1)-(4.4) we will use a decoupling method, known as *Gummel's map*. The main idea of the method, which was proposed for the first time in 1964 by H.K. Gummel [9], is successively solve the nonlinear Poisson equation (4.8) and then update the electrochemical potentials φ_α^{ec} by solving the continuity equation for each ion α.

In the following the steps for the solution of the iterative algorithm are reported. One can notice that the Gummel map is a block nonlinear Gauss-Seidel iteration for the variable $\boldsymbol{\varphi}^{ec} = [\varphi_1^{ec}, ..., \varphi_{M_{ion}}^{ec}]$.

🔍 **Gummel's map**

1. Set suitable initial data for the electric potential ψ^0 and the ionic concentrations c_α^0, $\quad \forall \alpha = 1, .., M_{ion}$.

   Fix a positive tolerance $tol_{Gummel} > 0$ for the inner loop related to the nonlinear Poisson equation, and a positive tolerance $tol_{NLP} > 0$, for the outer loop;

2. By using the Newton method, $\forall k = 0, ...$ find ψ^{k+1} solving the linearized Non Linear Poisson equation until the following stopping criterion is met

$$||\delta\psi^k||_{L^\infty} > tol_{NLP}$$

   where k is the counter of the newton iteration. Then, set

$$\psi^{j+1} = \psi^{k+1}$$

3. Find c_α^{j+1} by solving the linear continuity equations for each ion α;

4. Update the electrochemical potential φ_α^j, $\quad \forall \alpha = 1, .., M_{ion}$:

$$\varphi_\alpha^{ec,j+1} = \psi^{j+1} + \frac{V_{th}}{z_\alpha} \ln\left(\frac{c_\alpha^{j+1}}{c_{ref}}\right) \qquad (5.1)$$

   Restart from step 2 until the following convergence criterion is met

$$\max_\alpha ||\varphi_\alpha^{ec,j+1} - \varphi_\alpha^{ec,j}||_{L^\infty} < tol_{Gummel}$$

   restart from step 2.

5.2 Newton's method

Equation (4.8) is semilinear because of the presence of the exponential term in the right hand side. To treat the nonlinearity we apply the Newton iterative method, which is briefly recalled in the following.

Let us consider the generic nonlinear equation

$$N(u) = f \qquad in \ \Omega \tag{5.2}$$

coupled with suitable boundary conditions on $\partial\Omega$. In eq. (5.2) u is the dependent variable, N is a nonlinear differential operator and f is a given function. Denoting by V the Hilbert space in which we seek the solution of (5.2), we want to solve the following nonlinear problem:

Find $u \in V$ such that

$$G(u) := N(u) - f = 0 \tag{5.3}$$

where $G : V \to V$ is a nonlinear differential operator.

The iterative algorithm for the solution of (5.3) reads:

Given $u^0 \in V$, for all $j \geq 0$ until convergence, solve the following linearized problem:

$$G'(u^j)\delta u^j = -G(u^j) \tag{5.4}$$

$$u^{j+1} = u^j + \delta u^j \tag{5.5}$$

Definition 5.1 (Frechet derivative) *Given a non linear operator G, evaluated at $u \in V$, the operator $G' : V \to L(V; V)$ is defined as*

$$G'(u) := \lim_{\eta \to 0} \frac{G(u + \eta v) - G(u)}{\eta} \qquad \forall v \in V \tag{5.6}$$

where $L(V; V)$ is the space of linear operator from V to V.

5.2.1 Nonlinear Poisson equation

In the case of eq. (4.8), the operator G is

$$G(\psi) = \frac{\partial}{\partial s}\left(-\varepsilon_m \frac{\partial \psi}{\partial s}\right) - Fc_{ref}\sum_{\alpha=1}^{M_{ion}} z_\alpha \exp\left(z_\alpha \frac{\varphi_\alpha^{ec} - \psi}{V_{th}}\right) - Fc_{fixed} = 0 \quad (5.7)$$

Evaluating the Frechet derivative one obtains:

$$G'(\psi)\delta\psi = -\frac{\partial}{\partial s}\left(\varepsilon_m \frac{\partial \delta\psi}{\partial s}\right) + \left(\frac{Fc_{ref}}{V_{th}}\sum_{\alpha=1}^{M_{ion}} z_\alpha^2 \exp\left(z_\alpha \frac{\varphi_\alpha^{ec} - \psi}{V_{th}}\right)\right)\delta\psi = 0$$

$$(5.8)$$

Introducing the following notation

$$\sigma^k = \frac{Fc_{ref}}{V_{th}}\sum_{\alpha=1}^{M_{ion}} z_\alpha^2 \exp\left(z_\alpha \frac{\varphi_\alpha^{ec,k} - \psi^k}{V_{th}}\right) \qquad (5.9)$$

we obtain the Newton linearization of the nonlinear Poisson equation (4.8):

$$\begin{cases} -\frac{\partial}{\partial s}\left(\varepsilon_m \frac{\partial \delta\psi^k}{\partial s}\right) + \sigma^k \delta\psi^k = -G(\psi^k) & \text{in } \Omega_i, i = 1, ..., 11 \\ \psi^{k+1} = \psi^k + \delta\psi^k \end{cases} \qquad (5.10)$$

which has the structure of a diffusion-reaction problem.

The system reported above should be completed introducing suitable compatibility conditions at the nodes of the network.

To this purpose, we observe that

$$\begin{aligned} \delta\mu^k(s) &:= (D^{k+1}(s) - D^k(s)) \cdot \mathrm{n}(s) \\ &= -\varepsilon_m\left(\frac{\partial \psi^{k+1}}{\partial s} - \frac{\partial \psi^k}{\partial s}\right) \cdot \mathrm{n}(s) \qquad (5.11) \\ &= -\varepsilon_m \frac{\partial \delta\psi^k}{\partial s} \cdot \mathrm{n}(s) \end{aligned}$$

To obtain the conditions for $\delta\psi^k$ at the network nodes we proceed as follows.

At node A, using (4.13), one obtains (unlike the previous chapter, we now

indicate the edge as subscript to ease the notation):

$$\delta\mu_1^k(A) := D_1^{k+1}(A) \cdot \mathrm{n}_1(A) - D_1^k(A) \cdot \mathrm{n}_1(A)$$
$$= c_{m,A}(\psi_1^{k+1}(A) - \psi_S) - c_{m,A}(\psi_1^{k+1}(A) - \psi_S)$$
$$= c_{m,A}\delta\psi_1^k(A)$$

Similarly, for nodes B, F, and G, using (4.14), (4.21) and (4.22), we retrieve the following relations:

$$\delta\mu_4^k(B) = c_{m,B}\delta\psi_4^k(B)$$
$$\delta\mu_{10}^k(F) = c_{m,F}\delta\psi_{10}^k(F) \tag{5.12}$$
$$\delta\mu_{11}^k(G) = c_{m,G}\delta\psi_{11}^k(G)$$

At node C, which links two edges of the network, using (4.15)-(4.16) one obtains:

$$\delta\mu_2^k(C) = c_{m,C}(\delta\psi_2^k(C) - \delta\psi_3^k(C)) \tag{5.13}$$
$$\delta\mu_3^k(C) = c_{m,C}(\delta\psi_3^k(C) - \delta\psi_2^k(C)) \tag{5.14}$$

and the same reasoning could be applied to find suitable conditions at nodes D and E.

At nodes $L^j, j = 1, ..., 4$, denoting by e_1^j, e_2^j, e_3^j the edges that converge at node j, we have:

$$\delta\psi_{e_1^j}^k(L^j) = \delta\psi_{e_2^j}^k(L^j) \tag{5.15}$$
$$\delta\psi_{e_1^j}^k(L^j) = \delta\psi_{e_3^j}^k(L^j) \tag{5.16}$$
$$\delta\mu_{e_1^j}^k(L^j) + \delta\mu_{e_2^j}^k(L^j) + \delta\mu_{e_3^j}^k(L^j) = 0 \tag{5.17}$$

5.3 Linear continuity equations

Once the updated electric potential ψ^{j+1} has been obtained, according to the structure of Gauss-Seidel iteration, one needs to solve M_{ion} linear boundary value problems for the ion concentrations c_α^{j+1}:

For each ion $\alpha = 1, .., M_{ion}$, in $\Omega_i, i = 1, .., M_{ion}$, solve

$$\begin{cases} \frac{\partial J_\alpha^{j+1}}{\partial s} = \beta_\alpha^{j+1} \\ J_\alpha^{j+1} = \mu_\alpha^{el} \frac{z_\alpha}{|z_\alpha|} c_\alpha^{j+1} \frac{\partial \psi^{j+1}}{\partial s} - D_\alpha \frac{\partial c_\alpha^{j+1}}{\partial s} \end{cases} \qquad (5.18)$$

From a physical standpoint a crucial characteristic of system (5.18) is that ion concentrations are strictly positive, thus one should be aware of the fact that a numerical algorithm for the solution of (5.18) must guarantee a strictly positive solution in the computational domain. In the following this requirement will be satisfied by introducing a stabilized finite element discretization scheme, referred to as Scharfetter-Gummel method, which adds an artificial viscosity to the formulation.

To close the system (5.18) we must give a form to the molar flux density passing through the boundary of each edge of the network. In section 4.2.2 we deduced the mathematical formula for each $J_\alpha, \alpha = 1, .., M_{ion}$. Unfortunately, the derived equations are nonlinear, thus we need to introduce an alternative linearized form, taking advantage of the fact that we are dealing with an iterative algorithm.

The idea is to write the molar flux density evaluated at step $j + 1$ for each transporter at node ζ as:

$$J_\alpha^{M \to N, j+1}(\zeta) = \beta_\alpha^M c_\alpha^{M, j+1}(\zeta) + \beta_\alpha^N c_\alpha^{N, j+1}(\zeta) \qquad (5.19)$$

where $c_\alpha^{M, j+1}(\zeta)$ and $c_\alpha^{N, j+1}(\zeta)$ represent the ion concentrations at ζ respectively on the M and N sides, β_α^M and β_α^N are two coefficients such that:

$$\beta_\alpha^i = \beta_\alpha^i(\psi^{M,j}(\zeta), \psi^{N,j}(\zeta), c_1^{M,j}(\zeta), c_1^{N,j}(\zeta), ..., c_{M_{ion}}^{M,j}(\zeta), c_{M_{ion}}^{N,j}(\zeta)), \quad i = M, N \qquad (5.20)$$

For example, the molar flux density due to the $Na^+/K^+ ATPase$ pump at node ζ is obtained inserting in eq.(2.10) the ion concentrations computed at

the previous step and multiplying it by the factor $c_{Na}^{M,j+1}(\zeta)/c_{Na}^{M,j}(\zeta)$ for the sodium continuity equation and $c_K^{N,j+1}(\zeta)/c_K^{N,j}(\zeta)$ for the potassium continuity equation:

$$J_{pump,Na}^{M\to N,j+1}(\zeta) = \frac{c_{Na}^{M,j+1}(\zeta)}{c_{Na}^{M,j}(\zeta)}\gamma[ATP]\left(\frac{c_{Na}^{M,j}}{\phi_{Na}^j}\right)^3\left(\frac{c_K^{N,j}}{\phi_K^j}\right)^2 \qquad (5.21)$$

$$J_{pump,K}^{M\to N,j+1}(\zeta) = -\frac{2}{3}\frac{c_K^{N,j+1}(\zeta)}{c_K^{N,j}(\zeta)}\gamma[ATP]\left(\frac{c_{Na}^{M,j}}{\phi_{Na}^j}\right)^3\left(\frac{c_K^{N,j}}{\phi_K^j}\right)^2 \qquad (5.22)$$

From equations (5.21) and (5.22) we obtain for this particular active transporter the following coefficients:

$$\beta_{Na}^M = \gamma c_{Na}^{M,j}(\zeta)[ATP]\left(\frac{c_{Na}^{M,j}}{\phi_{Na}^j}\right)^3\left(\frac{c_K^{N,j}}{\phi_K^j}\right)^2, \qquad \beta_{Na}^N = 0 \qquad (5.23)$$

$$\beta_K^M = 0, \qquad \beta_K^N = -\frac{2}{3}\gamma c_K^{N,j}(\zeta)[ATP]\left(\frac{c_{Na}^{M,j}}{\phi_{Na}^j}\right)^3\left(\frac{c_K^{N,j}}{\phi_K^j}\right)^2 \qquad (5.24)$$

Observing the coefficients just calculated it is clear how important it is to correctly orient the transporter within the network. Since the role of the pump is to extrude Na^+ into an extracellular environment, in this case the M region represents the cytoplasm.

On the contrary, the equations obtained in section 2.2 for the remaining transporters are characterized by a symmetric shape with respect to the M and N sides. Let us examine for example the HCO_3^-/Cl^- anion exchanger:

$$J_{exch1,HCO_3}^{M\to N,j+1}(\zeta) = \kappa_{HCO_3^-/Cl^-}\left[\frac{c_{Cl}^{N,j}(\zeta)\,c_{HCO_3^-}^{M,j+1}(\zeta) - c_{Cl}^{M,j}(\zeta)\,c_{HCO_3^-}^{N,j+1}(\zeta)}{\phi_{exch1}^j}\right] \qquad (5.25)$$

$$J_{exch1,Cl}^{M\to N,j+1}(\zeta) = -\kappa_{HCO_3^-/Cl^-}\left[\frac{c_{Cl}^{N,j+1}(\zeta)\,c_{HCO_3}^{M,j}(\zeta) - c_{Cl}^{M,j+1}(\zeta)\,c_{HCO_3}^{N,j}(\zeta)}{\phi_{exch1}^j}\right] \qquad (5.26)$$

where $\phi_{exch1}^j = \phi_{exch1}(c_{Cl^-}^{M,j}(\zeta), c_{Cl^-}^{N,j}(\zeta), c_{HCO_3^-}^{M,j}(\zeta), c_{HCO_3^-}^{N,j}(\zeta))$. In this case the coefficients take the following form:

$$\beta_{HCO_3^-}^M = \kappa_{HCO_3^-/Cl^-} \frac{c_{Cl^-}^{N,j}(\zeta)}{\phi_{exch1}^j}, \quad \beta_{HCO3^-}^N = -\kappa_{HCO_3^-/Cl^-} \frac{c_{Cl^-}^{M,j}(\zeta)}{\phi_{exch1}^j} \quad (5.27)$$

$$\beta_{Cl^-}^M = \kappa_{HCO_3^-/Cl^-} \frac{c_{HCO_3^-}^{N,j}(\zeta)}{\phi_{exch1}^j}, \quad \beta_{Cl^-}^N = -\kappa_{HCO3^-/Cl^-} \frac{c_{HCO_3^-}^{M,j}(\zeta)}{\phi_{exch1}^j} \quad (5.28)$$

5.4 Weak formulation

Let $\Omega = \sum_{i=1}^{11} \Omega_i$ be the domain formed by the edges of the network. Let us introduce the Sobolev space $V := H^1(\Omega)$ defined as

$$V = \{\phi \in L^2(\Omega) : \frac{\partial \phi}{\partial s} \in L^2(\Omega)\} \quad (5.29)$$

5.4.1 Weak form of the nonlinear Poisson equation

In order to use the Finite Element method for the numerical solution of the problem, we will now proceed finding the weak formulation.

Let us first multiply (5.10) by a test function $\phi \in V$ and then integrate over the domain Ω

$$\int_\Omega \frac{\partial}{\partial s}(-\varepsilon \frac{\partial \delta \psi^k}{\partial s})\phi \, d\Omega + \int_\Omega \sigma^k \delta \psi^k \phi \, d\Omega = \int_\Omega -G(\psi^k)\phi \, d\Omega \quad \forall \phi \in V \quad (5.30)$$

Integrating by parts the first integral on the left hand side one obtains:

$$\int_\Omega \varepsilon \frac{\partial \delta \psi^k}{\partial s} \frac{\partial \phi}{\partial s} \, d\Omega + \int_\Omega \frac{\partial}{\partial s}(\delta \mu^k \phi) \, d\Omega + \int_\Omega \sigma^k \delta \psi^k \phi \, d\Omega = \int_\Omega -G(\psi^k)\phi \, d\Omega \quad (5.31)$$

where we used (5.11).

Applying the divergence theorem, we derive the following weak formulation:

Given ψ^k, find $\delta\psi^k \in V$ such that, for each $\phi \in V$

$$\int_\Omega \varepsilon \frac{\partial\delta\psi^k}{\partial s}\frac{\partial\phi}{\partial s}\, d\Omega + \int_{\partial\Omega} \phi\delta\mu^k \mathrm{n}\, d(\partial\Omega) + \int_\Omega \sigma^k\delta\psi^k\phi\, d\Omega = \int_\Omega -G(\psi^k)\phi\, d\Omega \tag{5.32}$$

where $\mathrm{n}(s)$ is the outward unit normal vector.

In order to introduce the interface conditions at each node of the domain, we now virtually detach every edge of the network and we treat them separately. Let us consider the local coordinate x for the single edge i. We define a_i the point with $x = 0$ (see figure 5.1) and b_i the point at $x = l_i$ (l_i is the length of the edge i). Moreover, we define $\delta\psi_i^k = \delta\psi^k|_{\Omega_i}$ that is the solution $\delta\psi^k$ evaluated on edge i.
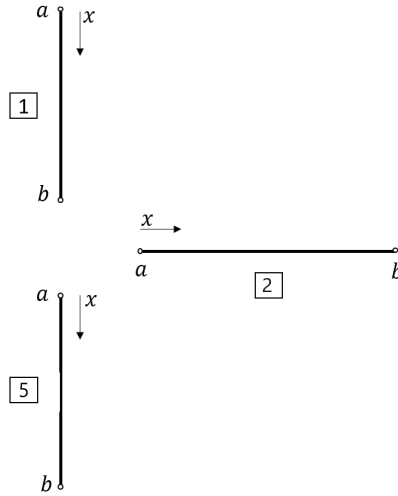

Figure 5.1: Schematic representation of 3 edges of the network. Each side is "detached" from the network and studied as a single one dimensional domain.

Given these assumptions, the weak formulation of the problem applied to the network reads:

For each $i = 1, .., 11$, find $\delta\psi_i^k \in V^i := H^1(\Omega_i)$, such that, for each $\phi \in V^i$

$$
\phi(a_i)\delta\mu_i^k(a_i) + \phi(b_i)\delta\mu_i^k(b_i) + \int_{\Omega_i} \varepsilon \frac{\partial\delta\psi_i^k(x)}{\partial x} \frac{\partial\delta\phi(x)}{\partial x} \, d\Omega_i +
$$
$$
\int_{\Omega_i} \sigma^k \delta\psi_i^k \phi \, d\Omega_i = -\int_\Omega G(\psi_i^k(x))\phi(x) \, d\Omega_i
$$
(5.33)

where

$$
\delta\mu_i^k(a_i) = (D_i^{k+1}(a_i) - D_i^k(a_i)) \, \mathrm{n}(a_i) = (D_i^k(a_i) - D_i^{k+1}(a_i))
$$
$$
\delta\mu_i^k(b_i) = (D_i^{k+1}(b_i) - D_i^k(b_i)) \, \mathrm{n}(b_i) = (D_i^{k+1}(b_i) - D_i^k(b_i))
$$

Note that to close (5.33) one needs to impose 22 boundary/interface conditions, that we already described in section 5.2.1.

5.4.2 Weak form of the linear continuity equation

Let us now consider the weak formulation of (5.18) for each ion species α. For the net production rate β_α we can suppose the following general relation:

$$
\beta_\alpha^{j+1} = \sigma_\alpha c_\alpha^{j+1} + \pi_\alpha
$$
(5.34)

thus we obtain the general form of an advection-diffusion-reaction problem. As above, multiplying by a test function $\phi \in V$, integrating over the volume Ω and applying the divergence theorem, the weak form reads:

Given ψ^{j+1} and c_α^j, $\forall\alpha = 1, .., M_{ion}$, find $c_\alpha^{j+1} \in V$ such that, for each $\phi \in V$:

$$
\int_\Omega D_\alpha \frac{\partial c_\alpha^{j+1}}{\partial s} \frac{\partial\phi}{\partial s} \, d\Omega - \int_\Omega \mu_{el} \frac{z_\alpha}{|z_\alpha|} \frac{\partial\psi^{j+1}}{\partial s} \frac{\partial\phi}{\partial s} c_\alpha^{j+1} \, d\Omega +
$$
$$
\int_{\partial\Omega} \phi J_\alpha^{j+1} \mathrm{n} \, d(\partial\Omega) - \int_\Omega \sigma_\alpha c_\alpha^{j+1} \phi \, d\Omega = \int_\Omega \pi_\alpha \phi \, d\Omega
$$
(5.35)

while, considering the detached structure described above, the weak form is:

For each $i = 1, ..., 11$, given ψ^{j+1} and c_α^j, $\forall\alpha = 1, .., M_{ion}$, find $c_{i,\alpha}^{j+1} :=$

$c_\alpha^{j+1}|_{\Omega_i} \in V^i$ such that, for each $\phi \in V^i$:

$$\int_{\Omega_i} D_\alpha \frac{\partial c_{i,\alpha}^{j+1}}{\partial x} \frac{\partial \phi}{\partial x} \, d\Omega_i - \int_{\Omega_i} \mu_{el} \frac{z_\alpha}{|z_\alpha|} \frac{\partial \psi_i^{j+1}}{\partial x} \frac{\partial \phi}{\partial x} c_{i,\alpha}^{j+1} \, d\Omega_i - \int_{\Omega_i} \sigma_\alpha c_{i_\alpha}^{j+1} \phi \, d\Omega_i +$$

$$\phi(b_i) J_{i,\alpha}^{j+1}(b_i) \mathrm{n}_i(b_i) + \phi(a_i) J_{i,\alpha}^{j+1}(a_i) \mathrm{n}_i(a_i) = \int_{\Omega_i} \pi_\alpha \phi \, d\Omega_i$$

$$(5.36)$$

To close (5.36) we need to impose 22 boundary/interface conditions that we discussed in section 5.3

5.5 Finite element approximation

We now discretize problems (5.33) and (5.36) using a Galerkin formulation. Let us define a discrete space $V_h \in V$, such that $\dim(V_h) = N_h$ and the discrete spaces $V_h^i \in V$, $\forall i = 1, ..., 11$, such that $\dim(V_h^i) = N_h^i$. Note that $V_h = \sum_{i=1}^{11} V_h^i$. Moreover, let us take $\{\phi_j^i\}_{j=1}^{N_h^i}$ as basis for V_h^i.

5.5.1 FEM for the nonlinear Poisson equation

Given $\psi_{h,i}^k$, for each $i = 1, ..., 11$, find $\delta\psi_{h,i}^k \in V_h^i$, such that, for each $m = 1, .., N_h^i$

$$\phi_m^i(a_i)\delta\mu_i^k(a_i) + \phi_m^i(b_i)\delta\mu_i^k(b_i) + \int_{\Omega_i} \varepsilon \frac{\partial \delta\psi_{h,i}^k(x)}{\partial x} \frac{\partial \phi_m^i(x)}{\partial x} \, d\Omega_i +$$
$$\int_{\Omega_i} \sigma^k \delta\psi_{h,i}^k \phi_m^i \, d\Omega_i = - \int_\Omega G(\psi_{h,i}^k(x))\phi_m^i(x) \, d\Omega_i \quad \forall m = 1, .., N_h^i$$

$$(5.37)$$

Since $\delta\psi_{h,i}^k \in V_h^i$, we can express it as a linear combination of the basis $\{\phi_j^i\}_{j=1}^{N_h^i}$:

$$\delta\psi_{h,i}^k(x) = \sum_{n=1}^{N_h^i} \delta\psi_{h,i}^{k,n} \phi_n^i(x) \tag{5.38}$$

We define the matrices $\boldsymbol{A}_i^k$ and $\boldsymbol{R}_i^k$, and the vectors $\delta\Psi_i^k$, F_i^k and δM_i^k:

$$A_{i,mn}^k = \int_{\Omega_i} \varepsilon \frac{\partial \phi_m^i(x)}{\partial x} \frac{\partial \phi_n^i(x)}{\partial x} \, d\Omega_i \tag{5.39}$$

$$R_{i,mn}^k = \int_{\Omega_i} \sigma^k \; \phi_m^i \phi_n^i \; d\Omega_i \tag{5.40}$$

$$F_{i,m}^k = -\int_{\Omega_i} G(\psi_{h,i}^k(x))\phi_m^i(x) \; d\Omega_i \tag{5.41}$$

$$\delta\Psi_i^k = [\delta\psi_{h,i}^{k,1}, ..., \delta\psi_{h,i}^{k,N_h^i}]^T \tag{5.42}$$

$$\delta M_i^k = [\delta\mu_i^k(a_i), 0, ...0, \delta\mu_i^k(b_i)]^T \tag{5.43}$$

Then, the final algebraic formulation of (5.37) is:
Find $\delta\Psi_i^k$ such that

$$(\boldsymbol{A}_i^k + \boldsymbol{R}_i^k)\delta\Psi_i^k + \delta M_i^k = F_i^k \tag{5.44}$$

The system above of size $N_h^i \times (N_h^i + 2)$, thus one needs to include 2 interface conditions.

In order to derive a FEM formulation, let us now introduce a suitable triangulation $\mathcal{T} = \sum_{i=1}^{11} \mathcal{T}_i$ for the domain Ω. We divide each edge i into N_{el}^i elements of equal length (see figure 5.2).
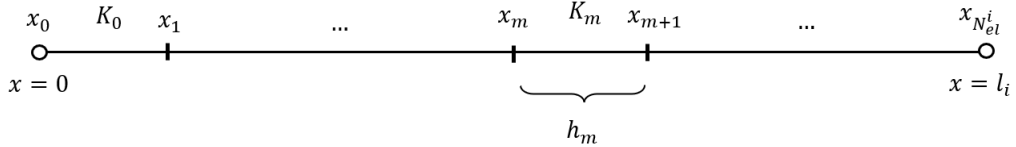

Figure 5.2: Triangulation for the one dimensional domain Ω_i.

As space of basis functions V_h^i we choose

$$V_h^i := \{\phi \in C(\bar{\Omega}_i) \; : \; \phi|_K \in P^1(K) \; \forall K \in \mathcal{T}_i\} \tag{5.45}$$

where $P^1(K)$ is the space of polynomials of degree at most 1 in K. As basis functions we use the hat functions defined on the node of the triangulation.

5.5.2 The Scharfetter-Gummel method

The Scharfetter-Gummel method [18] is an exponential fitting discretization scheme for convection-dominated problems, thus it provides an appropriate tool to approximate the Nernst-Planck equation.

Let us now consider $\beta_\alpha = 0$. For each edge i, we have:

$$\frac{d}{dx} J_\alpha(x) = 0, \quad \forall x \in (0, l_i) \tag{5.46}$$

where

$$J_\alpha = \mu_\alpha^{el} \frac{z_\alpha}{|z_\alpha|} E c_\alpha(x) - D_\alpha \frac{dc_\alpha(x)}{dx} \tag{5.47}$$

Assuming that μ_α^{el}, E, D_α and J_α are constant within K_m (see figure 5.2), we have from (5.47):

$$\frac{dc_{\alpha(x)}}{dx} = \mu_\alpha^{el} \frac{z_\alpha}{|z_\alpha|} \frac{E}{D_\alpha} c_\alpha(x) - \frac{J_\alpha}{D_\alpha} = \gamma_\alpha c_\alpha(x) - \frac{J_\alpha}{D_\alpha} \tag{5.48}$$

where we introduced the coefficient $\gamma_\alpha = \mu_\alpha^{el} \frac{z_\alpha}{|z_\alpha|} \frac{E}{D_\alpha}$. We now manipulate (5.48) in the following manner [13]:

$$
\begin{aligned}
\gamma_\alpha &= \frac{1}{c_\alpha(x) - \frac{J_\alpha}{\gamma_\alpha D_\alpha}} \frac{dc_\alpha(x)}{dx} = \\
\gamma_\alpha &= \frac{d}{dx} \ln \left| c_\alpha(x) - \frac{J_\alpha}{\gamma_\alpha D_\alpha} \right| \\
\gamma_\alpha x + c &= \ln \left| c_\alpha(x) - \frac{J_\alpha}{\gamma_\alpha D_\alpha} \right| \quad (c \text{ is a constant}) \\
e^{\alpha x + c} &= \pm \left(c_\alpha(x) - \frac{J_\alpha}{\gamma_\alpha D_\alpha} \right) \quad \text{on } K_m
\end{aligned}
\tag{5.49}
$$

The molar flux density $J_{\alpha,m+1/2} = J_\alpha(x_{m+1/2})$ $(x_{m+1/2} = \frac{x_m + x_{m+1}}{2})$ can

be written as:

$$\frac{c_{\alpha,m+1} - \frac{J_{m+1/2}}{\gamma_\alpha D_\alpha}}{c_{\alpha,m} - \frac{J_{m+1/2}}{\gamma_\alpha D_\alpha}} = e^{\gamma_\alpha h_m}, \quad \text{where } c_{\alpha,m} = c_\alpha(x_m)$$

$$c_{\alpha,m+1} - \frac{J_{m+1/2}}{\gamma_\alpha D_\alpha} = \left(c_{\alpha,m} - \frac{J_{m+1/2}}{\gamma_\alpha D_\alpha}\right)e^{\gamma_\alpha h_m}$$

$$(e^{\gamma_\alpha h_m} - 1)\frac{J_{m+1/2}}{\gamma_\alpha D} = (-c_{\alpha,m+1} + e^{\gamma_\alpha h_m}c_{\alpha,m}) \tag{5.50}$$

$$J_{m+1/2} = \frac{\gamma_\alpha D_\alpha}{e^{\gamma_\alpha h_m} - 1}(-c_{\alpha,m+1} + e^{\gamma_\alpha h_m}c_{\alpha,m})$$

$$= \frac{D_\alpha}{h_m}[-Be(-\eta_m)c_{\alpha,m+1} + Be(\eta_m)c_{\alpha,m}]$$

where $Be(x) = x/(e^t - 1)$ is the inverse of the Bernoulli function and $\eta_m = (\psi_{m+1} - \psi_m)/V_{th}$.

Therefore, the Scharfetter-Gummel approximation for (5.46) is:

$$\frac{d}{dx}J_\alpha(x_m) \approx \frac{2}{h_m + h_{m-1}}(J_{m+1/2} - J_{m-1/2})$$

$$= \frac{2}{h_m + h_{m-1}}\left[\frac{D}{h_m}(-Be(-\eta_m)c_{\alpha,m+1} + Be(\eta_m)c_{\alpha,m}) + \right.$$

$$\left.\frac{D}{h_{m-1}}(-Be(-\eta_{m-1})c_{\alpha,m} + Be(\eta_{m-1})c_{\alpha,m-1})\right]$$

$$= -Be(\eta_{m-1})c_{\alpha,m-1} + [Be(-\eta_{m-1}) + Be(\eta_m)]c_{\alpha,m} - Be(-\eta_m)c_{\alpha,m+1} = 0 \tag{5.51}$$

The approximation in (5.51) can be derived in an alternative manner, by adding artificial viscosity to the scheme, which has the aim of prevent spurious oscillations (see [1]).

Let us consider the following discrete formulation of (5.36) (where we assume $\beta_{\alpha=0}$):

For each $i = 1, ..., 11$, given ψ_h^{j+1} and $c_{h,\alpha}^j$, $\forall \alpha = 1, .., M_{ion}$, find $c_{h,i,\alpha}^{j+1} :=$

$c_{h,\alpha}^{j+1}|_{\Omega_i} \in V^i$ such that, for each $m = 1, ..., N_h^i$:

$$\int_{\Omega_i} D_\alpha \frac{\partial c_{h,i,\alpha}^{j+1}}{\partial x} \frac{\partial \phi_m^i}{\partial x} \, d\Omega_i + \int_{\Omega_i} v_\alpha^{j+1} \frac{\partial \phi_m^i}{\partial x} c_{h,i,\alpha}^{j+1} \, d\Omega_i +$$

$$\phi_m^i(b_i) J_{i,\alpha}^{j+1}(b_i) \mathrm{n}_i(b_i) + \phi_m^i(a_i) J_{i,\alpha}^{j+1}(a_i) \mathrm{n}_i(a_i) = 0 \tag{5.52}$$

where $v_\alpha^{j+1} = -\mu_{el} \frac{z_\alpha}{|z_\alpha|} \frac{\partial \psi_{h,i}^{j+1}}{\partial x}$. Since $c_{h,i,\alpha}^{j+1} \in V_h^i$ we can express it by the following linear combination:

$$c_{h,i,\alpha}^{j+1}(x) = \sum_{n=1}^{N_h^i} c_{h,i,\alpha}^{j+1,n} \phi_n^i(x) \tag{5.53}$$

Let us introduce now the matrices $\boldsymbol{A}_{i,\alpha}$, $\boldsymbol{B}_{i,\alpha}$ and the vectors $\boldsymbol{C}_{i,\alpha}$ and $\boldsymbol{J}_{i,\alpha}$, such that:

$$A_{mn} = \int_{\Omega_i} D_\alpha \frac{\partial \phi_m^j}{\partial x} \frac{\partial \phi_n^i}{\partial x} \, d\Omega_i \tag{5.54}$$

$$B_{mn} = \int_{\Omega_i} \phi_n^i \frac{\partial \phi_m^i}{\partial x} c_{h,i,\alpha}^{j+1} \, d\Omega_i \tag{5.55}$$

$$\boldsymbol{C}_{i,\alpha} = [c_{h,i,\alpha}^{j+1,1}, ..., c_{h,i,\alpha}^{j+1,N_h^i}]^T \tag{5.56}$$

$$\boldsymbol{J}_{i,\alpha} = [J_{i,\alpha}^{j+1}(a_i)\mathrm{n}_i(a_i), 0, ..., 0, J_{i,\alpha}^{j+1}(b_i)\mathrm{n}_i(b_i)]^T \tag{5.57}$$

The algebraic formulation reads:

Find $\boldsymbol{C}_{i,\alpha}$ such that

$$(\boldsymbol{A}_{i,\alpha} + \boldsymbol{B}_{i,\alpha})\boldsymbol{C}_{i,\alpha} + \boldsymbol{J}_{i,\alpha} = \boldsymbol{0} \tag{5.58}$$

that must be completed with suitable interface conditions.

Finally, we introduce the same discrete space of test functions and the same basis as in the previous section. Moreover, let us define the *local Peclet number*

$$Pe_k = \frac{|v_\alpha^{j+1,m}| h_m}{2 D_\alpha^m} \tag{5.59}$$

where $v_\alpha^{j+1,m} = v_\alpha^{j+1}((x_{m+1} - x_m)/2)$ and $D_\alpha^m = D_\alpha((x_{m+1} - x_m)/2)$. In order to add artificial viscosity to the scheme, we replace the diffusion coefficient

D_α in the finite element formulation, introducing the Scharfetter-Gummel modified coefficient:

$$D_\alpha^{SG} = D_\alpha(1 + \Phi_{SG}(Pe_k)) \tag{5.60}$$

where $\Phi_{SG}(x) = x - 1 + Be(2x)$.

Chapter 6

Numerical simulations

The aim of this chapter is to illustrate some numerical results obtained by running a computer code written in Matlab, implementing the methodologies described in chapter 5. To start, we will investigate some test cases in a simplified geometry and we will comment the main relevant results.

In particular, we are interested in the Na^+ molar flux densitiy and the Cl^- molar flux density, since we know that a net current of Na^+ and Cl^- ions from the Stroma to the PC is crucial in AH secretion (see section 2.1.1).

In our simplified models, we assume a membrane specific capacitance of $10^{-2} Fm^{-2}$ for each membrane. The specific capacitance of biological membranes can be estimated dividing the dielectric constant of lipids ε_m by the thickness of the bilayer t_m [11].

Values for membrane permeabilities P_α for each ion species α at each membrane and the diffusion coefficients D_α used in the simulations are set equal to those proposed in [7] and they are reported in tables 6.2 and 6.3. Boundary conditions used for ψ and c_α in the (S) and (PC) compartments, taken from [19], are reported in table 6.1.

	Value	Unit		Value	Unit
ψ^S	0.0	V	ψ^{PC}	0.02	V
c_{Na}^S	137.5	mM	c_{Na}^{PC}	143.0	mM
$c_{K^+}^S$	4.25	mM	$c_{K^+}^{PC}$	4.0	mM
$c_{H^+}^S$	7.4	mM	$c_{H^+}^{PC}$	7.21	mM
$c_{Cl^-}^S$	110.0	mM	$c_{Cl^-}^{PC}$	131.0	mM
$c_{HCO_3^-}^S$	27.0	mM	$c_{HCO_3^-}^{PC}$	20.0	mM

Table 6.1: Boundary conditions: Values of the electric potential and ion concentrations in the Stroma and in the posterior chamber ([19]).

	$D_\alpha \ [m^2 s^{-1}]$
Na^+	$1.33 \cdot 10^{-9}$
K^+	$1.96 \cdot 10^{-9}$
H^+	$1.96 \cdot 10^{-9}$
Cl^-	$2.03 \cdot 10^{-9}$
HCO_3^-	$1.18 \cdot 10^{-9}$

Table 6.2: Values for the ions diffusion coefficients [7]

6.1 Test cases for the Debye length

Figure 6.1: Geometrical domain used in the following tests. We consider the presence of ion channels for each species α in the membranes at $x = 0$ and $x = l$.

Membrane	Na^+	K^+	H^+	Cl^-	HCO_3^-
PE Basoloateral membrane	0	$5.20 \cdot 10^{-7}$	0	$1.08 \cdot 10^{-7}$	0
NPE Basoloateral membrane	$3.0 \cdot 10^{-8}$	$1.58 \cdot 10^{-5}$	0	$4.5 \cdot 10^{-7}$	0
Tight junction	$3.0 \cdot 10^{-7}$	$4.42 \cdot 10^{-8}$	$4.42 \cdot 10^{-8}$	$3.0 \cdot 10^{-8}$	$1.74 \cdot 10^{-8}$
PS-S & PS-PC membrane	$3 \cdot 10^{-2}$	$4.42 \cdot 10^{-3}$	$4.42 \cdot 10^{-2}$	$3.0 \cdot 10^{-3}$	$1.74 \cdot 10^{-2}$

Table 6.3: Values for membrane permeabilities. [7]

The principal objective of this series of test problem is to verify whether the code is able to correctly describe the condition of electroneutrality away from membranes. For this purpose, we take as domain $\Omega = [0, l]$, and we consider only the presence of ion channels for each ion $\alpha \in [Na^+, K^+, H^+, Cl^-, HCO_3^-]$ in the membranes placed in $x = 0$ and $x = l$. We take $P_\alpha = 10^{-4} ms^{-1}$ for each ion α and we set $c_\alpha^-(0) = \bar{c}_\alpha^L$ and $c_\alpha^+(l) = \bar{c}_\alpha^R$ (see figure 6.1).

Since we know that the Debye length is inversely proportional to the quantity

$$c_{ref} = \max \left\{ \max_\alpha (\bar{c}_\alpha^L), \max_\alpha (\bar{c}_\alpha^R) \right\} \qquad (6.1)$$

we simulate different tests by varying the concentrations at the boundary $\bar{c}_\alpha^L$ and $\bar{c}_\alpha^R$: first we consider $\bar{c}_\alpha^L = \bar{c}_\alpha^R = 100 \ mM$, then $\bar{c}_\alpha^L = \bar{c}_\alpha^R = 1 \ mM$, then $\bar{c}_\alpha^L = \bar{c}_\alpha^R = 10^{-2} \ mM$ and finally $\bar{c}_\alpha^L = \bar{c}_\alpha^R = 10^{-4} \ mM$. Based on the different choices of $\bar{c}_\alpha^L, \bar{c}_\alpha^R$, we expect the Debye length to assume increasing values. This has the consequence that the boundary layers in the neighborhood of the membranes will be larger as $\bar{c}_\alpha^L, \bar{c}_\alpha^R$ become smaller. For each test we plot the electric potential ψ and the total charge density Q

($[Cm^{-3}]$), defined as

$$Q(x) = F \sum_{\alpha=1}^{M_{ion}} z_\alpha c_\alpha(x) \qquad (6.2)$$

Test 1. $\bar{c}_\alpha^L = \bar{c}_\alpha^R = 100 \ mM$

Considering $c_{ref} = 100mM$ as reference value, the resulting Debye length is

$$r_d = \sqrt{\frac{\varepsilon_W V_{th}}{F c_{ref}}} = 1.4004 \cdot 10^{-9} \qquad (6.3)$$

where $\varepsilon_W = \varepsilon_0 \epsilon_W$ ($\epsilon_W = 80$) ($[Fm^{-1}]$) is the dielectric permittivity of water.

Since we have $l = 10^{-6} \ m$, in our computation we need to use a mesh with 1000 elements at least, in order to correctly catch the scale of the boundary layers. We choose $n_{el} = 2000$ elements.

The Gummel map required 6 iterations to converge, with a final relative error $err_{Gummel} = 4.0136 \cdot 10^{-11}$, where

$$err_{Gummel} = \max_\alpha \frac{||\psi_\alpha^{ec,j+1} - \psi_\alpha^{ec,j}||_{L^\infty}}{||\psi_\alpha^{ec,j+1}||_{L^\infty}} \qquad (6.4)$$

Figure 6.2 shows the spatial distribution of electric potential and total charge density. Figure 6.3 shows that a proper choice of the mesh size allows us to numerically resolve the boundary layers and, away from membranes, verify the electroneutrality of the ionic solution. Consistently, the spatial distribution of the electric potential turns out to be linear.

In figure 6.4, we decreased the number of elements used in the mesh. In particular, we can note that as soon as we choose an unsuitable refinement (that is, a mesh size larger than r_d), the solution is unable to catch the boundary layers at the membranes.
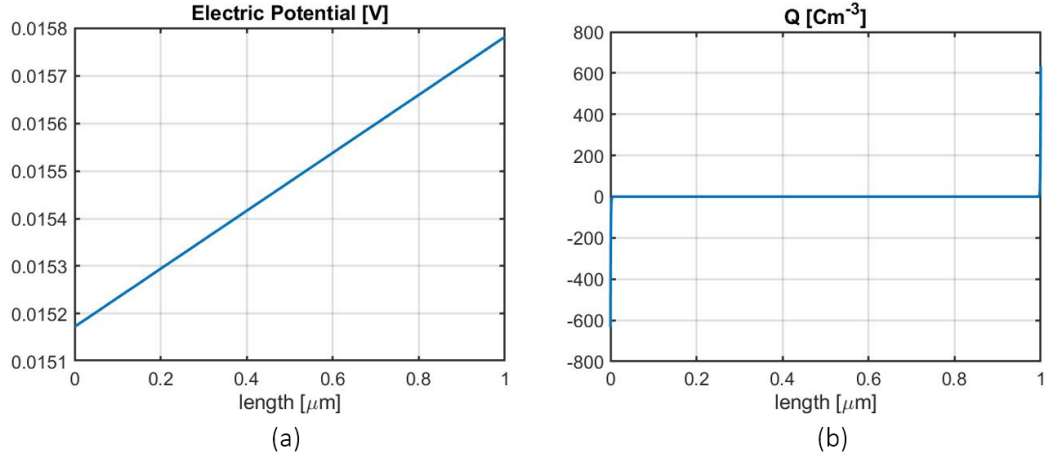
Figure 6.2: Test case 1: electric potential (a) and total charge density (b) obtained using a mesh with $n_{el} = 2000$ elements.
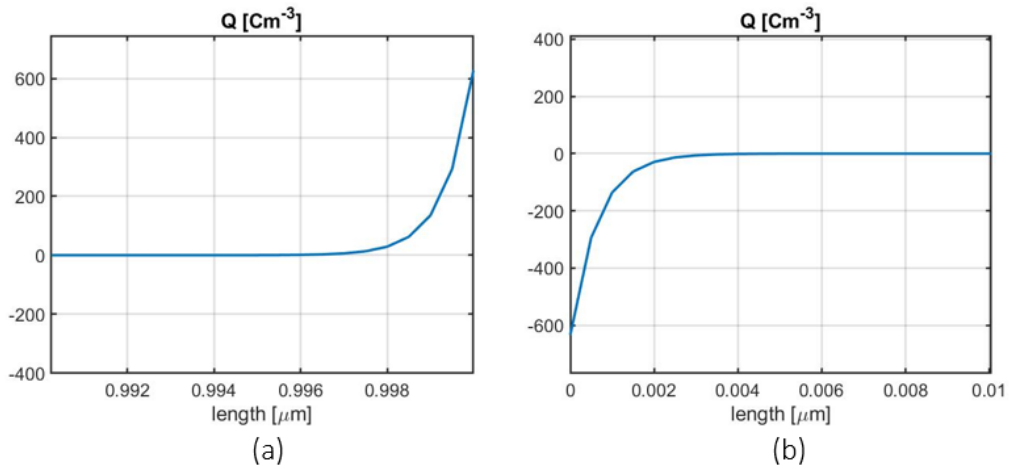

Figure 6.3: Test case 1: (a) zoom of $Q(x)$ in the neighborhood of $x = 0$. (b) zoom of $Q(x)$ in the neighborhood of $x = 0$. Notice the formation of two marked boundary layers of the order of r_d.
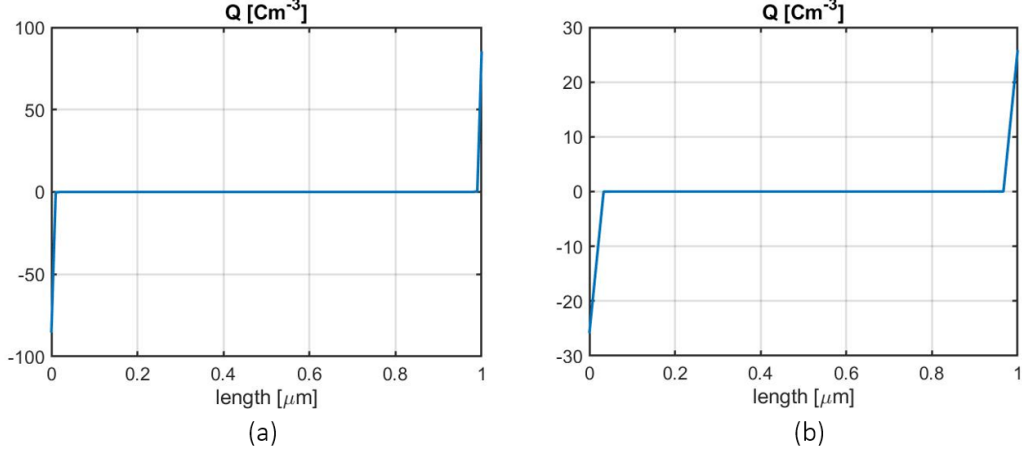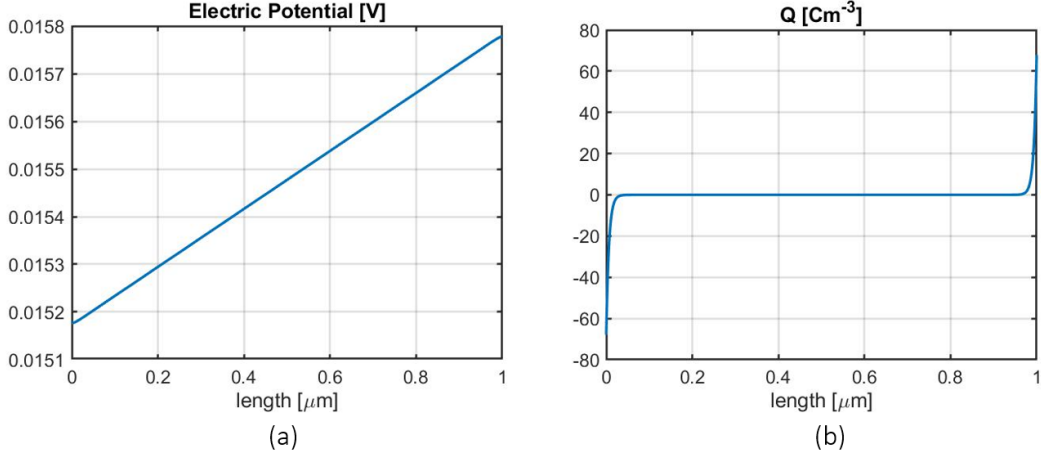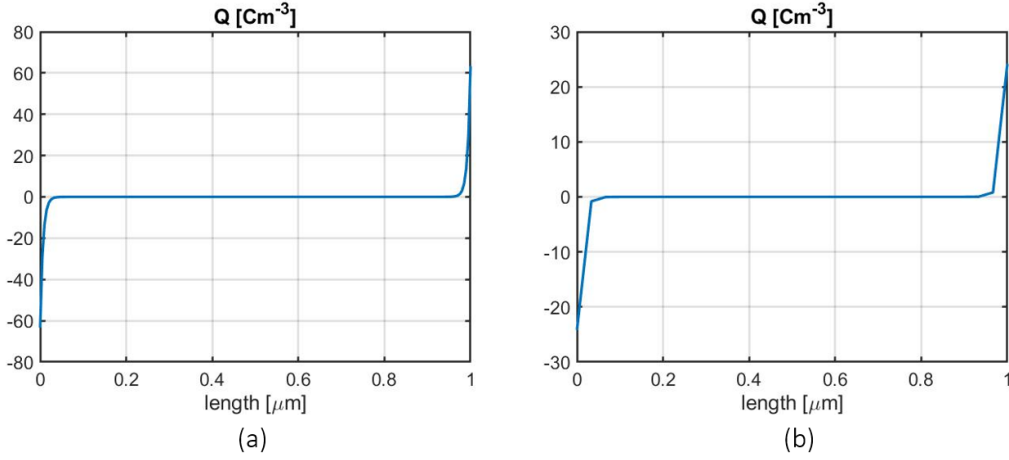
Figure 6.4: Test case 1: total charge density obtained using $n_{el} = 200$ (a) and $n_{el} = 30$(b).

Test 2. $\bar{c}_\alpha^L = \bar{c}_\alpha^R = 1 \ mM$

The resulting Debye length is $c_{ref} = 1.4004 \cdot 10^{-8}$, thus we should take a mesh refinement with $n_{el} = 100$ at least.

Using $n_{el} = 1000$, Gummel map requires 9 iterations to converge, with a final relative error $err_{Gummel} = 5.5369 \cdot 10^{-11}$.

Figure 6.5 shows the spatial distribution of electric potential and total charge density. In figure 6.6 we plot $Q(x)$ computed using two different values of n_{el}. We observe that taking $n_{el} = 200$ does not significantly spoil the accuracy of the result, as the graphs for the total charge Q are almost identical. This is not the case when $n_e l = 30$ (right panel of figure 6.6).
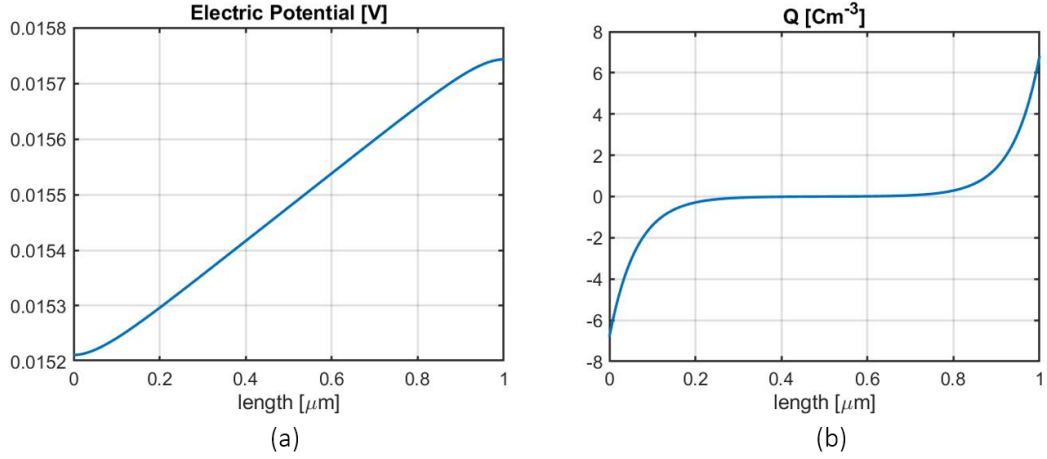
Figure 6.5: Test case 2: electric potential (a) and total charge density (b) obtained using a mesh with $n_{el} = 1000$ elements.

Figure 6.6: Test case 2: total charge density obtained using $n_{el} = 200$ (a) and $n_{el} = 30$(b).

Test 3. $\bar{c}_\alpha^L = \bar{c}_\alpha^R = 10^{-2} \ mM$ The resulting Debye length is $c_{ref} = 1.4004 \cdot 10^{-7}$, thus we should take a mesh refinement with $n_{el} = 10$ at least.

Using $n_{el} = 1000$, the code converges within 13 Gummel iterations, with a final relative error $err_{Gummel} = 6.4762 \cdot 10^{-11}$.

Figure 6.7: Test case 3: electric potential (a) and total charge density (b) obtained using a mesh with $n_{el} = 1000$ elements.

Comparing the spatial distribution of $Q(x)$ shown in figure 6.8 and figure 6.7, we see that the choice of the mesh size does affect model predictions, as expected.
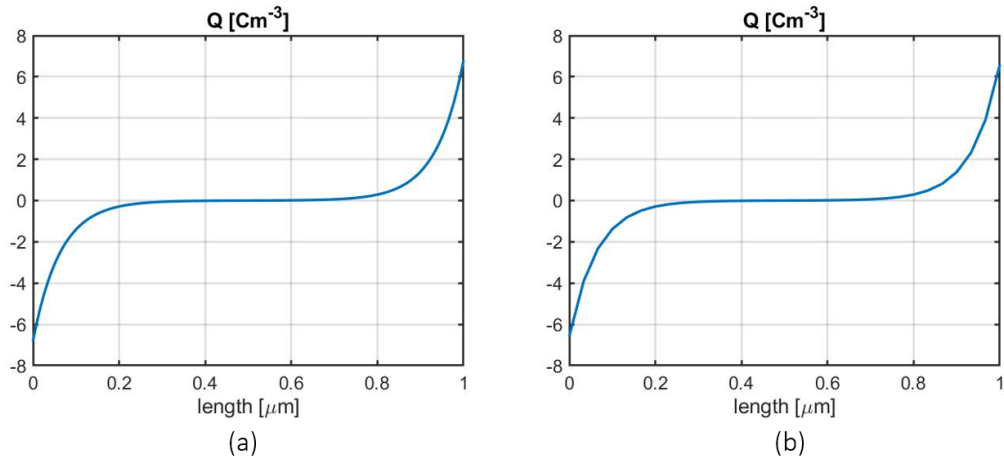
Figure 6.8: Test case 3: total charge density obtained using $n_{el} = 200$ (a) and $n_{el} = 30$(b).

Test 4. $\bar{c}_\alpha^L = \bar{c}_\alpha^R = 10^{-4} \ mM$ The resulting Debye length is $c_{ref} = 1.4004 \cdot 10^{-6}$, thus it is of the same order of magnitude as the domain length. In this case, we expect that we are not able to see any boundary layers.

Using $n_{el} = 1000$, the code converges in 17 iterations, with a final relative error $err_{Gummel} = 4.5566e - 11$. Results are shown in the figure 6.9 and 6.10 and they are in agreement with our expectation.
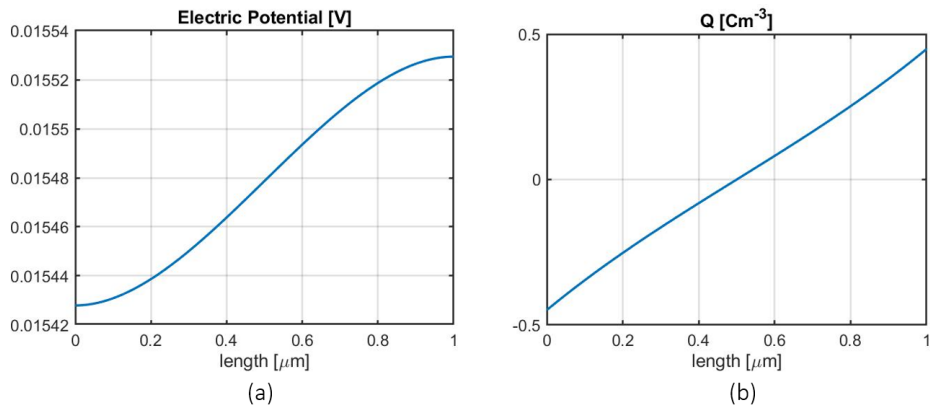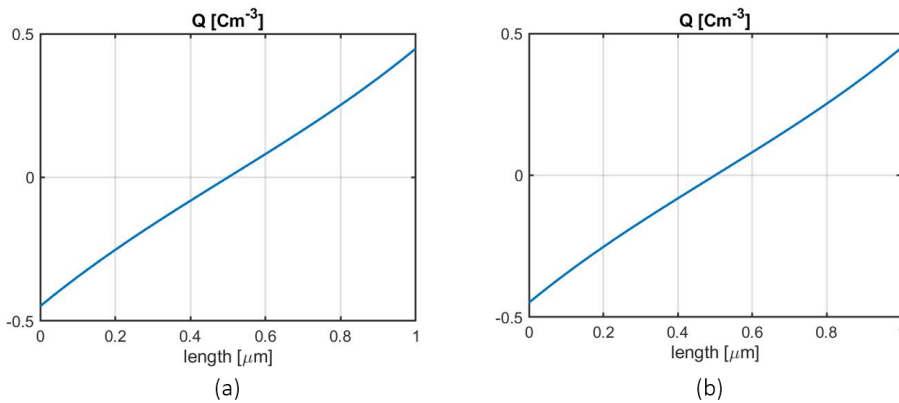

Figure 6.9: Test case 4: electric potential (a) and total charge density (b) obtained using a mesh with $n_{el} = 1000$ elements.

Figure 6.10: Test case 4: total charge density obtained using $n_{el} = 200$ (a) and $n_{el} = 30$(b).

6.2 1-edge domain: Unidirectional flow of Na^+ and from S to PC

Figure 6.11: Domain of the 1-edge domain. PE and NPE compartments are described by a single edge.

Here we want to implement the scheme described in figure 2.2, which we report in figure 6.12. The aim of this simulation is to study the unidirectional flow of ions from the Stroma to the PC taking into consideration just a transmembrane pathway. Under this configuration, we expect to observe a net molar flux density of sodium and chloride from S to PC and a flow of potassium in th opposite direction.
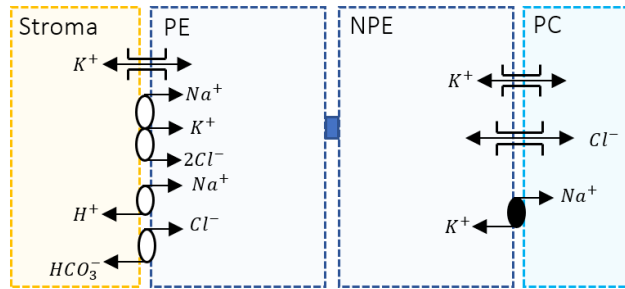
Figure 6.12: Scheme of the transmembrane transporters considered in this simulation

We will consider as computational domain a single edge structure of length $l = 10^{-6}m$, that represents the PE-NPE intercellular spaces (see figure 6.11). Moreover, since we have as reference concentration $c_{ref} = 10^1 \sim$

$10^2 mM$, we consider a mesh refinement with $n_{el} = 1000$, in order to have an element length of the order of the Debye length.

In figure 6.11, node S represents the basolateral membrane of the PE, thus values for membrane permeabilities for each ion species α are set as in table 6.3, first row. Node PC represents the basolateral membrane of the NPE, thus for the membrane permeabilities we refer to table 6.3, second row. Diffusion coefficients and boundary values are reported in table 6.2 and 6.1, respectively.

the molar densities for each ionα. Figure 6.15 shows the electric potential and the total electric charge density. In figure 6.13 we reported a graphic description of the values obtained for the molar flux densities J_α.

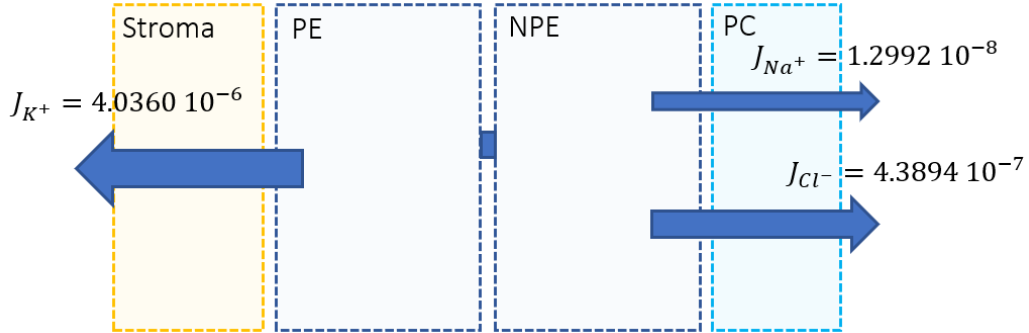
Figure 6.13: Molar flux densities obtained in the 1-edge simulation. The arrows represent the flow directions of the ions.

In agreement with biphysical expectations, we obtained zero molar flux densities for HCO_3^- and H^+, as we did not insert transporters for these ions on the NPE basolateral membrane. Furthermore, we obtained a net flow of Chlorine and Sodium from the Stroma to the posterior chamber.
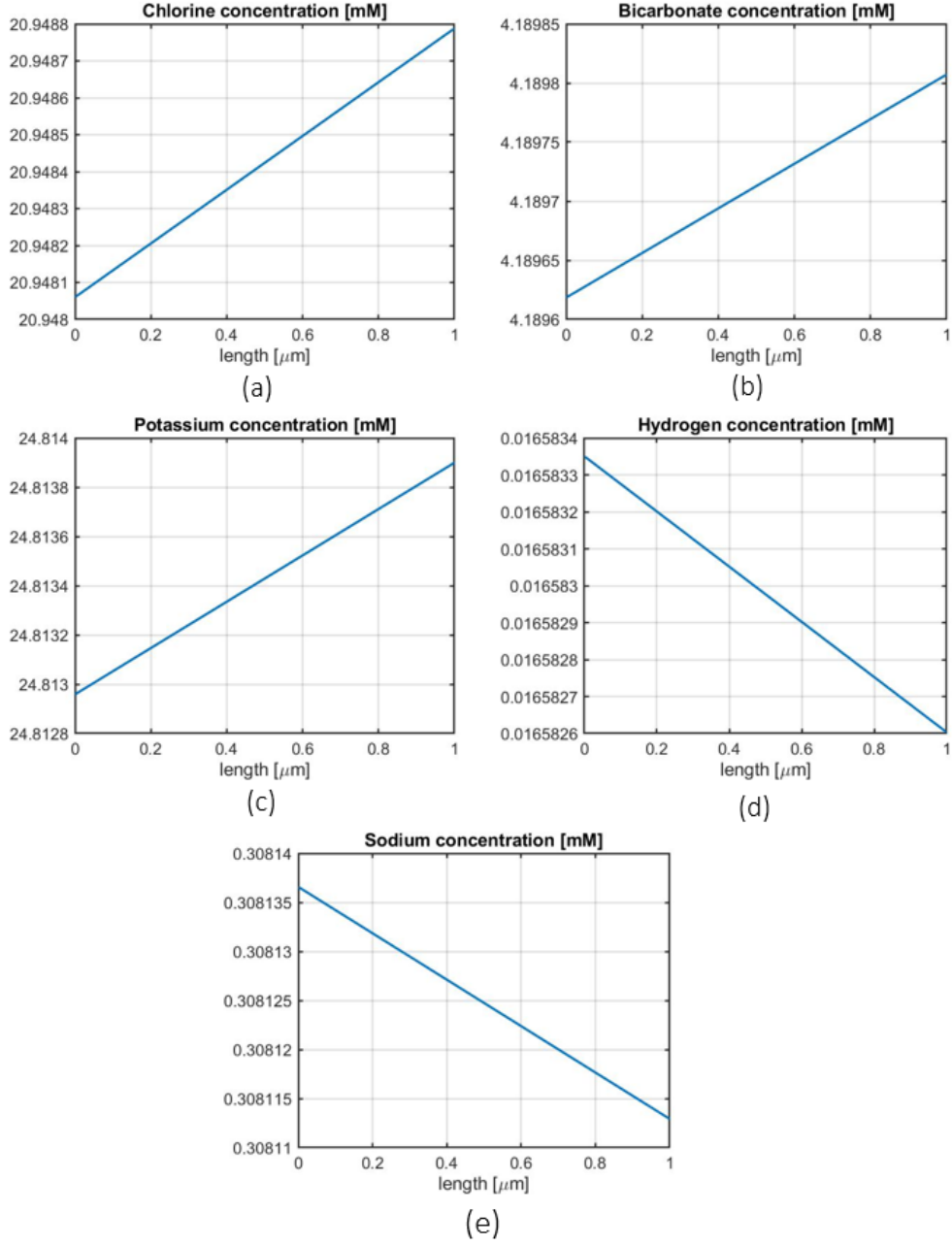
Figure 6.14: Results for the 1-edge test case: (a) Cl^- concentration, (b) HCO_3^- concentration, (c) K^+ concentration, (d) H^+ concentration, (e) Na^+ concentration.
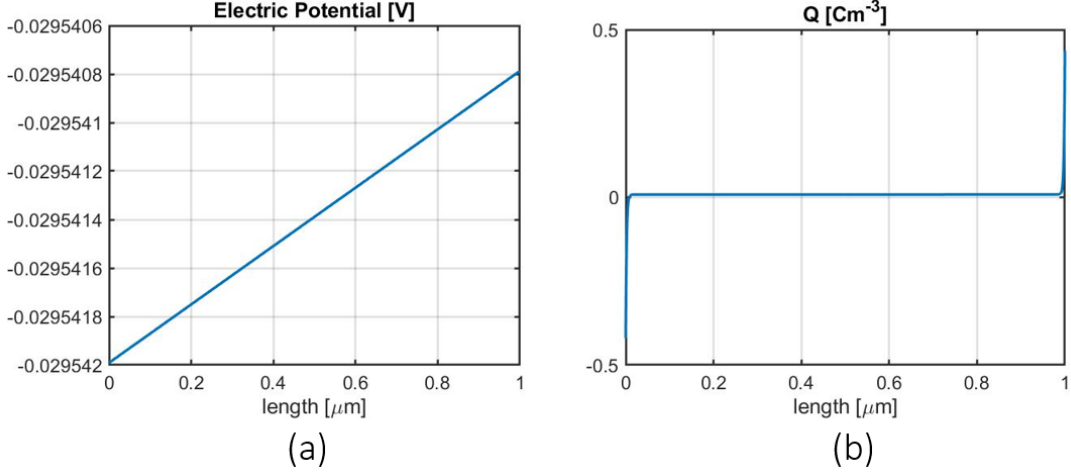
Figure 6.15: Results for the 1-edge test case: (a) Electric potential, (b) Total charge density

6.3 Network geometry

As final step we will now investigate the molar flux densities obtained using the Network geometry of figure 4.5, since we want to try to give a description of both transmbembrane and paracellular flows.

For the simulation we assume a length of 10^{-6} m for each edge of the Network and we will consider the presence of the transporters depicted in figure 2.10, which for convenience we report in figure 6.16. Boundary conditions are reported in table 6.1, in particular we assume ψ^S and c_α^S on the stromal side in A and B and ψ^S and c_α^S on the PC side in F and G. Membrane permeabilities and diffusion coefficients are reported in tables 6.3 and 6.2.

For the simulation, we used $n_{el} = 500$ element for each edge of the network. The algorithm converged in 43 iterations with $err_{Gummel} = 8.8920 \cdot 10^{-11}$. Results for the spatial distribution of each ion molar density and the electric potetial are plotted in the following graphs.
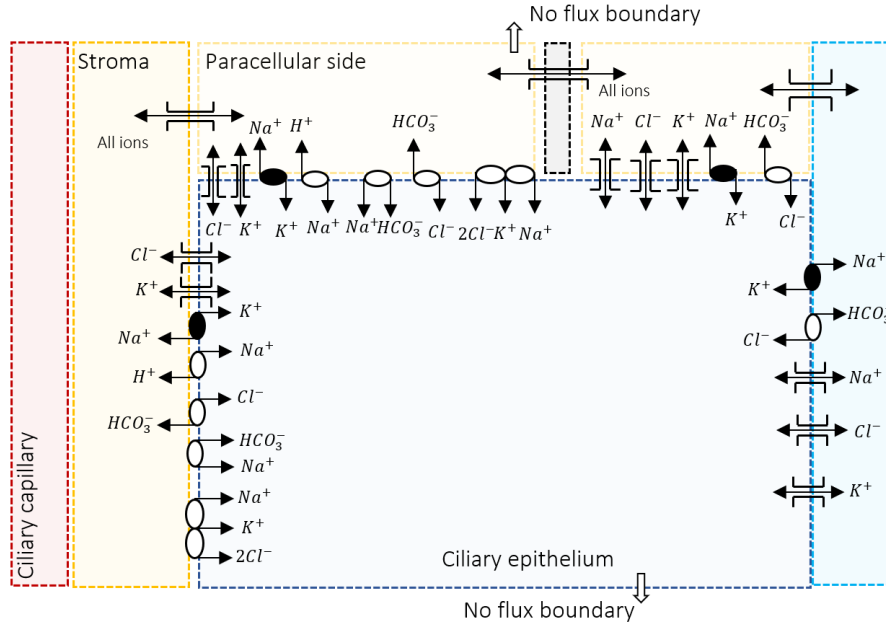
Figure 6.16: Scheme of the trasmembrane transporters included in the Network test case.
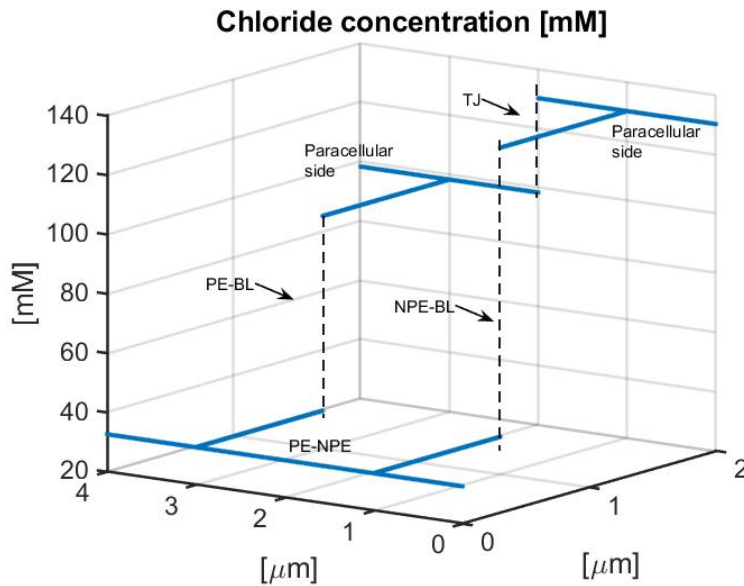

Figure 6.17: Network test: Cl^- concentration. TJ: Tight junction, NPE-BL: NPE basolateral membrane, PE-BL: PE basolateral membrane.

Figure 6.18: Network test: HCO_3^- concentration. TJ: Tight junction, NPE-BL: NPE basolateral membrane, PE-BL: PE basolateral membrane.

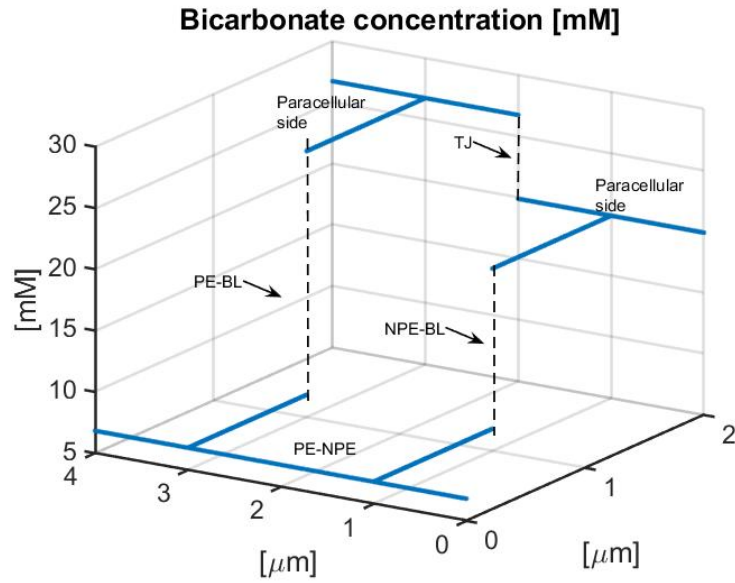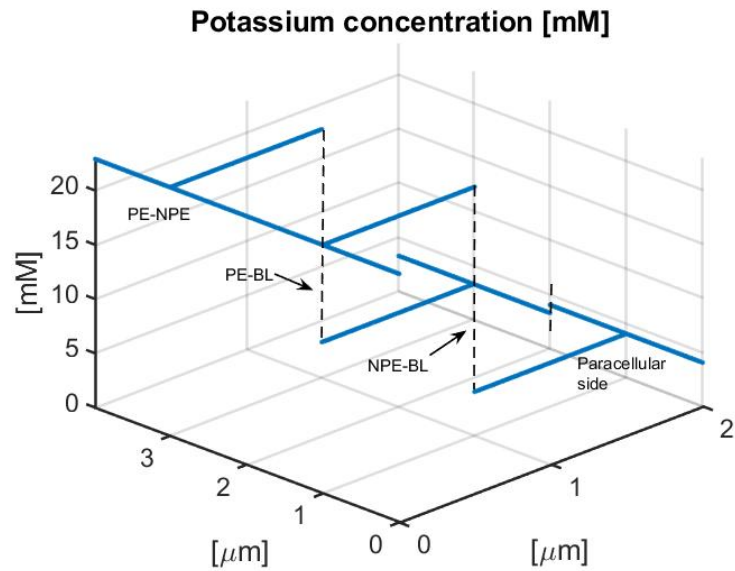Figure 6.19: Network test: K^+ concentration. TJ: Tight junction, NPE-BL: NPE basolateral membrane, PE-BL: PE basolateral membrane.

Figure 6.20: Network test: H^+ concentration. TJ: Tight junction, NPE-BL: NPE basolateral membrane, PE-BL: PE basolateral membrane.
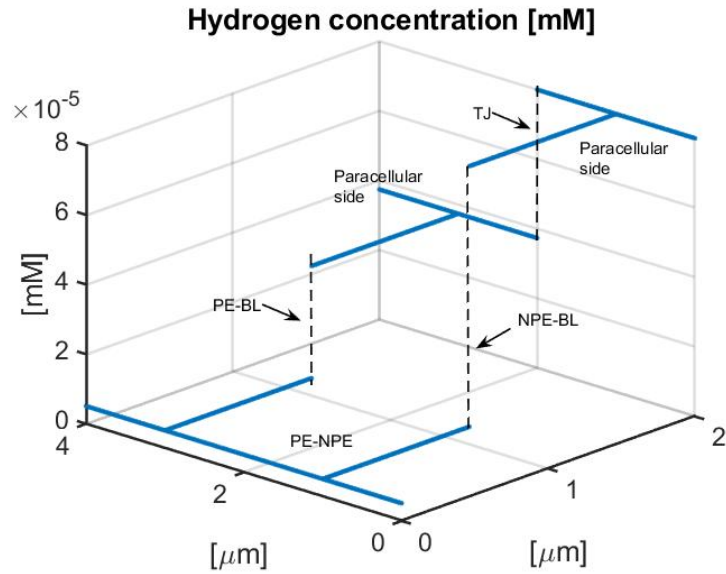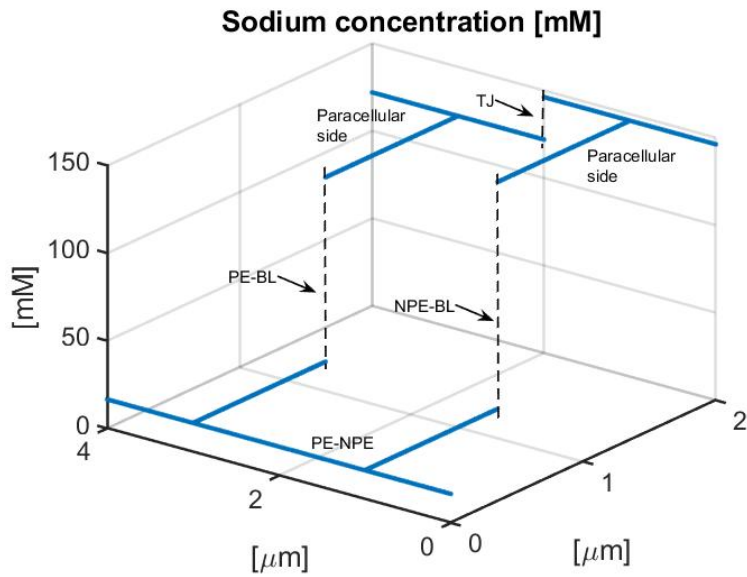

Figure 6.21: Network test: Na^+ concentration. TJ: Tight junction, NPE-BL: NPE basolateral membrane, PE-BL: PE basolateral membrane.
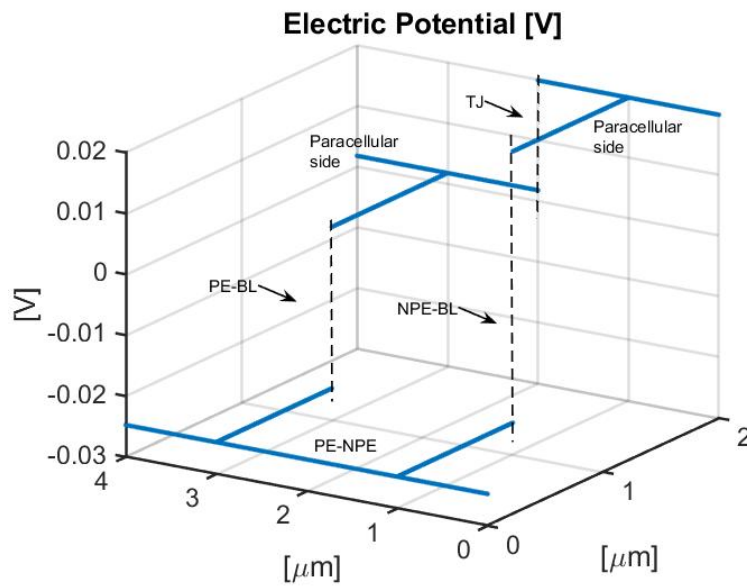
96

Figure 6.22: Network test: Electric potential distribution. TJ: Tight junction, NPE-BL: NPE basolateral membrane, PE-BL: PE basolateral membrane.

Figure 6.23 is a schematic representation of the Na^+ molar flux density obtained in the simulation. In accordance with biophysical expectations, we can observe the Na^+ is flowing from S to PC following a transmembrane pathway. Nevertheless, the paracellular side is characterized by a backward flow of sodium, which recirculates from PC to the stroma. Therefore, the total flux density is the sum of two contributions with opposite sign.

Although the orders of magnitude of the two molar flux densities are the same in figure 6.23, one should remember that the secretion surface of the NPE basolateral membrane is much higher than the secretion surface of the paracellular space. For this reason, in the calculation of the total ionic current, we can consider the contribution due to the paracellular pathway to be negligible.
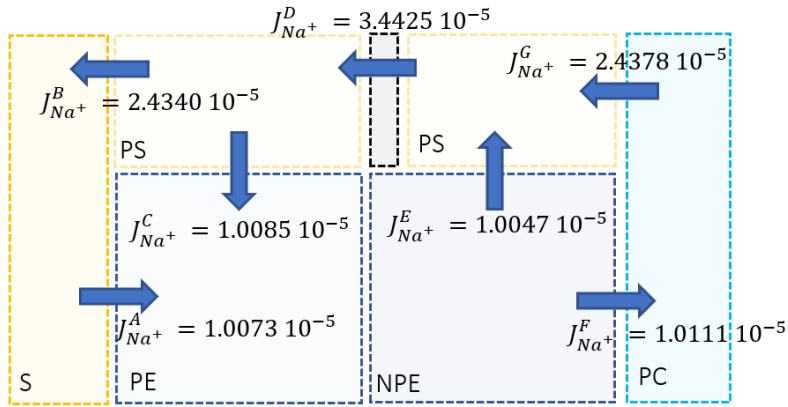

Figure 6.23: Schematic representation of J_{Na^+} along the Network. The arrow direction indicates the direction of the flux.
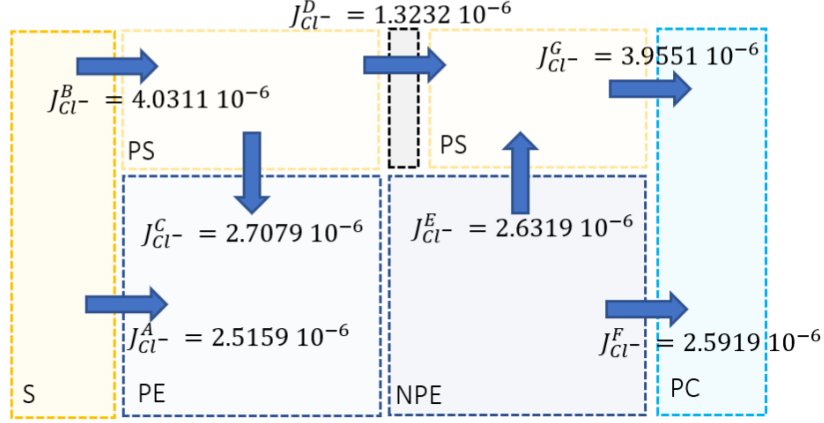
Figure 6.24: Schematic representation of J_{Cl^-} along the Network. The arrow direction indicates the direction of the flux.

In Figure 6.24 we illustrate the obtained Cl^- molar flux density. In this case we have that both the paracellular pathway and the transmembrane pathway promote a flow of chlorine from the stroma towards the posterior chamber. Moreover, as above, the orders of magnitude of the two contributions are the same, thus also in this case the transmembrane pathway plays a relevant role in the computation of th total current of Cl^- flowing across the ciliary epithelium.

It is interesting to notice that, besides having a similar intracellular pathway, Chloride and Sodium shows an opposite flow direction in the paracellular path.

Finally, in figure 6.25 we represented the obtained values for J_{K^+} along the Network. Consistently with what was expected, in this case we obtained that the the potassium flows from the posterior chamber to the Stroma.

$J_{K^+}^D = 1.4217\ 10^{-7}$

$J_{K^+}^G = 3.5204\ 10^{-6}$

$J_{K^+}^B = 3.0997\ 10^{-6}$

PS

PS

$J_{K^+}^C = 2.9576\ 10^{-6}$

$J_{K^+}^E = 2.5860\ 10^{-6}$

$J_{K^+}^A = 3.1488\ 10^{-6}$
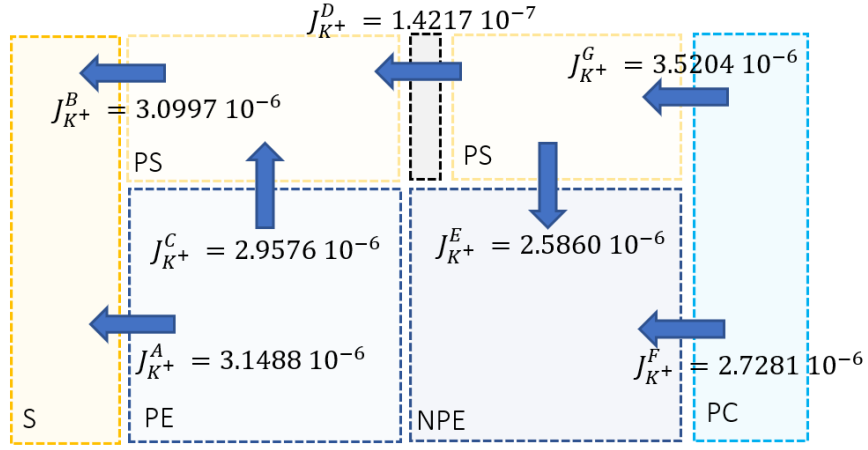
$J_{K^+}^F = 2.7281\ 10^{-6}$

S

PE

NPE

PC

Figure 6.25: Schematic representation of J_{K^+} along the Network.The arrow direction indicates the direction of the flux.

Chapter 7

Conclusions and perspectives

In this thesis we proposed and numerically implemented a continuum-based model for the description of ion electrodiffusion across the ciliary epithelium of the human eye. In particular, using the PNP equations we have developed a cellular scale model, treating the membrane scale by means of the inclusion of lumped models for the ionic molar flux densities passing through the different transporters present on the basolateral membranes of PE and NPE cells. Then, we performed several numerical tests in order to investigate if the model is able to predict correctly what we discussed in chapter 2, namely, that the osmotic pressure driving the secretion of AH is due to a flow of Na^+ and Cl^- through the ciliary epithelium from stroma to the posterior chamber.

The results of our simulations are in agreement with biological expectations. In particular, we observed that in the case of Na^+ we obtained a recirculation from PC to the stromal compartment through the paracellular pathway. However this contribution turns out to be negligible with respect to the transmembrane flow, thus the net molar flux density flows from the stroma to the posterior chamber.

For the Cl^- we found a positive flow of ions from S to PC both for the paracellular and the transmembrane pathway. Moreover, we concluded that also in this case the transmembrane pathway plays the major role.

Despite being able to accurate describe ion electrodiffusion across the ciliary epithelium, the proposed model is affected by several important limitations due to the numerous simplifying assumptions made in the description of the biological processes. In this sense, we can say that th model is at its early stages. In particular, we have neglected the intracellular chemical reactions and we the presence of a fixed charge inside the cytoplasm. The inclusion of these aspects, which are known to play an important role in determining the ion distribution in the compartments, could be a valid theme for future projects.

Moreover, the final step for model improvement is the inclusion of the fluid part in order to provide a complete description of AH secretion. To this purpose, one must include in the model the Navier-Stokes equations to describe the fluid component of the mixture.

Appendix A

A.1 Transport theorem

Theorem *(Transport theorem) Let $\phi = \phi(\boldsymbol{x}, t)$ be a scalar field defined on $\mathcal{V}_t \times (0, T)$, where $\mathcal{V}_t$ is a material volume. Let $\bar{\boldsymbol{v}}$ be the Eulerian velocity in $\mathcal{V}_t$, then:*

$$\frac{d}{dt} \int_{\mathcal{V}_t} \phi(\boldsymbol{x}, t) d\mathcal{V}_t = \int_{\mathcal{V}_t} \left(\frac{\partial \phi}{\partial t}(\boldsymbol{x}, t) + \nabla_{\boldsymbol{x}} \cdot (\phi \bar{\boldsymbol{v}})(\boldsymbol{x}, t) \right) d\mathcal{V}_t \qquad \text{(A.1)}$$

A.2 Divergence theorem

Theorem *(Divergence theorem) Let $\Omega \subset \mathbb{R}$ be a compact set with smooth boundary $\partial\Omega$, and $\boldsymbol{\phi}$ be a continuously differentiable vector field defined on $\bar{\Omega}$. The following relation holds:*

$$\int_{\Omega} \nabla_{\boldsymbol{x}} \cdot \underline{\boldsymbol{\phi}} \, d\Omega = \int_{\partial\Omega} \underline{\boldsymbol{\phi}} \cdot \underline{n} \, d(\partial\Omega) \qquad \text{(A.2)}$$

A.3 Reynold's theorem

The Reynold's theorem can be derived by applying the transport theorem to a scalar function ϕ of the form $\phi(\boldsymbol{x}, t) = \rho(\boldsymbol{x}, t)\eta(\boldsymbol{x}, t)$ where $\rho(\boldsymbol{x}, t)$ is the mass density and $\eta(\boldsymbol{x}, t)$ is a scalar field, and then applying the balance of mass in local form:

$$\frac{d}{dt} \int_{\mathcal{V}_t} \rho \eta d\mathcal{V}_t = \int_{\mathcal{V}_t} \rho \frac{D\eta}{Dt} d\mathcal{V}_t + \int_{\mathcal{V}_t} \beta \eta d\mathcal{V}_t \qquad (A.3)$$

Bibliography

[1] Sacco R. Guidoboni G. Mauri A.G. *A Comprehensive Physically Based Approach to Modeling in Bioengineering and Life Sciences.* Intermediate Physics for Medicine and Biology. Springer Cham, 2015. ISBN: 978-3-319-12681-4.

[2] Clay Armstrong. "The Na/K pump, Cl ion, and osmotic stabilization of cells". In: *Proceedings of the National Academy of Sciences of the United States of America* 100 (June 2003), pp. 6257–62. DOI: 10.1073/pnas.0931278100.

[3] M. Coca-Prados and J. Sánchez-Torres. "Chapter 2 Molecular Approaches to the Study of the Na+,K+ -ATPase and Chloride Channels in the Ocular Ciliary Epithelium". In: *Current Topics in Membranes* 45 (1997), pp. 25–53.

[4] Mary Frame David Rubenstein Wei Yin. *Biofluid Mechanics. An Introduction to Fluid Mechanics, Macrocirculation, and Microcirculation. Chapter 10.* Biomedical Engineering. Academic Press, 2015. ISBN: 9780128009444.

[5] Johnson G.J. Foster P.J. - Buhrmann R.- Quigley H.A. "The definition and classification of glaucoma in prevalence surveys." In: *The British*

journal of ophthalmology 86.2 (2002), pp. 238–42. DOI: `10.1136/bjo.86.2.238`.

[6]   B'Ann Gabelt and Paul Kaufman. "Production and Flow of Aqueous Humor". In: *Adler's Physiology of the Eye* (Jan. 2011), pp. 274–307. DOI: `10.1016/B978-0-323-05714-1.00011-X`.

[7]   Guilherme J.M. Garcia, Richard Boucher, and Timothy Elston. "Biophysical Model of Ion Transport across Human Respiratory Epithelia Allows Quantification of Ion Permeabilities". In: *Biophysical journal* 104 (Feb. 2013), pp. 716–26. DOI: `10.1016/j.bpj.2012.12.040`.

[8]   Manik Goel et al. "Aqueous Humor Dynamics: A Review". In: *The open ophthalmology journal* 4 (Sept. 2010), pp. 52–9. DOI: `10.2174/1874364101004010052`.

[9]   H.K. Gummel. "A self-consistent iterative scheme for one-dimensional steady state transistor calculations". In: *IEEE Transactions on Electron Devices* 11.10 (1964), pp. 455–465. DOI: `10.1109/T-ED.1964.15364`.

[10] Davson H. "Aqueous humor and the intraocular pressure. In: Davson, H., editor. Physiology of the Eye." In: Academic Press, 1990, pp. 9–81. ISBN: 978-953-307-591-4. DOI: `10.5772/26559`.

[11] Hobbie R - Russel K. *The Principles of Quantum Mechanics*. Intermediate Physics for Medicine and Biology. Springer Cham, 2015. ISBN: 978-3-319-12681-4.

[12] Anita T Layton and Aurélie Edwards. *Mathematical Modeling in Renal Physiology - Chaper 10*. 2014.

[13] Jinn-Liang Liu. *Scharfetter-Gummel Method*. URL: `http://www.nhcue.edu.tw/~jinnliu/proj/Device/SGMethod.pdf`.

[14] Yoichiro Mori. "A three-dimensional model of cellular electrical activity". In: (Jan. 2006).

[15] Delamere N.A. "Ciliary Body and Ciliary Epithelium". In: *Advances in organ biology* 10 (1905), pp. 127–148. DOI: `10.1016/S1569-2590(05) 10005-6`.

[16] G Raviola and E Raviola. "Intercellular junctions in the ciliary epithelium." In: *Investigative Ophthalmology Visual Science* 17.10 (Oct. 1978), pp. 958–981. ISSN: 1552-5783. eprint: `https://arvojournals. org/arvo/content\_public/journal/iovs/933308/958.pdf`.

[17] Giuseppina Raviola. "The structural basis of the blood-ocular barriers". In: *Experimental Eye Research* 25 (1977). The Ocular and Cerebrospinal Fluids, pp. 27–63. ISSN: 0014-4835. DOI: `https : / / doi . org / 10 . 1016 / S0014 - 4835(77 ) 80009 - 2`. URL: `https : / / www . sciencedirect.com/science/article/pii/S0014483577800092`.

[18] D.L. Scharfetter and H.K. Gummel. "Large-signal analysis of a silicon Read diode oscillator". In: *IEEE Transactions on Electron Devices* 16.1 (1969), pp. 64–77. DOI: `10.1109/T-ED.1969.16566`.

[19] Mohammad Shahidullah, Waleed Al-Malki, and Nicholas Delamere. "Mechanism of Aqueous Humor Secretion, Its Regulation and Relevance to Glaucoma". In: Nov. 2011. ISBN: 978-953-307-591-4. DOI: `10.5772/26559`.